

Distributionally Robust Transfer Learning with Structurally Missing Covariates, with Application to Cross-National Cardiac Arrest Prediction

Siqi Li^{1,2}, Chuan Hong^{3,4}, Ziye Tian³, Benjamin Sieu-Hon Leong⁵, Koshi Nakagawa⁶,
Hideharu Tanaka⁷, Sang Do Shin⁸, Khuong Quoc Dai⁹, Do Ngoc Son¹⁰,
Marcus Eng Hock Ong^{11,12,13}, Nan Liu^{†1,2,3,13,14}, and Molei Liu^{†15,16},
for the PAROS Clinical Research Network

¹Centre for Biomedical Data Science, Duke-NUS Medical School, Singapore

²Duke-NUS AI + Medical Sciences Initiative, Duke-NUS Medical School, Singapore

³Department of Biostatistics and Bioinformatics, Duke University, Durham, NC, USA

⁴Duke Clinical Research Institute, Durham, NC, USA

⁵Emergency Medicine Department, National University Hospital, Singapore

⁶Department of Sport and Medical Science, Faculty of Physical Education, Kokushikan University, Tokyo, Japan

⁷Graduate School of Emergency Medical System, Kokushikan University, Tokyo, Japan

⁸Department of Emergency Medicine, Seoul National University College of Medicine, Seoul, Republic of Korea

⁹Center for Emergency Medicine, Bach Mai Hospital, Hanoi, Vietnam

¹⁰Center for Critical Care Medicine, Bach Mai Hospital, Hanoi, Vietnam

¹¹Health Services Research Centre, Singapore Health Services, Singapore

¹²Department of Emergency Medicine, Singapore General Hospital, Singapore

¹³Pre-hospital & Emergency Research Centre, Health Services Research and Population Health, Duke-NUS Medical School, Singapore

¹⁴NUS Artificial Intelligence Institute, National University of Singapore, Singapore

¹⁵Department of Biostatistics, Peking University Health Science Center, Peking University, Beijing, China

¹⁶Beijing International Center for Mathematical Research, Peking University, Beijing, China

Abstract

Deploying clinical prediction models across diverse healthcare systems often fails when key covariates used during training are unavailable at deployment and labeled outcomes are limited or unavailable in the target domain. For example, high-performing models for out-of-hospital cardiac arrest (OHCA) rely on detailed prehospital measurements that are routinely collected in high-resource research settings but unavailable in many international registries. Existing methods commonly either discard these missing covariates, sacrificing predictive information, or rely

[†]Co-last authors. Correspondence should be addressed to Molei Liu: moleiliu@bjmu.edu.cn.

on untestable assumptions about their distribution in the target domain. We propose DRUM (Distributionally Robust Unsupervised transfer learning with structurally Missing covariates), a framework that transfers prediction models to target populations where certain covariates are structurally absent and target outcome labels are not used for model fitting. DRUM partitions covariates into shared components (X), observed across all settings, and missing components (A), observed only in the source. Rather than imputing the missing covariates, DRUM optimizes worst-case predictive performance over the unknown target distribution of $A | X$ using a neural network generator, with a robustness parameter δ controlling the allowable deviation from the source conditional distribution. We further develop a bias correction procedure that reduces sensitivity to nuisance estimation error, improving finite-sample performance. Simulation studies suggest substantial improvements in both mean and worst-case prediction error under distribution shift. Applied to cross-national OHCA prediction, transferring models from the US registry to multiple Asian registries where prehospital variables are unrecorded, DRUM yields substantially better-calibrated predictions and improved fixed-threshold clinical classification performance across deployment sites compared with existing baselines, providing a practical framework for deploying clinical prediction models when key covariates are unavailable at target sites.

Keywords: Unsupervised transfer learning, Distributionally robust optimization, Structural missingness, Generative models, Neyman orthogonality, Energy distance, Model generalizability, Clinical prediction, Cardiac arrest

1 Introduction

Clinical prediction models developed in high-resource research settings (Wahl et al., 2018) are increasingly deployed across diverse, multi-regional healthcare systems, yet ensuring their generalizability remains a fundamental challenge (de Hond et al., 2022). Transfer learning (TL) (Li et al., 2025a)¹, which leverages knowledge from models trained in one setting to improve prediction in new populations, has emerged as a promising framework for adapting clinical models across heterogeneous healthcare environments (Li et al., 2025c).

A common assumption underlying such knowledge transfer is that the conditional relationship between commonly observed covariates and outcome, $Y | X$, remains stable across populations, so that a model trained on the source can generalize to new settings where the same covariates X are observed. In many practical deployments, however, the source model relies on a richer set of covariates (X, A) , where certain variables A that are highly predictive and routinely recorded in the source can be entirely absent in target settings due to differences in clinical infrastructure or data collection protocols. We refer to such variables as *structurally missing covariates*: unlike standard missing data where individual observations are incomplete, structural missingness reflects a population-level absence, and the missingness itself is highly informative.

¹Sometimes referred to as domain adaptation in the machine learning literature; we use the term transfer learning throughout this paper.

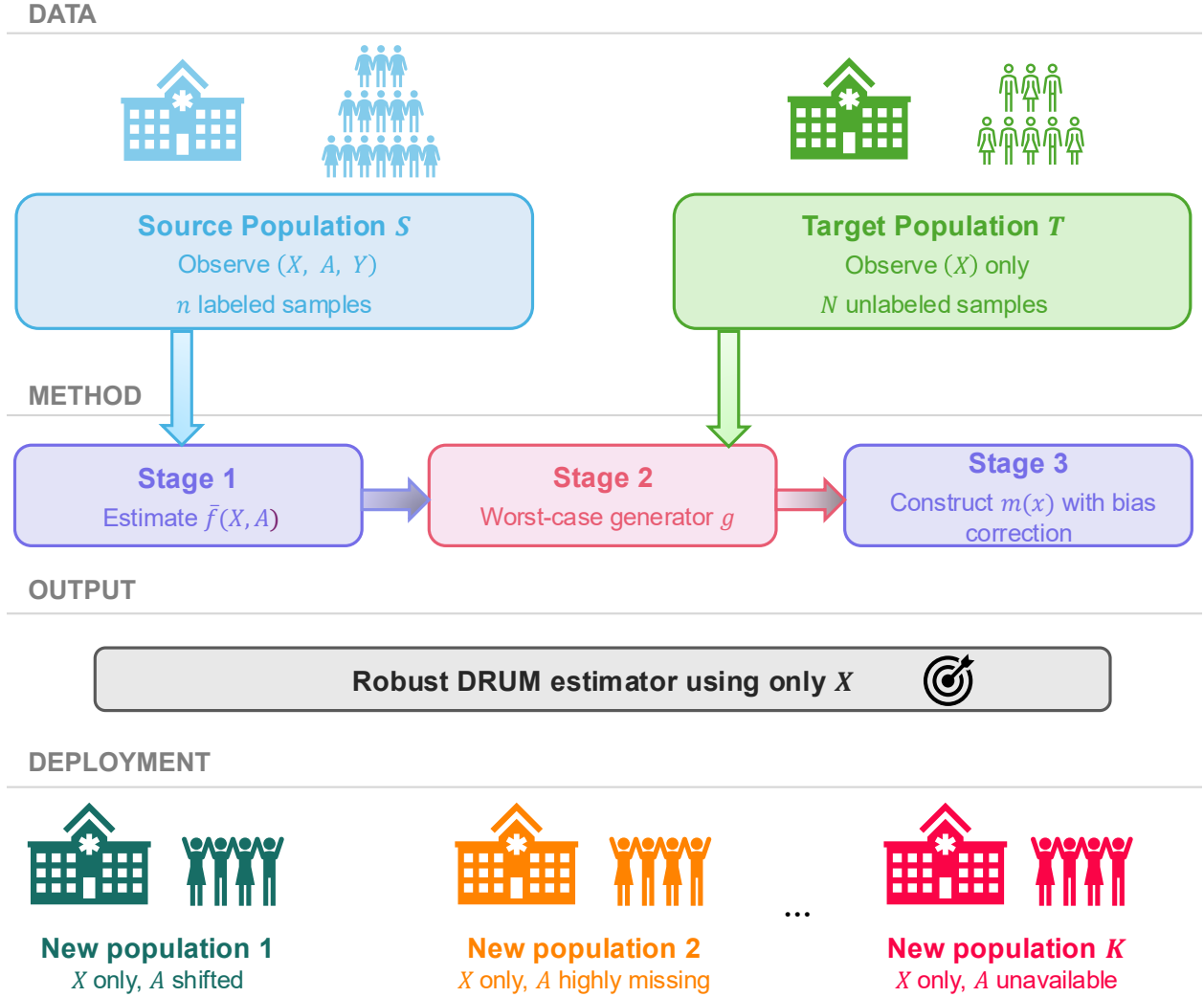


Figure 1: Overview of the DRUM framework. Source data with complete observations (X, A, Y) are used to estimate the conditional mean \bar{f} , while unlabeled target data with only X observed are used to train the worst-case generator g . The robustness parameter δ controls the allowable deviation from the source conditional distribution. The DRUM estimator $m(x)$ uses only covariates X .

When A is structurally missing in the target, prediction must rely on $\mathbb{E}[Y | X]$ alone, which requires integrating over the unknown distribution of $A | X$ in the new population. If this distribution differs from the source, as is likely when clinical practices vary across regions, directly applying the source model produces biased and miscalibrated predictions. Compounding this challenge, labeled outcome data are often unavailable, delayed, or too limited in the target population due to resource constraints or limited follow-up infrastructure, precluding retraining or supervised adaptation.

A critical application that exemplifies this challenge is predicting neurological outcomes after out-of-hospital cardiac arrest (OHCA). High-performing models trained on the US Resuscitation

Outcomes Consortium (ROC) Cardiac Epidemiologic Registry (National Heart, Lung, and Blood Institute, 2024) rely on detailed prehospital care measurements such as total epinephrine dose and arterial blood pH. When transferring these models to the Pan-Asian Resuscitation Outcomes Study (PAROS) network (Ong et al., 2011), which spans registries with heterogeneous populations and clinical practices, these prehospital variables are structurally absent across all sites, and the underlying prehospital care patterns vary substantially due to different emergency response protocols and resource levels.

This OHCA example illustrates a broader methodological challenge: transfer learning when certain covariates available in the source are structurally absent in the target, and the conditional distribution $A | X$ in the target differs from the source in unknown ways. Existing approaches fall short: imputation methods require assumptions about the distribution of A in the target domain that cannot be verified without target labels, while covariate shift corrections only address distributional differences in observed variables and cannot recover information about covariates that are entirely absent. This motivates a framework that accounts for uncertainty in the unobserved $A | X$ without relying on untestable distributional assumptions.

1.1 Related Work

Unsupervised transfer learning. Following Weiss et al. (2016), we operate in the *unsupervised transfer learning* paradigm, characterized by abundant labeled source data but no labeled target data. Classical methods typically rely on importance reweighting (Shimodaira, 2000; Sugiyama et al., 2007), which corrects for distributional mismatch by weighting source samples by the density ratio dQ_X/dP_X , with nonparametric extensions via kernel mean matching (Huang et al., 2006) or classifier-based estimation (Bickel et al., 2009). Representation-based approaches instead learn domain-invariant features by minimizing distributional discrepancy in a shared embedding space, for example through maximum mean discrepancy (Long et al., 2015) or adversarial domain classification (Ganin et al., 2016). Generative approaches such as CyCADA (Hoffman et al., 2018) leverage unlabeled target data via pixel- and feature-level adversarial alignment. Despite their methodological differences, all of these methods assume a shared covariate space between source and target. They cannot handle the case where certain outcome-relevant covariates are entirely absent in the target domain, as occurs in our setting.

Missing data and blockwise missingness. A parallel literature addresses missing covariate data through *blockwise missingness*, where entire groups of variables are absent for certain data sources during multi-source integration (Little and Rubin, 2019). Methods in this area—whether imputation-based (Xue and Qu, 2021), structured-sparsity approaches that partition samples by missingness pattern (Yuan et al., 2012; Xiang et al., 2014), covariance-based optimal prediction (Yu et al., 2020), modular regression for multi-modal covariates (Jin and Rothenhäusler, 2023), or adaptive learning under distributional shift (Li et al., 2025e)—share a common strategy: leveraging sources where a variable block is observed to recover information for sources where it is absent.

This literature diverges from our setting in two critical ways. First, these methods target estimation at a primary source or across pooled datasets, rather than out-of-sample prediction in an entirely unlabeled target domain. Second, they share an implicit assumption that the conditional distribution $A | X$ remains stable across sources, so that information learned where A is observed transfers directly to settings where it is absent. This assumption cannot be verified without target labels and is unlikely to hold in heterogeneous clinical data.

Distributionally robust optimization. To avoid relying on these untestable assumptions about the stability of $A | X$, distributionally robust optimization (DRO) offers a principled alternative by providing worst-case guarantees over a specified uncertainty set of distributions. For an outcome Y and a full set of covariates Z , the standard DRO formulation seeks a predictor $m(\cdot)$ that solves the minimax problem:

$$\min_{m(\cdot)} \max_{\mathbb{P} \in \mathcal{U}} \mathbb{E}_{(Z,Y) \sim \mathbb{P}} [\ell(Y, m(Z))],$$

where \mathcal{U} is an uncertainty set around the training distribution, typically constrained via divergence constraints such as f -divergence (Hu and Hong, 2013; Duchi and Namkoong, 2021) or Wasserstein distance (Esfahani and Kuhn, 2017; Blanchet and Murthy, 2017). This paradigm has been applied broadly, including to classification (Sagawa et al., 2020) and algorithmic fairness (Hashimoto et al., 2018; Li et al., 2025b).

However, conventional DRO formulations construct uncertainty sets over the *joint* distribution of all variables, treating the covariate space Z as a single, monolithic block. They do not distinguish between covariates that remain reliably available at deployment (X) and those that are structurally absent (A). For our setting, this joint-distribution approach is overly conservative and poorly targeted. The primary source of uncertainty when deploying to a new healthcare system is not the marginal distribution of the stable variables $P(X)$, but rather the unknown conditional distribution $A | X$ of the missing covariates.

1.2 Contributions

We propose DRUM (Distributionally Robust Unsupervised transfer learning with structurally Missing covariates), a framework for transferring prediction models to unlabeled target populations where certain covariates are structurally absent. DRUM partitions covariates into stable components X , consistently observed across all settings, and structurally missing components A , unobserved in the target domain. Rather than imputing A under untestable distributional assumptions, DRUM learns a prediction function that optimizes worst-case predictive performance over an uncertainty set on the target distribution of $A | X$. Our specific contributions are as follows.

First, we develop a DRO framework that isolates the uncertainty to the conditional distribution $A | X$ using an energy distance-based uncertainty set, governed by a single robustness parameter δ . By parameterizing this conditional distribution through a generative model, we reduce an otherwise intractable infinite-dimensional robust optimization problem into a finite-dimensional neural

network objective solvable via gradient-based training. This parameterization offers substantial flexibility: neural networks accommodate complex nonlinear relationships between covariates and outcome and naturally extend to diverse prediction modeling tasks.

Second, to ensure reliable finite-sample performance, we derive a bias-correction procedure based on Neyman-orthogonal estimation and cross-fitting. This procedure formally reduces the estimator’s sensitivity to first-order biases arising from nuisance function estimation. Extensive simulation studies show that this correction yields substantial improvements in mean and worst-case prediction errors over uncorrected DRUM and standard baselines under varying degrees of distribution shift.

Third, we apply DRUM to cross-national OHCA outcome prediction under genuine structural missingness. Using the US-ROC registry as the labeled source, we deploy DRUM across three distinct Asian PAROS registries (Singapore, Japan, Korea) where prehospital care variables are absent from the data collection infrastructure. DRUM yields consistently well-calibrated predictions across all deployment sites, substantially outperforming empirical risk minimization, importance weighting, and imputation-based baselines.

Beyond this specific application, DRUM provides a principled framework for transferring clinical prediction models from high-resource to low-resource healthcare settings when important predictors are unavailable, with direct implications for the generalizability and equity of clinical decision support across diverse populations.

1.3 Organization of the Article

The remainder of the paper is organized as follows. Section 2 describes the cross-national OHCA prediction challenge and the study populations. Section 3 formulates the DRO framework and derives the dual-form robust predictor. Section 4 presents the computational approach, including generator parameterization and bias correction. Section 5 presents simulation studies. Section 6 reports the results of applying DRUM to cross-national cardiac arrest outcome prediction. Theoretical justifications, additional experimental details, and supplementary results are provided in the Appendix.

2 Data Description

2.1 Cross-National Generalizability of Clinical Prediction Models

Clinical prediction models are increasingly developed at high-resource academic centers using rich data, yet are intended for deployment across heterogeneous healthcare systems whose data collection infrastructure may be substantially leaner. A growing methodological literature has documented systematic degradation in predictive performance when models trained at a single site are transported to populations differing in case-mix, measurement practices, or outcome prevalence (de Hond et al., 2022), and recent reviews of clinical AI emphasize that external validation

across geographically and institutionally distinct cohorts remains the central bottleneck to clinical adoption (Yang et al., 2022).

A common failure mode occurs when target sites do not record a subset of the training covariates, a structural missingness driven by differing clinical and regulatory infrastructures (Yang et al., 2024). Standard responses, such as discarding the missing variables or restricting deployment to sites with complete data, force a trade-off between predictive power and generalizability. A principled alternative is to leverage the rich source data during training, but design a deployable predictor that uses only universally available covariates while explicitly accounting for uncertainty in the unobserved variables.

2.2 Out-of-Hospital Cardiac Arrest as a Motivating Application

We illustrate this challenge using prediction of neurological outcomes after out-of-hospital cardiac arrest (OHCA). OHCA prediction is a natural setting for studying cross-national deployment under structural missingness for two reasons. First, the conditional relationship between clinical state at presentation and neurological outcome is plausibly stable across populations (Li et al., 2025c). Second, the data infrastructure supporting OHCA registries differs sharply across regions, producing exactly the kind of structural missingness our framework addresses. As with other critical care and emergency medicine models, OHCA prediction is increasingly used to guide resource allocation, for example by identifying patients most likely to benefit from aggressive interventions such as mechanical circulatory support or early coronary angiography (Nolan et al., 2019). In such contexts, well-calibrated predicted probabilities are essential for clinical deployment.

Source Data We use the Resuscitation Outcomes Consortium (ROC) Cardiac Epidemiologic Registry (National Heart, Lung, and Blood Institute, 2024) as source data ($n = 9,755$). ROC was a North American clinical research network funded by the National Heart, Lung, and Blood Institute, designed to standardize prehospital data capture across participating EMS agencies. As a consequence, the ROC registry provides granular prehospital care variables mandated by its standardized data dictionary. The outcome is favorable neurological status at hospital discharge, defined as Cerebral Performance Category 1 or 2 (Y , binary). Patient-level covariates (X) include age, sex, initial cardiac rhythm (shockable vs. non-shockable), and witness/bystander CPR status. The prehospital care variables are denoted A .

Target and External Data To emulate a realistic deployment scenario in which only stable covariates are available, we treat the Singapore OHCA cohort from the Pan-Asian Resuscitation Outcomes Study (PAROS) registry (Ong et al., 2011) ($N = 5,933$) as unlabeled target data, using only X for generator training. PAROS is a collaborative network of Asia-Pacific EMS systems whose data dictionary is deliberately leaner than ROC’s: across participating sites, prehospital care variables such as drug dosing and blood gases are inconsistently captured or absent altogether (Doctor et al., 2017). Although outcome labels are available in PAROS for retrospective

Table 1: Baseline characteristics of the OHCA study populations. Continuous variables are presented as mean (SD) or median [IQR]; categorical variables as n (%). The prehospital care variables (A) were available only in the US-ROC source data.

		Source	Target	External	
		US-ROC $n = 9,755$	Singapore $n = 5,933$	Japan $n = 64,262$	Korea $n = 8,484$
<i>Stable covariates (X)</i>					
Age, mean (SD)		63.8 (16.0)	65.2 (18.4)	72.4 (18.3)	64.6 (19.1)
Sex, n (%)	Female	3,427 (35.1)	2,072 (34.9)	27,460 (42.7)	3,079 (36.3)
	Male	6,328 (64.9)	3,861 (65.1)	36,802 (57.3)	5,405 (63.7)
Rhythm, n (%)	Non-shock.	5,519 (56.6)	4,901 (82.6)	59,795 (93.0)	7,284 (85.9)
	Shockable	4,236 (43.4)	1,032 (17.4)	4,467 (7.0)	1,200 (14.1)
Witness/CPR, n (%)	No/No	1,869 (19.2)	1,354 (22.8)	21,706 (33.8)	2,498 (29.4)
	No/Yes	1,503 (15.4)	1,057 (17.8)	15,829 (24.6)	1,535 (18.1)
	Yes/No	2,351 (24.1)	1,475 (24.9)	11,530 (17.9)	1,862 (21.9)
	Yes/Yes	4,032 (41.3)	2,047 (34.5)	15,197 (23.6)	2,589 (30.5)
<i>Missing covariates (A, source only)</i>					
Response time (min)		5.40 [4.15, 6.90]	—	—	—
Epinephrine dose (mg)		2.00 [1.00, 3.00]	—	—	—
Blood pH		7.18 [7.02, 7.29]	—	—	—
<i>Outcome (Y)</i>					
Neuro outcome, n (%)	Good	1,885 (19.3)	183 (3.1)	2,217 (3.4)	354 (4.2)
	Poor	7,870 (80.7)	5,750 (96.9)	62,045 (96.6)	8,130 (95.8)

evaluation, DRUM does not use target labels during model training, generator estimation, or bias correction. In the real-data analysis, a labeled Singapore validation subset was used only for final hyperparameter selection, while held-out Singapore outcomes and all Japan/Korea outcomes were reserved for performance assessment.

External validation is performed on the PAROS cohorts from Japan ($n = 64,262$) and Korea ($n = 8,484$), in which the prehospital variables A are likewise unavailable. The three Asian cohorts also exhibit substantial heterogeneity in patient characteristics and outcomes relative to the source: the prevalence of favorable neurological outcome is 19.3% in the US-ROC source population but only 3.1–4.2% in the three PAROS cohorts (Table 1), reflecting differences in bystander response rates, EMS dispatch times, and post-arrest care pathways. This prevalence shift is consistent with the Conditional Stability Assumption, as it can arise from differences in the distribution of (X, A) rather than changes in the outcome mechanism. Together, structural missingness in A , covariate shift in X , and substantial prevalence shift make the OHCA setting a stringent test of our transfer learning methodology.

3 Problem Setup and DRO framework

3.1 Problem Setup

We consider a transfer learning setting where a prediction model will be deployed in a new target population using only the covariates X that are consistently observed across all settings, while certain covariates A are structurally missing in the target. Let $\mathcal{D}_S = \{X_i, A_i, Y_i\}_{i=1}^n$ denote labeled source data from population \mathcal{S} and let $\mathcal{D}_T = \{X_j\}_{j=1}^N$ denote unlabeled target data from population \mathcal{T} where only X is observed. We make the following assumption on the stability of the outcome mechanism.

Assumption (Conditional Stability). The conditional distribution of outcome is identical in source and target populations: $\mathbb{P}_{Y|X,A}^S = \mathbb{P}_{Y|X,A}^T$.

The marginal distribution of X may shift from \mathbb{P}_X (source) to \mathbb{Q}_X (target), and the distribution of A , either marginal or conditional on X , may shift arbitrarily and A can become entirely unobserved. Since A is structurally absent in the target, conditional stability cannot be empirically verified at deployment, analogous to the covariate shift assumption in standard transfer learning (Shimodaira, 2000). Under this premise, the sole remaining source of unidentifiability is the unknown target distribution of $A | X$.

Our goal is to learn a predictor $m : \mathbb{R}^{d_X} \rightarrow \mathbb{R}$ that uses only X and achieves robust predictive performance under worst-case realizations of A . We formalize this as a distributionally robust optimization problem:

$$\max_{m(\cdot)} \min_{\mathbb{P}_{A|X} \in \mathcal{C}(\delta)} \mathbb{E}_{X \sim \mathbb{Q}_X, A \sim \mathbb{P}_{A|X}, Y \sim \mathbb{P}_{Y|X,A}^S} [Y^2 - (Y - m(X))^2], \quad (1)$$

where $\mathcal{C}(\delta)$ is an uncertainty set of conditional distributions of $A | X$ controlled by a radius parameter $\delta \geq 0$. The objective is a robust squared-error-reduction criterion: $Y^2 - (Y - m(X))^2$ measures the improvement in squared prediction error achieved by $m(X)$ relative to the null predictor $m_0(x) = 0$. The choice of zero as the reference predictor is without loss of generality: replacing $m_0(x) = 0$ with any fixed baseline yields an equivalent optimization after centering Y . Maximizing the worst-case value over $\mathcal{C}(\delta)$ therefore selects a predictor whose predictive utility remains favorable under adverse target distributions of the structurally missing covariates.

The parameter δ controls the degree of robustness. When $\delta = 0$, the uncertainty set contains only the source conditional $\mathbb{P}_{A|X}^S$, recovering standard transfer learning without robustness. For $\delta > 0$, the uncertainty set expands to include conditional distributions $A | X$ within a bounded neighborhood of the source, protecting against bounded perturbations in the conditional relationship between missing and observed covariates. We additionally consider a separate formulation, referred to as the *unconstrained* setting, in which the adversary is restricted to selecting a marginal distribution $\rho \in \mathcal{P}_A$ independent of X . This corresponds to parameterizing the generator as $g_\theta(\epsilon)$ with no dependence on X , enforcing $A \perp X$ by construction. The unconstrained setting provides

robustness against arbitrary marginal shifts in A while remaining computationally tractable, at the cost of discarding conditional structure between A and X that may be informative for prediction.

3.2 Dual-Form DRO Predictor

At the population level, for fixed $\mathbb{P}_{A|X}$, the objective in (1) is a pointwise quadratic in $m(x)$ with a unique maximizer; for fixed m , it is linear in $\mathbb{P}_{A|X}$. Since the maximization over m admits a closed-form solution (shown below), Sion's minimax theorem (Sion, 1958) (conditions given in Appendix A.2) permits exchanging the order of optimization:

$$\min_{\mathbb{P}_{A|X} \in \mathcal{C}(\delta)} \max_{m(\cdot)} \mathbb{E}_{X \sim \mathbb{Q}_X, A \sim \mathbb{P}_{A|X}, Y \sim \mathbb{P}_{Y|X,A}^S} [Y^2 - (Y - m(X))^2]. \quad (2)$$

Expanding $Y^2 - (Y - m(X))^2 = 2Ym(X) - m(X)^2$ and taking the conditional expectation over Y given (X, A) yields

$$\min_{\mathbb{P}_{A|X} \in \mathcal{C}(\delta)} \max_{m(\cdot)} \mathbb{E}_{X \sim \mathbb{Q}_X, A \sim \mathbb{P}_{A|X}} [2\bar{f}(X, A)m(X) - m^2(X)], \quad (3)$$

where $\bar{f}(x, a) = \mathbb{E}[Y \mid X = x, A = a]$ is the conditional mean function.

For a fixed $\mathbb{P}_{A|X}$, the inner maximization over m is a point-wise quadratic problem. Taking the first-order condition with respect to $m(x)$ gives

$$m_{\mathbb{P}}^*(x) = \mathbb{E}_{A \sim \mathbb{P}_{A|X=x}} [\bar{f}(x, A)]. \quad (4)$$

Substituting (4) back into (3), the problem reduces to finding the worst-case conditional distribution:

$$\min_{\mathbb{P}_{A|X} \in \mathcal{C}(\delta)} \mathbb{E}_{X \sim \mathbb{Q}_X} \left\{ \mathbb{E}_{A \sim \mathbb{P}_{A|X}} [\bar{f}(X, A)] \right\}^2. \quad (5)$$

In the unconstrained setting, the energy distance constraint is removed and the generator depends only on ϵ , enforcing $A \perp X$; the optimization (5) reduces to minimization over marginal distributions $\rho \in \mathcal{P}_A$.

Theorem (Existence of Robust Predictor). Under the Conditional Stability Assumption and regularity conditions on \bar{f} (Assumption 2 in Appendix A.2), the unconstrained problem admits a solution $\rho^* \in \mathcal{P}_A$. The robust prediction function is

$$m^*(x) = \mathbb{E}_{A \sim \rho^*} [\bar{f}(x, A)]. \quad (6)$$

For $\delta > 0$, an analogous existence result holds under an additional compactness condition on $\mathcal{C}(\delta)$; see Proposition 1 in Appendix A.2 along with additional convergence properties of the estimators.

4 Estimation and Computation

4.1 Generator-Based Parameterization

Direct optimization of (5) over the infinite-dimensional space of conditional distributions $\mathbb{P}_{A|X}$ is intractable. A key challenge is that the robust predictor $m^*(x) = \mathbb{E}_{A \sim \mathbb{P}_{A|X}}[\bar{f}(x, A)]$ depends on the full conditional distribution of $A | X$, not merely its conditional mean $\mathbb{E}[A | X]$. When \bar{f} is nonlinear in A , $\mathbb{E}[\bar{f}(x, A)]$ depends on the full conditional distribution of $A|X$, not merely $\mathbb{E}[A | X]$; the two coincide only when \bar{f} is linear in A , a restrictive condition that rarely holds in real-world data where outcome-covariate relationships are typically complex and nonlinear.

We therefore parameterize the conditional distribution of $A | X$ through a generative model that maps latent noise to the space of A , enabling Monte Carlo approximation of $\mathbb{E}[\bar{f}(x, A)]$ for arbitrary \bar{f} . Parameterizing the generator as a neural network offers considerable modeling flexibility: neural networks can approximate arbitrarily complex conditional distributions on compact domains (Hornik et al., 1989), and the resulting finite-dimensional optimization over network parameters is solvable via standard gradient-based training.

Specifically, we introduce the generator $g_\phi : \mathbb{R}^{d_X} \times \mathbb{R}^q \rightarrow \mathbb{R}^{d_A}$ with parameters ϕ to model the conditional distribution $A | X$:

$$A = g_\phi(X, \epsilon), \quad \epsilon \stackrel{\text{iid}}{\sim} \mathcal{N}(0, I_q), \quad (7)$$

where the latent dimension q controls the expressiveness of the generator; empirically, setting $q \in [d_A, 2d_A]$ yields good performance across settings (Sections 5 and 6). In the unconstrained setting, the generator reduces to $g_\theta : \mathbb{R}^q \rightarrow \mathbb{R}^{d_A}$, depending only on ϵ , which ensures $A \perp X$ by construction.

Substituting (7) into (5), the optimization becomes:

$$\min_{g_\phi \in \mathcal{C}_g(\delta)} \mathbb{E}_{X \sim \mathbb{Q}_X} \left[\mathbb{E}_{\epsilon \stackrel{\text{iid}}{\sim} \mathcal{N}(0, I_q)} [\bar{f}(X, g_\phi(X, \epsilon))] \right]^2, \quad (8)$$

which in the unconstrained setting simplifies to unconstrained minimization over $\theta \in \Theta$. The robust prediction function is $m^*(x) = \mathbb{E}_\epsilon[\bar{f}(x, g^*(\cdot, \epsilon))]$ once an optimal generator is obtained.

4.2 Energy-Based Uncertainty Set

To operationalize the uncertainty set $\mathcal{C}_g(\delta)$ in (8), we require a discrepancy measure between conditional distributions that (i) measures distance between *distributions*, not merely between their means; (ii) provides a consistent training objective with a unique minimizer at the true conditional; and (iii) is computationally efficient and compatible with gradient-based optimization.

We adopt the energy distance (Székely and Rizzo, 2013), operationalized through the Engression framework of Shen and Meinshausen (2024). The energy score is a strictly proper scoring rule, uniquely minimized when the generated distribution matches the true conditional without requiring

density estimation or kernel selection. In addition, the Egression framework has been shown to produce generators that extrapolate well beyond the training distribution (Shen and Meinshausen, 2024), a useful property when the worst-case generator must explore conditional distributions that depart from the source.

For a conditional generator $g(x, \epsilon)$, the energy score $En(g)$ measures how well g captures the source conditional distribution $\mathbb{P}_{A|X}^{\mathcal{S}}$:

$$En(g) = \mathbb{E}_{(X,A) \sim \mathbb{P}^{\mathcal{S}}, \epsilon \sim \text{iid } \mathcal{N}(0, I_q)} \|A - g(X, \epsilon)\|_2 - \frac{1}{2} \mathbb{E}_{X \sim \mathbb{P}_X^{\mathcal{S}}, \epsilon, \epsilon' \sim \text{iid } \mathcal{N}(0, I_q)} \|g(X, \epsilon) - g(X, \epsilon')\|_2, \quad (9)$$

where (X, A) are drawn from the source distribution $\mathbb{P}^{\mathcal{S}}$. The first term measures the expected distance between generated and observed values of A ; the second measures the expected distance between independent generated samples, encouraging the generator to capture the spread of the conditional distribution rather than collapsing to a point estimate.

The source conditional generator $g^{\mathcal{S}} = \arg \min_{g \in \mathcal{G}} En(g)$ minimizes this score (Eq. (9)), achieving the best fit to the source $A | X$. The uncertainty set is then defined by allowing generators that deviate from this best fit by at most δ :

$$\mathcal{C}_g(\delta) = \{g \in \mathcal{G} : En(g) - En(g^{\mathcal{S}}) \leq \delta\}. \quad (10)$$

The energy gap $En(g) - En(g^{\mathcal{S}})$ is smooth and differentiable in the generator parameters, enabling enforcement of the constraint via primal-dual gradient methods (Section 4.3). In practice, finite δ can be selected via held-out source validation or informed by domain expertise about the plausible magnitude of $A | X$ shift; when no prior knowledge or labeled validation data are available, the unconstrained setting provides a conservative default.

4.3 Estimation Procedure

The estimation proceeds in three stages.

Stage 1: Conditional mean estimation. Train a neural network $\hat{f}_{\psi}(x, a)$ on source data $\mathcal{D}_{\mathcal{S}}$ to approximate $\bar{f}(x, a) = \mathbb{E}[Y | X = x, A = a]$ by minimizing the mean squared error:

$$\hat{\psi} = \arg \min_{\psi} \frac{1}{n} \sum_{i=1}^n (Y_i - \hat{f}_{\psi}(X_i, A_i))^2. \quad (11)$$

For binary outcomes, the Stage 1 training loss is replaced by binary cross-entropy; the subsequent stages apply the squared objective to the estimated probabilities and remain unchanged.

Stage 2: Worst-case generator training. With $\hat{f}_{\hat{\psi}}$ fixed, train the generator by minimizing the empirical version of (8). We first learn the source conditional generator $g_{\phi}^{\mathcal{S}}$ by minimizing the empirical energy score (9) on source data, then solve the energy-constrained problem via the primal-dual method:

$$\mathcal{L}(\phi, \lambda) = \frac{1}{N} \sum_{j=1}^N \left(\frac{1}{L} \sum_{l=1}^L \hat{f}_{\hat{\psi}}(X_j, g_{\phi}(X_j, \epsilon_{jl})) \right)^2 + \lambda(\Delta En(g_{\phi}, g^{\mathcal{S}}) - \delta), \quad (12)$$

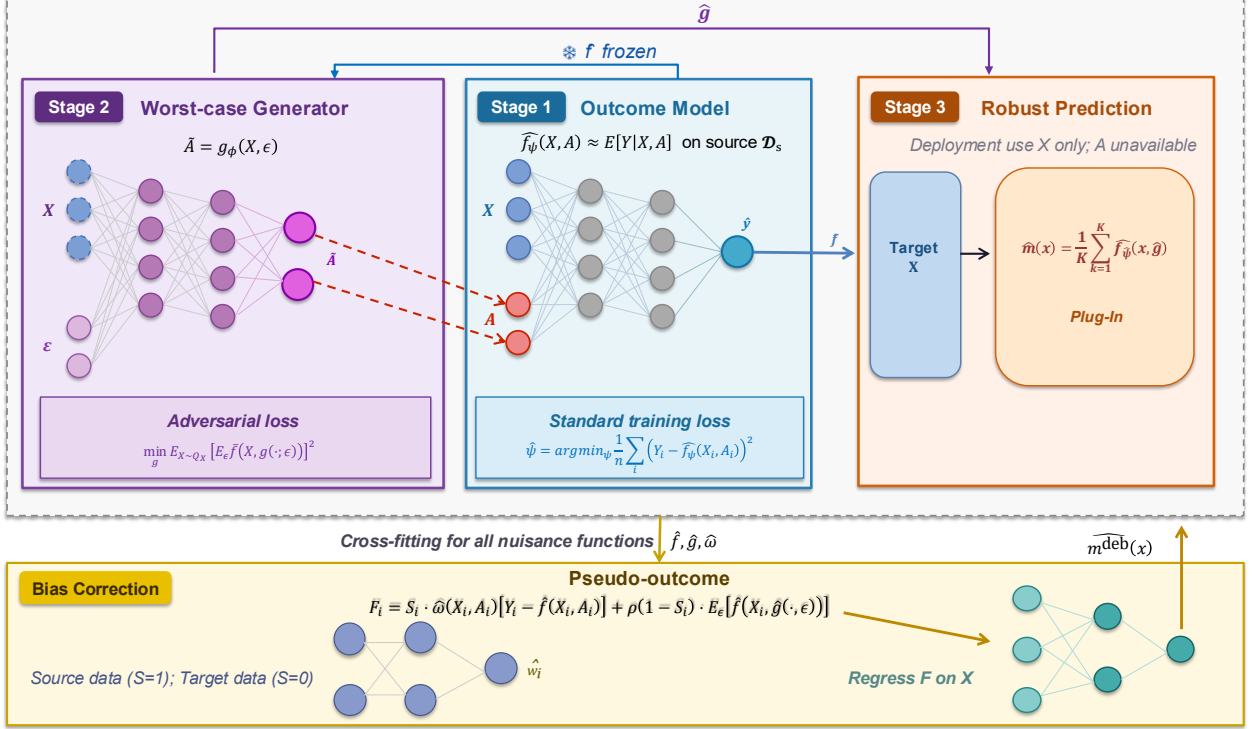


Figure 2: Estimation procedure for DRUM. Stage 1: a neural network $\hat{f}_\psi(X, A)$ is trained on labeled source data to estimate $\bar{f}(x, a)$. Stage 2: with \hat{f} fixed, a worst-case generator is trained on unlabeled target covariates; the generator $g_\phi(X, \epsilon)$ is conditional on X and constrained by the energy distance budget δ (in the unconstrained setting, $g_\theta(\epsilon)$ depends only on latent noise). Stage 3: the robust predictor $\hat{m}(x)$ averages \hat{f} over L Monte Carlo draws, producing predictions that use only X at deployment. A bias correction stage regresses pseudo-outcomes F_i on X to reduce sensitivity to estimation error in \hat{f} .

where $\{\epsilon_{jl}\}_{l=1}^L \stackrel{\text{iid}}{\sim} \mathcal{N}(0, I_q)$ are Monte Carlo samples, $\{X_j\}_{j=1}^N$ are target covariates, $\lambda \geq 0$ is the dual variable, and $\Delta \text{En}(g_\phi, g^S) = \text{En}(g_\phi) - \text{En}(g^S)$ is the energy gap. The optimization alternates between updating ϕ to minimize (12) and updating λ via dual gradient ascent: $\lambda \leftarrow \max(0, \lambda + \eta_\lambda(\Delta \text{En} - \delta))$. In the unconstrained setting, the energy constraint is removed and the generator $g_\theta(\epsilon)$ depends only on latent noise.

Stage 3: Robust prediction. Given the trained generator \hat{g} , the robust predictor is:

$$\hat{m}(x) = \frac{1}{L} \sum_{l=1}^L \hat{f}_\psi(x, \hat{g}(\cdot, \epsilon_l)), \quad (13)$$

where $\{\epsilon_l\}_{l=1}^L \stackrel{\text{iid}}{\sim} \mathcal{N}(0, I_q)$. Here $\hat{g}(\cdot, \epsilon_l)$ denotes the generated value of A under the fitted worst-case generator: in the general setting, $\hat{g}(\cdot, \epsilon_l) = \hat{g}(x, \epsilon_l)$ when evaluating $\hat{m}(x)$, whereas in the unconstrained setting, $\hat{g}(\cdot, \epsilon_l) = \hat{g}(\epsilon_l)$.

Figure 2 illustrates the estimation procedure for the plug-in DRUM estimator. The plug-in

estimator $\hat{m}(x)$ can be further improved through bias correction, described in Section 4.4. Complete algorithms, including bias correction, are provided in Algorithms 1–4 in Appendix B.

4.4 Bias Correction

The plug-in estimator $\hat{m}(x) = \frac{1}{L} \sum_l \hat{f}(x, \hat{g}(\cdot, \epsilon_l))$ inherits the estimation error of \hat{f} , which is estimated in the higher-dimensional (x, a) space. However, the target function $m(x) = \mathbb{E}_A[\bar{f}(x, A)]$ depends only on x and is a lower-complexity object than $\bar{f}(x, a)$: in an oracle setting where \bar{f} is known, estimating $m(x)$ reduces to a regression problem in x alone. The plug-in estimator does not exploit this complexity reduction. Since \hat{f} is used both to train the generator and to form the final prediction, estimation errors in \hat{f} accumulate systematically rather than canceling upon averaging. Moreover, the worst-case optimization further amplifies this sensitivity by steering the generator toward regions where \hat{f} produces extreme predictions.

Motivated by semiparametric efficiency theory (Chernozhukov et al., 2018; Kennedy, 2023), we construct a bias-corrected estimator that adapts to the complexity of $m(x)$ rather than $\bar{f}(x, a)$. The key idea is to augment the plug-in prediction with a correction term that cancels the first-order bias from estimating \bar{f} , leaving only second-order remainders. Specifically, we form the pseudo-outcome:

$$F_i = S_i \cdot \hat{\omega}(X_i, A_i) [Y_i - \hat{f}(X_i, A_i)] + r(1 - S_i) \cdot \mathbb{E}_\epsilon[\hat{f}(X_i, \hat{g}(\cdot, \epsilon))], \quad (14)$$

where $S_i = 1$ for source observations, $S_i = 0$ for target observations, and $r = n/N$.

Here $\hat{\omega}(x, a) = \mathbb{Q}_{X,A}^{\hat{g}}(x, a) / \mathbb{P}_{X,A}^S(x, a)$ is a density ratio that reweights source observations to match the distribution induced by the preliminary (plug-in) generator from Stages 1–2, where $\mathbb{Q}_{X,A}^{\hat{g}}$ denotes the joint distribution of $X \sim \mathbb{Q}_X$ and $A = \hat{g}(\cdot, \epsilon)$. In practice, $\hat{\omega}$ is estimated via probabilistic classification: source observations (X_i, A_i) and synthetic pairs $(X_j, \hat{g}(\epsilon_j))$ are pooled, a classifier $\hat{p}(S=1 | X, A)$ is trained to distinguish the two populations, and the density ratio is obtained as $\hat{\omega} = (1 - \hat{p})/\hat{p}$. Because $\hat{\omega}$ is normalized to unit mean within each cross-fitting fold (Algorithm 4), any constant class-prior factor in $(1 - \hat{p})/\hat{p}$ cancels.

The first term of (14) reweights source residuals from the source distribution to the generator-induced distribution via the density ratio $\hat{\omega}$, correcting for the systematic bias introduced by using \hat{f} in place of \bar{f} ; the second term provides the plug-in prediction on target data. The bias-corrected estimator $\hat{m}^{\text{deb}}(x)$ is obtained by regressing F on X using a neural network.

The pseudo-outcome construction renders the estimator Neyman-orthogonal (Chernozhukov et al., 2018; Kennedy, 2023) with respect to \bar{f} , canceling the first-order term from estimating \bar{f} and leaving only second-order remainders; both \hat{f} and $\hat{\omega}$ must be consistent, but neither requires the parametric \sqrt{n} rate individually (Corollary 1). To avoid overfitting, we employ K -fold cross-fitting ($K = 3$ in all experiments) for all nuisance functions (\hat{f} , $\hat{\omega}$, \hat{g}). The formal derivation is provided in Appendix A.1, and the complete procedure is summarized in Algorithm 4 in Appendix B.

5 Simulations

We evaluate the proposed DRUM methods through simulation studies designed to assess predictive robustness under varying degrees of conditional shift in $A | X$. All experiments compare DRUM against the following baselines:

- *Standard baselines*: Baseline-ERM, a neural network regressing Y on X alone via empirical risk minimization using source data only; and Baseline-DRO, the distributionally robust optimization method of Duchi and Namkoong (2021) applied to the same $Y \sim X$ regression.
- *Importance weighting baselines*: IW-KMM, which estimates target/source density ratio weights $\hat{w}(x) = p_{\mathcal{T}}(x)/p_{\mathcal{S}}(x)$ via kernel mean matching (Huang et al., 2006) using unlabeled target X , then trains a weighted $Y \sim X$ regression on source data; and IW-Classify, which estimates the same density ratio via a logistic regression classifier trained to distinguish source from target observations (Shimodaira, 2000; Bickel et al., 2009).
- *Pseudo-label baselines*: PL-Mean, PL-MICE, and PL-MissForest, which treat the target Y as missing, impute it using source $Y | X$ relationships (via mean imputation, MICE, or MissForest respectively), pool the imputed target data with source data, and train $Y \sim X$ models on the completed dataset. Each imputation method is combined with both ERM and DRO training, yielding six variants (10 baselines in total).

The importance weighting and pseudo-label baselines each use unlabeled target X but no target Y , matching the information available to DRUM. The key distinction is that all baselines model $Y | X$ directly, either by reweighting source observations to match the target covariate distribution or by augmenting the training set with imputed pseudo-labels. Neither approach accounts for the influence of the unobserved A on Y : importance weighting corrects for shifts in $P(X)$ but assumes $P(Y | X)$ is shared across populations, while pseudo-labeling reinforces the source $Y | X$ relationship through the imputed values. In contrast, DRUM explicitly models the role of A through $\bar{f}(X, A)$ and optimizes over the worst-case conditional distribution of $A | X$. The implementation details are provided in Appendix C.1.

5.1 Setting I: Linear Conditional Relationship

Data-generating Process Let $d_X = 15$ and $d_A = 5$. Source covariates are generated as $X_i \stackrel{\text{iid}}{\sim} \mathcal{N}(0, I_{d_X})$ for $i = 1, \dots, n$ with $n = 5,000$. Covariates A follow a linear conditional model:

$$A_i = B^\top X_i + \varepsilon_i, \quad \varepsilon_i \sim \mathcal{N}(0, \sigma_S^2 I_{d_A}), \quad (15)$$

where $B \in \mathbb{R}^{d_X \times d_A}$ is a fixed coefficient matrix (see details in Appendix C.1) with structured sparsity: the first 10 rows contain nonzero entries ranging from 0.1 to 1.0 that encode differential dependence of each component of A on subsets of X , while the remaining rows are zero. The noise scale is $\sigma_S = 0.8$.

The conditional mean function is specified as:

$$\bar{f}^{\text{setting I}}(x, a) = 0.1 \sum_{j=1}^{d_A} a_j + 0.1 \sum_{j=1}^{d_A} a_j^2 + 0.1 \sum_{i=1}^{d_A} x_i a_i + 0.3(x_1 a_2 + x_2 a_1) + 0.2 \sum_{i=1}^{d_A} \text{sign}(a_i) x_i^2,$$

which includes linear, quadratic, interaction, and non-smooth components in A ; as a result, the dependence of Y on A cannot be captured by simple averaging over A . Outcomes are generated as $Y_i = \bar{f}(X_i, A_i) + \eta_i$ with $\eta_i \sim \mathcal{N}(0, 0.05^2)$.

Target covariates are drawn from a mildly shifted distribution: $X_j \stackrel{\text{iid}}{\sim} \mathcal{N}(0.1 \cdot \mathbf{1}_{d_X}, 1.1^2 I_{d_X})$ for $j = 1, \dots, N$ with $N = 1,000$. Only $\{X_j\}_{j=1}^N$ is observed in the target population.

Evaluations To evaluate robustness under varying degrees of distributional shift in $A | X$, we generate Monte Carlo test datasets in which the conditional relationship (15) is perturbed. Specifically, for a perturbation scale $s > 0$, each test dataset is generated with:

$$A_{\text{test}} = \tilde{B}^\top X_{\text{test}} + \varepsilon, \quad \tilde{B} = B \odot U, \quad U_{kl} \stackrel{\text{iid}}{\sim} \text{Uniform}(-s, s), \quad (16)$$

where \odot denotes element-wise multiplication and $\varepsilon \sim \mathcal{N}(0, \sigma_S^2 I_{d_A})$. The parameter s controls the severity of the conditional shift: as s increases, the entries of \tilde{B} undergo sign reversals and magnitude changes, producing increasingly severe departures from the source conditional $A | X$.

The noiseless outcomes $\bar{f}(X_{\text{test}}, A_{\text{test}})$ serve as the ground truth for evaluation. We consider perturbation scales $s \in \{0.6, 1.0, 1.4, 1.8\}$ and generate 100 independent Monte Carlo test datasets at each scale.

For each method and perturbation scale, we report: (i) the worst-case normalized MSE, defined as $\max_{l=1, \dots, 100} \text{MSE}_l / \widehat{\text{Var}}(Y^{\mathcal{S}})$, where MSE_l is the mean squared error on the l -th Monte Carlo test set evaluated against the noiseless outcome $\bar{f}(X_{\text{test}}, A_{\text{test}})$ and $\widehat{\text{Var}}(Y^{\mathcal{S}})$ is the sample variance of Y in the source data (we report both this sample maximum and the mean to characterize tail and average-case performance, respectively); and (ii) the mean normalized MSE, averaged over the 100 Monte Carlo draws. The worst-case metric is an empirical analogue of the robust objective (1); the mean metric reflects average-case performance.

Results The results of Setting I are presented in Figure 3, Figure 8 and Table 6. The standard baselines (ERM, DRO) and importance reweighting baselines (IW-KMM, IW-Classify) all exhibit worst-case normalized MSE above 3.4, suggesting that correcting the marginal shift in $P(X)$ does not address the conditional shift in $A | X$. Among the pseudo-label baselines, PL-Mean+DRO is the strongest competitor.

DRUM-Debiased (unconstrained) achieves the best worst-case MSE across all scales shown, representing roughly a 30% reduction over PL-Mean+DRO. DRUM-Debiased (unconstrained) also achieves the best mean MSE across all perturbation scales. A full comparison across all perturbation scales and all four DRUM variants is provided in Figure 8 and Table 6 in Appendix C.2.

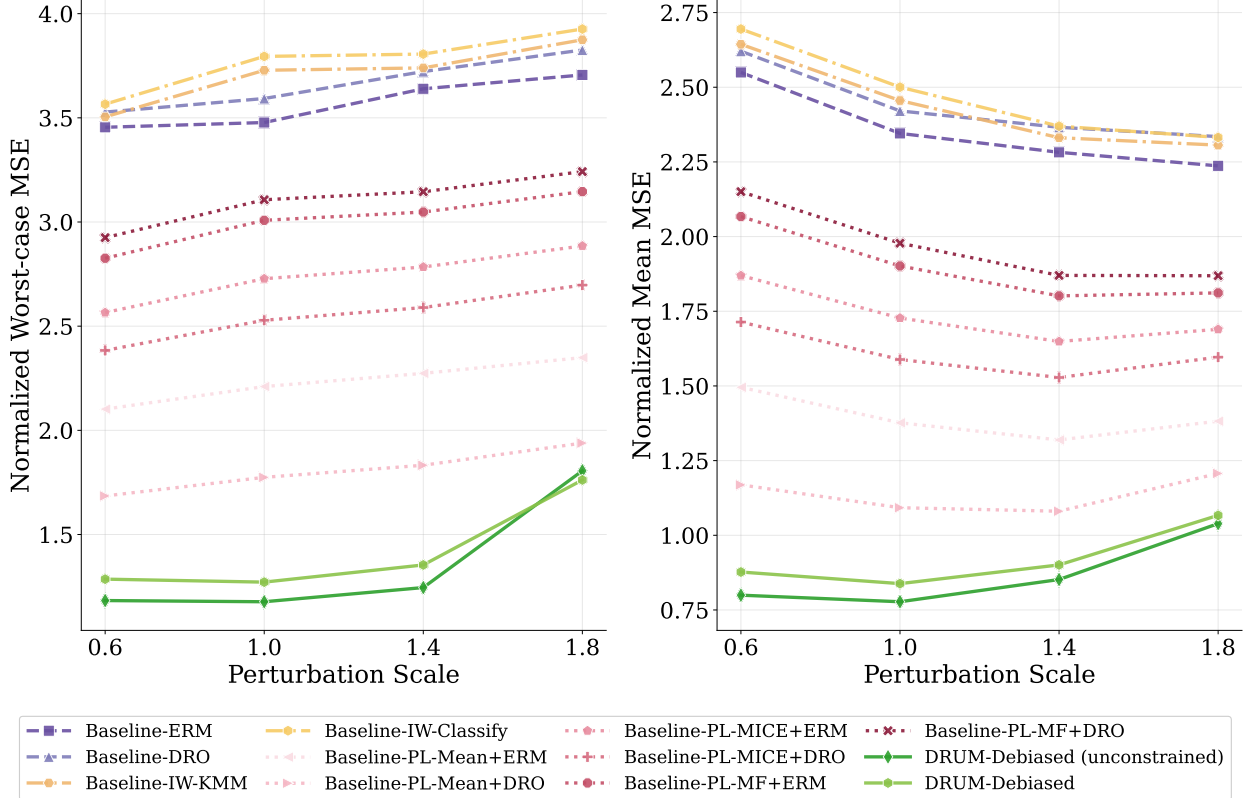


Figure 3: Worst-case and mean normalized MSE across perturbation scales s for Setting I. Results are computed over 100 Monte Carlo test datasets at each scale. MSE is normalized by the source outcome variance $\widehat{\text{Var}}(Y^{\mathcal{S}})$.

5.2 Setting II: Nonlinear Conditional Relationship

We modify Setting I in two ways to examine performance when the conditional relationship between A and X is nonlinear. First, we replace the linear data-generating mechanism for $A | X$ with a nonlinear one. While the source conditional distribution in Setting I takes the form $A = B^\top X + \varepsilon$, here we instead generate

$$A_j = \sum_i B_{ij} X_i + \sum_i 0.1 B_{ij} X_i X_{i+1} + \sum_i 0.1 B_{ij} \text{sign}(X_i) X_i^2 + \varepsilon_j, \quad j = 1, \dots, d_A,$$

where the sums over i run over $i = 1, \dots, \min(5, d_X - 1)$ for the interaction terms and $i = 1, \dots, \min(5, d_X)$ for the sign-quadratic terms, and $\varepsilon \sim \mathcal{N}(0, \sigma_{\text{noise}}^2 I_{d_A})$. The coefficient matrix B is the same as in Setting I. This introduces structured nonlinearity into $A | X$ through both pairwise interactions ($X_i X_{i+1}$) and sign-dependent quadratic effects ($\text{sign}(X_i) X_i^2$), making the conditional distribution substantially harder to approximate via marginal (unconstrained) methods that ignore X .

Second, we modify the outcome function $\bar{f}(X, A)$ by adding a directional interaction term:

$$\bar{f}^{\text{setting II}}(x, a) = \bar{f}^{\text{setting I}}(x, a) + 0.5 \sum_{i=1}^{d_A} \tanh(x_i) a_i, \quad (17)$$

This new term creates a smooth, bounded interaction between X and A that rewards methods capable of capturing the conditional structure of $A | X$: since $\tanh(X_i)$ saturates for large $|X_i|$, the direction of the A -effect on Y depends nonlinearly on X , favoring general methods that model $A | X$ directly.

We set $d_A = 2$ (reduced from $d_A = 5$ in Setting I) and reduce the source noise scale to $\sigma_{\text{noise}} = 0.3$ (compared to 0.8 in Setting I), which strengthens the signal-to-noise ratio of the conditional relationship. The matrix $B \in \mathbb{R}^{d_X \times d_A}$ is also modified (see details in Appendix C.1). All other parameters remain identical to Setting I. The Monte Carlo evaluation samples are generated analogously, with the perturbation now applied to both the linear and nonlinear components of $A | X$.

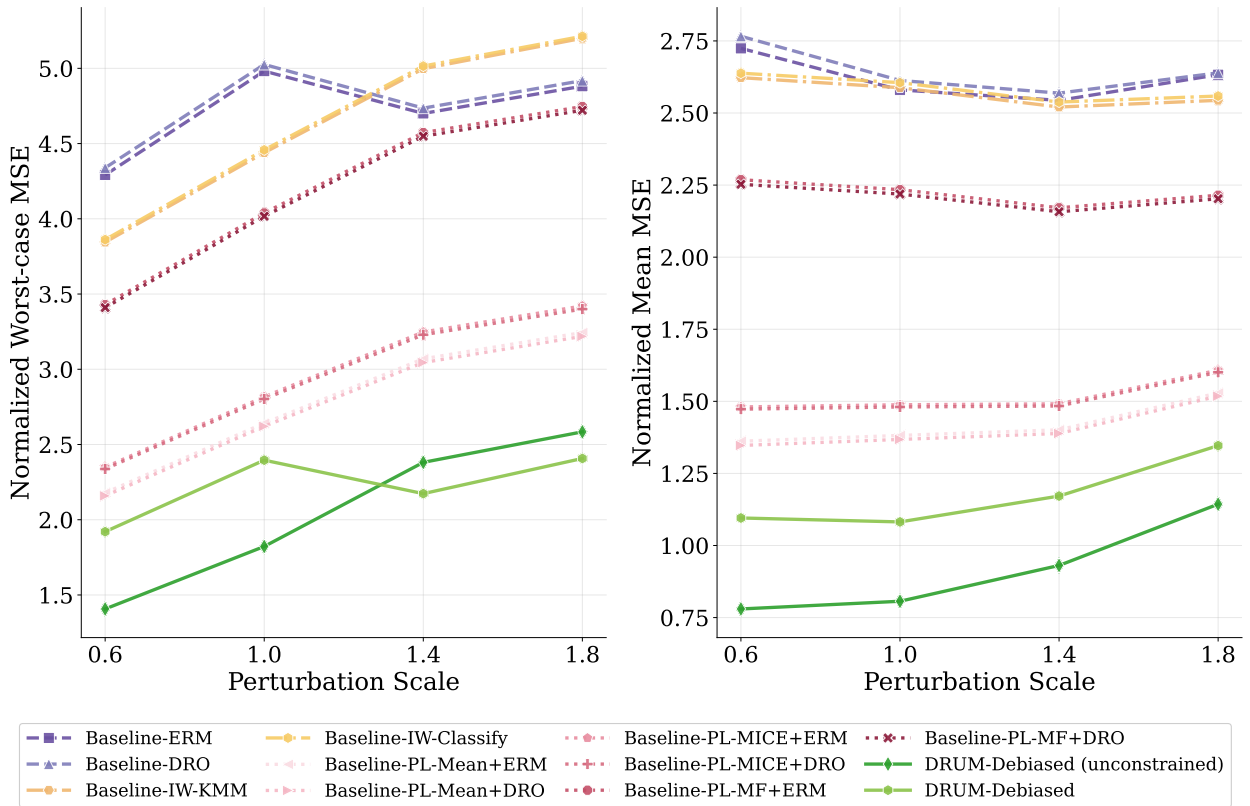


Figure 4: Worst-case and mean normalized MSE across perturbation scales s for Setting II. Results are computed over 100 Monte Carlo test datasets at each scale. MSE is normalized by the source outcome variance $\widehat{\text{Var}}(Y^S)$.

Results The results for Setting II are shown in Figure 4 and Table 7. The nonlinear conditional relationship $A | X$ makes this setting more challenging, as reflected in higher baseline MSE values. The standard baselines (ERM, DRO) and importance reweighting baselines (IW-KMM, IW-Classify) all exhibit worst-case normalized MSE above 3.8, with IW methods occasionally exceeding 5.0 at larger perturbation scales. Among the pseudo-label baselines, PL-Mean+DRO is again the strongest competitor, while PL-MissForest performs notably worse in this setting, approaching the standard baselines. DRUM-Debiased (unconstrained) achieves the best worst-case MSE at smaller perturbation scales and the best mean MSE across all scales shown. A comparison among all four DRUM variants is provided in Figure 9 in Appendix C.3.

5.3 Setting III: Varying Dimension of A

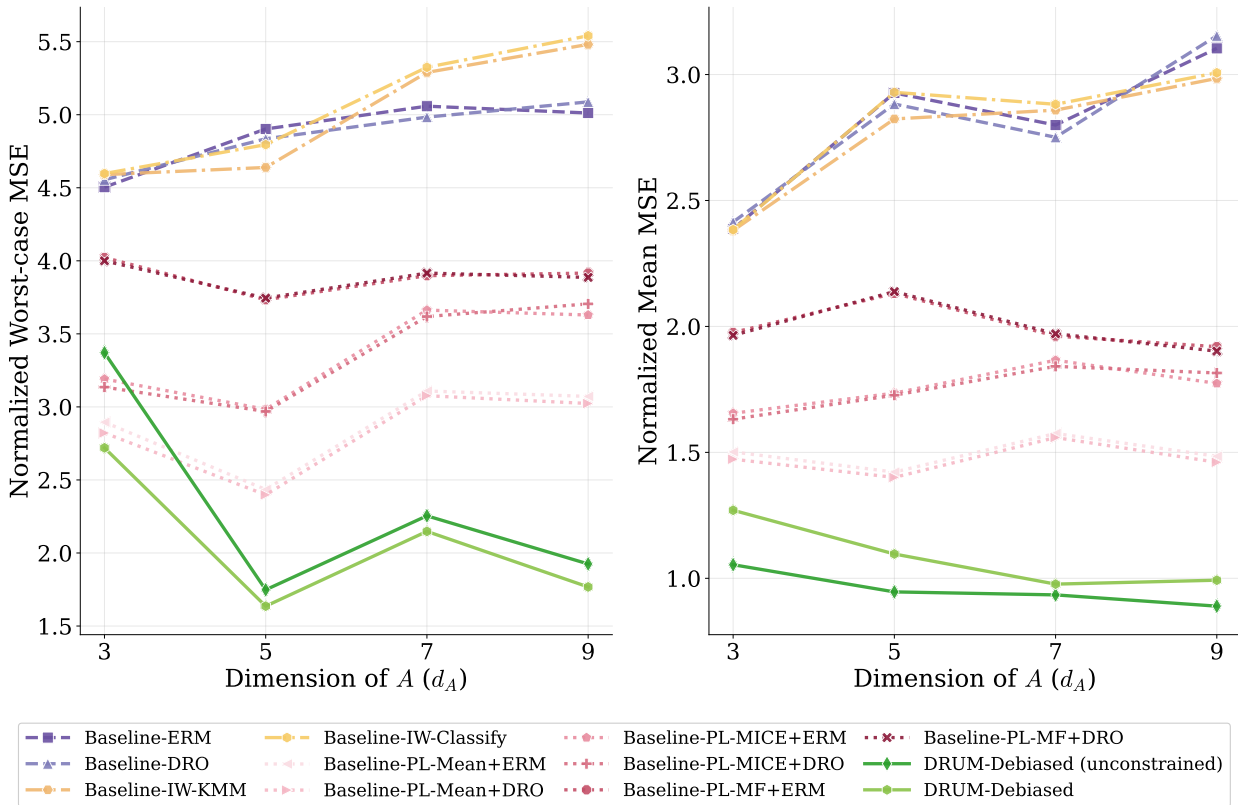


Figure 5: Worst-case and mean normalized MSE across different d_A with perturbation scales fixed at $s = 1.8$. Results are computed over 100 Monte Carlo test datasets at each scale. MSE is normalized by the source outcome variance $\widehat{\text{Var}}(Y^S)$.

We further extend Setting II to examine how performance scales with the d_A . We vary $d_A \in \{3, 5, 7, 9\}$ while keeping $d_X = 15$ fixed. To accommodate each value of d_A , the coefficient matrix $B \in \mathbb{R}^{d_X \times d_A}$ is extended by appending columns that follow the same structured sparsity pattern as Setting II (see Appendix C.1 for the full matrix). All other parameters remain identical to

Setting II. We fix the MC perturbation scale at $s = 1.8$ and evaluate each method on 100 Monte Carlo test datasets at each d_A .

Results The results of Setting III are shown in Figure 5 and Table 8. As d_A increases, the prediction problem becomes harder: more variance in Y is attributable to the unobserved A . The standard and importance weighting baselines degrade accordingly, with worst-case normalized MSE exceeding 5.0 at larger d_A . Among the pseudo-label baselines, PL-Mean+DRO is again the strongest competitor and achieves competitive worst-case MSE at several values of d_A .

DRUM-Debiased (unconstrained) achieves the best mean MSE at every d_A value shown, indicating the most accurate predictor on average. For worst-case MSE, the DRUM-Debiased variants achieve the best performance at all d_A values shown. A comparison including all four DRUM variants is provided in Figure 10 in Appendix C.4.

6 Real Data Analysis

We apply DRUM and its debiased variants to the cross-national OHCA prediction task described in Section 2, comparing against empirical risk minimization (ERM), standard DRO, importance weighting (IW-KMM, IW-Classify), and pseudo-label imputation baselines. We used the US-ROC registry as the labeled source for training $\hat{f}(X, A)$. For the target population, Singapore shared covariates were used as unlabeled data for generator training. Because DRUM is designed for settings where target labels may be unavailable, no target outcome labels were used in the estimation of \hat{f} , generator training, or bias correction. In this retrospective evaluation, a small labeled Singapore validation subset was used only for final hyperparameter selection (Appendix C.5, Table 11); the remaining Singapore observations were held out for evaluation. Sensitivity analyses showed that performance was stable across a broad range of hyperparameter values, supporting the use of default choices when labeled target data are unavailable. The Japan and Korea cohorts were used solely for independent external validation, and no data from these sites entered any training or selection step.

Figure 6 presents Brier scores across all Asian populations. The standard baselines (ERM, DRO) and importance weighting baselines (IW-KMM, IW-Classify) perform similarly, suggesting that correcting the marginal covariate shift in $P(X)$ alone provides limited benefit when the primary challenge is unobserved prehospital care variables. The pseudo-label baselines show marginal improvement by leveraging unlabeled target data, but remain substantially above the DRUM-Debiased variants. To avoid visual clutter, the pseudo-label baselines in Figure 6 report only the oracle-best imputation method per site (selecting among Mean, MICE, and MissForest separately for each population), which favors these baselines by giving them the benefit of hindsight. All six pseudo-label variants are shown individually in Figure 11 in the Appendix. DRUM-Debiased (unconstrained) achieves the lowest Brier score on the target population (Singapore) and both external sites, with statistically significant improvement over the best baseline on each site.

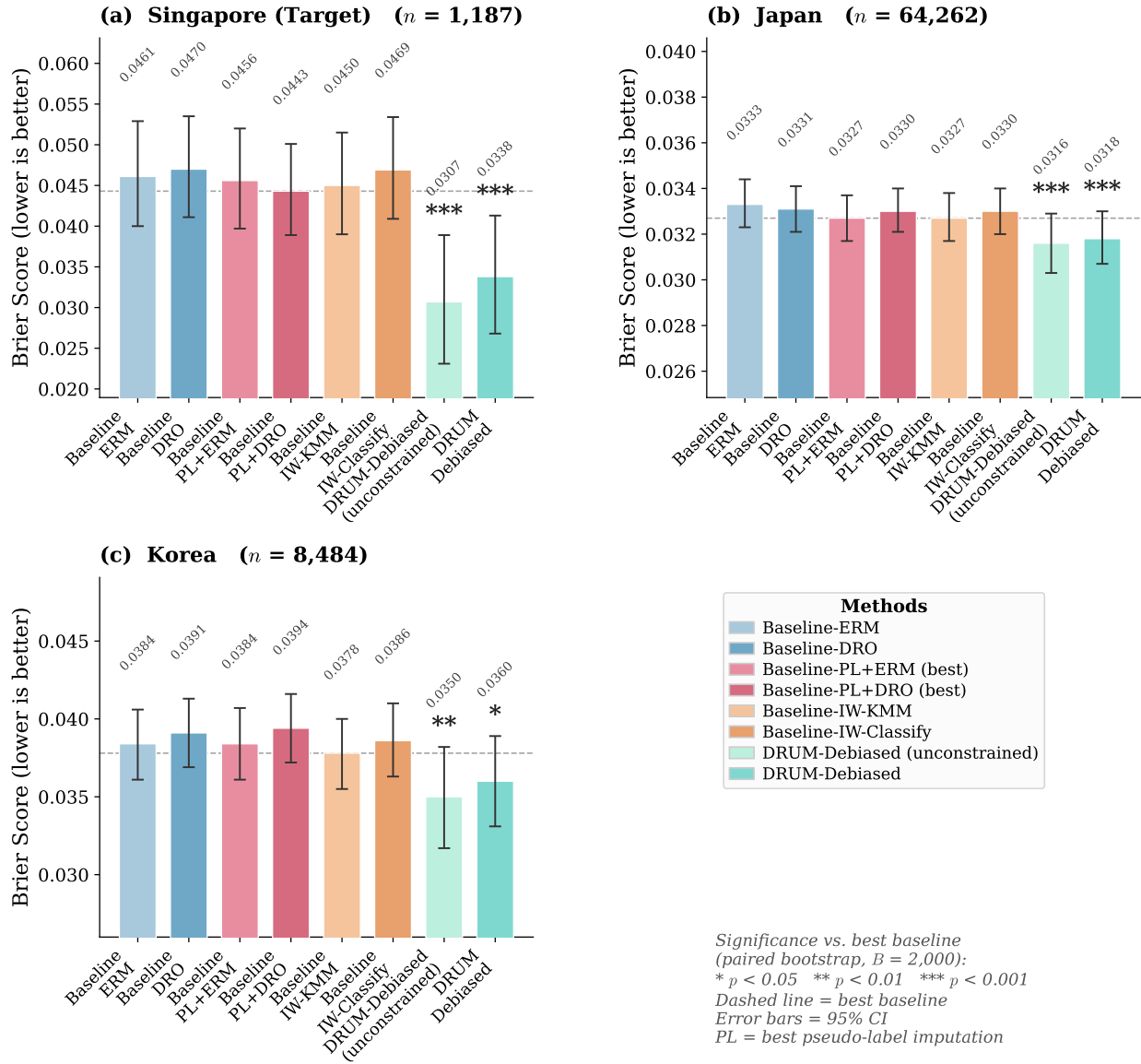


Figure 6: Brier scores across three OHCA populations. Bars show Brier scores (lower is better) with 95% bootstrap CIs. Panel (a): target population (Singapore); panels (b)–(c): external validation sites. Dashed line = best baseline. Stars: paired bootstrap significance vs. best baseline ($B = 2,000$). PL = best pseudo-label imputation per site.

Figure 7 shows calibration plots across all sites. Baseline methods trained on US source data systematically over-predict good neurological outcome probabilities when applied to Asian populations, with predicted probabilities extending well beyond observed event rates. This reflects the large difference in outcome prevalence between the US source (19.3%) and Asian populations (3–5%). The DRUM-Debiased variants track closer to the diagonal, indicating that explicitly accounting for uncertainty in unobserved prehospital care variables produces better-calibrated predictions under distribution shift. DRUM-Debiased (unconstrained) also achieves the lowest expected

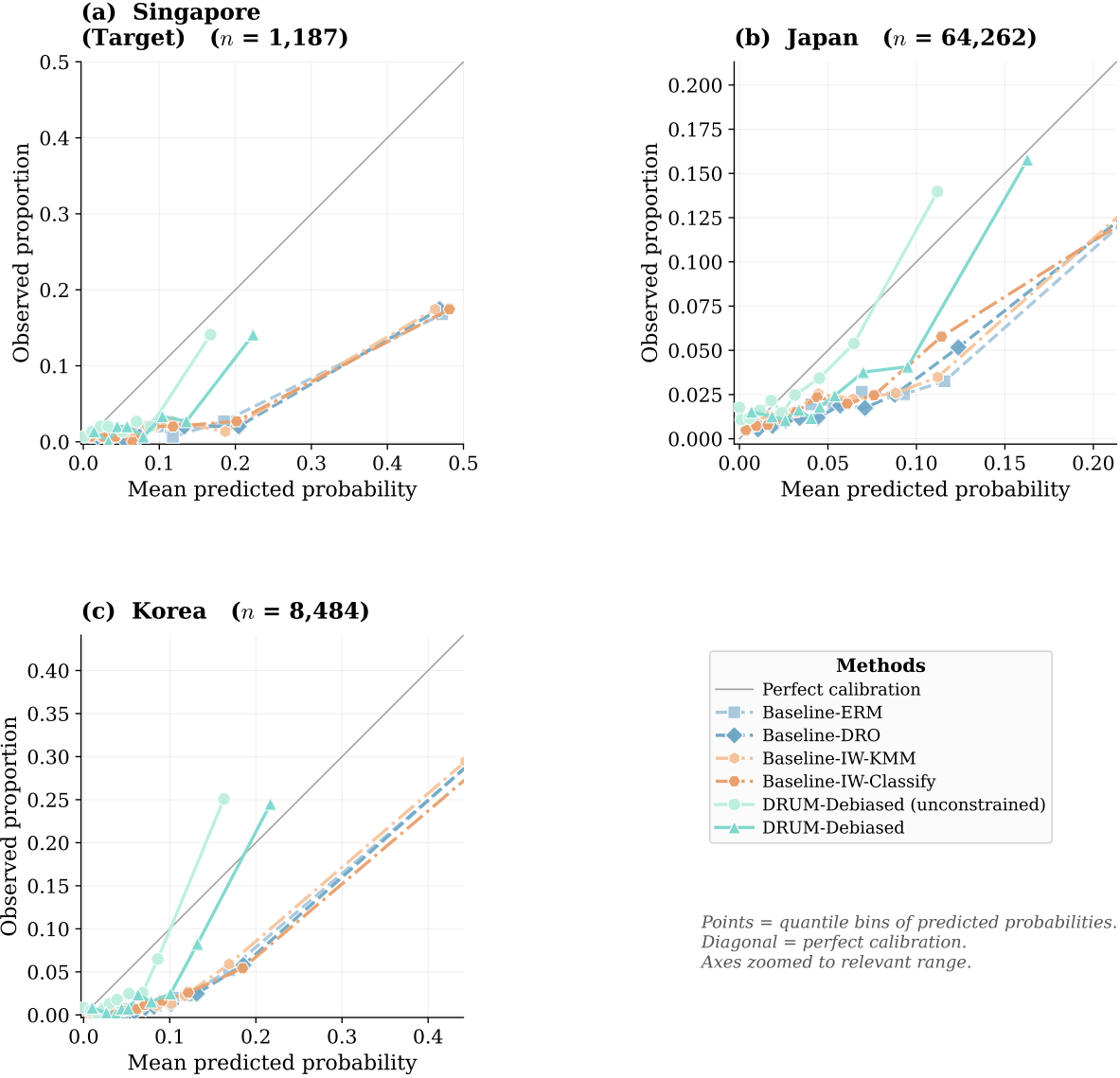


Figure 7: Calibration plots across three OHCA populations. Points show mean predicted probability vs observed proportion in quantile bins (axes truncated for visibility). Diagonal = perfect calibration.

calibration error (ECE) across all three sites (Table 2).

To evaluate clinical utility under resource constraints, Table 3 reports classification performance at fixed probability cutoffs $t \in \{0.03, 0.05, 0.10, 0.15\}$. These cutoffs span the observed and published range of favorable neurological outcome rates in Asia-Pacific OHCA cohorts (Ong et al., 2011; Doctor et al., 2017) and correspond to clinically interpretable triage rules: classify a patient as high priority when the predicted probability of favorable outcome exceeds a prespecified risk threshold. The higher precision and specificity of DRUM-Debiased (unconstrained) indicate that its calibrated probabilities produce fewer but more reliable positive classifications, a desirable prop-

Table 2: Expected calibration error (ECE) across three OHCA populations. Lower is better. ECE computed using quantile binning consistent with Figure 7 (10 bins). Best baseline selected per site from all 10 baselines (oracle selection). Bold indicates the lowest ECE at each site. 95% bootstrap CIs ($B = 2,000$).

Method	Singapore (Target)	Japan	Korea
Best baseline*	0.093 (0.083, 0.104)	0.030 (0.029, 0.032)	0.067 (0.063, 0.071)
DRUM (unconstrained)	0.119 (0.109, 0.129)	0.094 (0.093, 0.095)	0.111 (0.107, 0.115)
DRUM	0.101 (0.091, 0.112)	0.041 (0.039, 0.042)	0.077 (0.073, 0.080)
DRUM-Debiased (unconstrained)	0.025 (0.020, 0.036)	0.011 (0.010, 0.012)	0.026 (0.022, 0.030)
DRUM-Debiased	0.054 (0.045, 0.064)	0.022 (0.021, 0.024)	0.040 (0.037, 0.045)

*Best baseline: IW-KMM (Singapore), PL-MICE+ERM (Japan, Korea).

erty when downstream interventions are scarce, costly, or clinically intensive. Additional evaluation metrics and full method comparisons are reported in Appendix C.5, including Brier scores for all methods (Figure 11), calibration plots (Figure 12), AUROC and AUPRC as secondary discrimination analyses (Figures 13–14), and expanded fixed-cutoff classification results (Table 12).

Taken together, these results are consistent with the hypothesis that unobserved prehospital-care covariates contribute to cross-national miscalibration, though because A is not observed in the PAROS sites, the target $A|X$ distribution cannot be directly identified. Regardless of the underlying mechanism, DRUM’s worst-case formulation yields well-calibrated predictions across deployment sites without requiring assumptions about the target distribution of A .

7 Discussion

This study addresses unsupervised transfer learning under structural covariate missingness, where outcome-relevant variables are available during source training but absent at deployment and target labels are unavailable. Across simulations and cross-national OHCA prediction, DRUM improved robust prediction performance by using rich source covariates to learn the outcome mechanism while producing a deployable predictor that depends only on shared covariates X . In the real-data application, DRUM’s advantage is concentrated in calibration-sensitive metrics (Brier score, ECE, and fixed-threshold precision/F1), which is expected given that the worst-case objective penalizes squared prediction error rather than ranking inversions. AUROC and AUPRC, reported in Appendix C.5, show smaller gains, consistent with DRUM targeting probability calibration rather than global discrimination.

The bias-corrected DRUM variants consistently outperform their plug-in counterparts across all simulation settings and deployment sites, as measured by mean squared error, Brier score, and calibration error. However, the degree of improvement depends on the quality of density ratio estimation: when the source and target-generator distributions overlap substantially, the density

Table 3: Classification performance at fixed probability cutoffs across three OHCA populations. Best baseline is selected per site from all 10 baselines. Bold indicates the best value across all methods at each site.

t	Method	F1 Score			Precision			Specificity		
		<i>Singapore</i>	<i>Japan</i>	<i>Korea</i>	<i>Singapore</i>	<i>Japan</i>	<i>Korea</i>	<i>Singapore</i>	<i>Japan</i>	<i>Korea</i>
0.03	Best BL*	0.084	0.115	0.110	0.044	0.062	0.058	0.279	0.528	0.305
	DRUM (unconstrained)	0.064	0.067	0.080	0.033	0.034	0.042	0.000	0.000	0.000
	DRUM	0.075	0.094	0.095	0.039	0.050	0.050	0.182	0.373	0.176
	DRUM-Debiased (unconstrained)	0.084	0.123	0.133	0.045	0.068	0.071	0.422	0.655	0.472
	DRUM-Debiased	0.071	0.084	0.095	0.037	0.044	0.050	0.164	0.315	0.186
0.05	Best BL*	0.096	0.140	0.135	0.051	0.074	0.073	0.413	0.658	0.455
	DRUM (unconstrained)	0.064	0.067	0.080	0.033	0.034	0.042	0.003	0.004	0.001
	DRUM	0.088	0.115	0.114	0.046	0.062	0.060	0.316	0.550	0.331
	DRUM-Debiased (unconstrained)	0.105	0.156	0.180	0.056	0.090	0.100	0.564	0.792	0.660
	DRUM-Debiased	0.089	0.122	0.129	0.047	0.067	0.069	0.380	0.626	0.445
0.10	Best BL*	0.134	0.213	0.214	0.073	0.128	0.121	0.633	0.841	0.711
	DRUM (unconstrained)	0.070	0.084	0.091	0.036	0.044	0.048	0.149	0.288	0.135
	DRUM	0.112	0.165	0.173	0.060	0.095	0.096	0.564	0.775	0.612
	DRUM-Debiased (unconstrained)	0.207	0.221	0.354	0.128	0.208	0.253	0.875	0.968	0.924
	DRUM-Debiased	0.127	0.200	0.229	0.070	0.126	0.134	0.687	0.878	0.773
0.15	Best BL*	0.204	0.285	0.333	0.118	0.208	0.210	0.814	0.939	0.868
	DRUM (unconstrained)	0.103	0.134	0.147	0.055	0.075	0.080	0.518	0.711	0.540
	DRUM	0.171	0.261	0.285	0.097	0.175	0.171	0.764	0.914	0.822
	DRUM-Debiased (unconstrained)	0.216	0.165	0.379	0.167	0.279	0.352	0.948	0.989	0.967
	DRUM-Debiased	0.222	0.249	0.356	0.140	0.233	0.257	0.888	0.969	0.927

*Best baseline selected per site from ERM, DRO, IW-KMM, IW-Classify, and six PL variants.

Cutoff t : classify $\hat{Y} = 1$ if predicted probability $\geq t$.

ratio $\hat{\omega}$ is well-estimated and the correction is effective; when the distributions diverge more sharply, the correction can be less stable. The choice between DRUM and DRUM (unconstrained) should reflect domain knowledge about the plausibility of the source conditional $A | X$: practitioners with confidence that the source $A | X$ is approximately valid in the target should prefer DRUM with a moderate δ , while those facing entirely unknown deployment conditions should default to DRUM (unconstrained).

The proposed framework addresses a recurring problem in clinical prediction: models developed in high-resource research settings (Van Zyl et al., 2021) frequently rely on measurements that are unavailable at deployment sites due to differences in clinical infrastructure, data collection protocols, or resource constraints. The OHCA application illustrates this concretely with prehospital care

variables, but the same structural pattern arises whenever prediction models cross institutional or regional boundaries with heterogeneous data collection capabilities. DRUM provides a principled alternative to the two dominant current approaches: restricting deployment to sites that mirror the source infrastructure, or discarding the covariates that are unavailable. The former limits the reach of well-developed models, while the latter sacrifices predictive performance by ignoring information learned from the source.

More broadly, DRUM is directly applicable beyond the structurally missing covariate setting studied in this work, as any problem where predictive covariates are available during training but absent or restricted at deployment shares the same mathematical structure. In pharmaceutical stability prediction, for example, models trained under controlled laboratory conditions with environmental factors such as temperature or humidity (Guideline et al., 2003) must generalize to real-world settings where these factors shift unpredictably; here A represents covariates that are observed but *unstable* rather than absent, and the robustness parameter δ controls the degree of protection against environmental variation. In algorithmic fairness (Li et al., 2025b,d), protected attributes such as race or sex may be available during training but impermissible to use at deployment; here A represents covariates that are observed but *deliberately excluded*, and worst-case optimization over their conditional distribution may reduce dependence on the realized distribution of protected attributes at deployment.

Limitations and future directions. Several directions for extension remain. First, the current generator-based parameterization assumes continuous unstable covariates A . When A is high-dimensional, discrete or mixed-type, extensions such as Gumbel-Softmax relaxations (Jang et al., 2017) or hybrid architectures may be required. Second, the framework currently assumes a single source population; when multiple source sites have heterogeneous conditional distributions, integrating DRUM into a federated learning framework (Li et al., 2024) that leverages multiple sources while preserving data privacy remains an open direction. Third, while the present derivation focuses on squared-error and cross-entropy losses, extending DRUM to structured outcomes such as time-to-event data (Wang et al., 2026), or multi-class and ordinal outcomes, would broaden its applicability beyond the binary and continuous settings considered in this work.

Acknowledgments

Pan-Asian Resuscitation Outcomes Study Clinical Research Network (PAROS CRN).

Participating Site Investigators: K Kajino (Kansai Medical University, Osaka, Japan), T Nishiuchi (Graduate School of Medical Sciences and Faculty of Medicine, Kindai University, Osaka, Japan); T Tagami (Nippon Medical School Tama Nagayama Hospital, Tokyo, Japan); KJ Hong (Seoul National University Hospital, Seoul, South Korea); JH Park (Seoul National University Hospital, Seoul, South Korea); KW Lee (Keimyung University Dongsan Hospital, Daegu, South Korea); WC Cha (Samsung Medical Center, Seoul, South Korea); KJ Song (Boramae Medical Center, Seoul, South Korea); YS Ro (Seoul National University Hospital, Seoul, South Korea); JY Kim (Seoul National University Hospital, Seoul, South Korea); YJ Lee (Seoul National University Hospital, Seoul, South Korea); S Moon (Korea University Ansan Hospital, Gyeonggi, South Korea); DA Nguyen (Bach Mai Hospital, Hanoi, Viet Nam); QTA Hoang (Hue Central General Hospital, Hue, Viet Nam); TT Tra (Cho Ray Hospital, Ho Chi Minh, Vietnam); PD Quyet (115 Emergency Center, Ho Chi Minh, Viet Nam); CQ Luong (Bach Mai Hospital, Hanoi, Viet Nam); D Pflug (Singapore Civil Defence Force, Singapore); BSH Leong (National University Hospital, Singapore); WM Ng (Ng Teng Fong General Hospital, Singapore); NE Doctor (Sengkang General Hospital, Singapore); MYC Chia (Tan Tock Seng Hospital, Singapore); HN Gan (Changi General Hospital, Singapore); L Tiah (Changi General Hospital, Singapore); WL Tay (Ng Teng Fong General Hospital, Singapore); SY Low (Sengkang General Hospital, Singapore); LP Tham (KK Women's and Children's Hospital, Singapore); SL Lim (National University Heart Centre Singapore, Singapore); ES Goh (Woodlands Health, Singapore); SO Cheah (Urgent Care Clinic International, Singapore); Mao DRH (Koo Teck Puat Hospital, Singapore); YY Ng (National University Singapore, Singapore); G Nadarajan (Singapore General Hospital, Singapore); ISY Chua (Singapore General Hospital, Singapore); AFW Ho (Singapore General Hospital, Singapore); S Arulananandam (previously from Singapore Civil Defence Force, Singapore); KC Tan (previously from Singapore Civil Defence Force, Singapore); SL Chong (KK Women's and Children's Hospital, Singapore).

The authors would like to thank Ms Maeve Pek from Pre-hospital and Emergency Research Centre, Duke-NUS Medical School, Singapore; the late Ms Susan Yap from Department of Emergency Medicine, Singapore General Hospital, Singapore; Ms Noor Azuin, Ms Nurul Asyikin and Ms Liew Le Xuan from Unit for Pre-hospital Emergency Care, Singapore; Ms Charlene Ong and Ms Anju Devi from Accident & Emergency, Changi General Hospital, Singapore and Ms Woo Kai Lee from Department of Cardiology, National University Heart Centre Singapore for their contributions and support to the Singapore PAROS registry; Ms Patricia Tay from Singapore Clinical Research Institute for providing secretariat support to the PAROS CRN, and Unit for Pre-hospital Emergency Care, Singapore for facilitating/implementing the initiatives that have brought about improved response to OHCA. The authors would also like to extend their sincere gratitude to all coordinators, researchers, and EMS providers from the PAROS CRN for their invaluable support of the registry.

Ethics Statement

This study used data from two sources. The US Resuscitation Outcomes Consortium (ROC) data were approved by the National University of Singapore Institutional Review Board, which granted an exemption for this study (NUS-IRB-2023-451). The Pan-Asian Resuscitation Outcomes Study (PAROS) data were approved by the relevant ethics committees at each participating site and by the Centralized Institutional Review Board and Domain Specific Review Board for Singapore (reference numbers: 2010-270-C, C-10-545, 2013/604/C, and 2013/00929). Informed consent was waived for both datasets due to the retrospective, observational nature of the study, and all data were de-identified prior to analysis.

Data and Code Availability

The Python implementation of the proposed algorithm, along with code for reproducing the simulation studies, is available at <https://github.com/siqili0325/DRUM>. The Resuscitation Outcomes Consortium (ROC) Epistry database (Version 3, April 2011–June 2015) can be requested through the NIH website at https://biolincc.nhlbi.nih.gov/studies/roc_cardiac_epistry_3/. The PAROS dataset contains confidential information and is governed by IRB restrictions. In accordance with these policies, the data are available to qualified researchers upon reasonable request, pending approval from the PAROS governing body.

Funding

This study was supported by the Khoo Postdoctoral Fellowship Award (Duke-NUS-KPFA/2025/0081) funded by the Estate of Tan Sri Khoo Teck Puat, awarded to SL; the National Medical Research Council, Singapore, through Clinician Scientist Awards (NMRC/CSA/024/2010 and NMRC/CSA/0049/2013), and the Ministry of Health, Singapore, through the Health Services Research Grant (HSRG/0021/2012), awarded to MEHO. The funders had no role in study design, data collection, analysis, interpretation, or manuscript preparation.

Conflict of Interest

Prof Marcus EH Ong is a member of the Editorial Board of Resuscitation. Prof Marcus EH Ong reports grants from the Laerdal Foundation, Laerdal Medical, and Ramsey Social Justice Foundation for funding of the Pan-Asian Resuscitation Outcomes Study; an advisory relationship with Global Healthcare SG, a commercial entity that manufactures cooling devices. He has a licensing agreement with ZOLL Medical Corporation and patent filed (Application no: 13/047,348) for a “Method of predicting acute cardiopulmonary events and survivability of a patient.” He is also the co-founder and scientific advisor of TIIM Healthcare, a commercial entity which develops

real-time prediction and risk stratification solutions for triage. These organizations have no role in conducting this research.

References

- Bartlett, P. L., Foster, D. J., and Telgarsky, M. J. (2017). Spectrally-normalized margin bounds for neural networks. In Guyon, I., Luxburg, U. V., Bengio, S., Wallach, H., Fergus, R., Vishwanathan, S., and Garnett, R., editors, *Advances in Neural Information Processing Systems*, volume 30. Curran Associates, Inc.
- Bickel, S., Brückner, M., and Scheffer, T. (2009). Discriminative learning under covariate shift. *Journal of Machine Learning Research*, 10(9).
- Blanchet, J. and Murthy, K. R. A. (2017). Quantifying distributional model risk via optimal transport.
- Chernozhukov, V., Chetverikov, D., Demirer, M., Dufo, E., Hansen, C., Newey, W., and Robins, J. (2018). Double/debiased machine learning for treatment and structural parameters. *The Econometrics Journal*, 21(1):C1–C68.
- de Hond, A. A., Leeuwenberg, A. M., Hooft, L., Kant, I. M., Nijman, S. W., van Os, H. J., Aardoom, J. J., Debray, T. P., Schuit, E., van Smeden, M., et al. (2022). Guidelines and quality criteria for artificial intelligence-based prediction models in healthcare: a scoping review. *NPJ digital medicine*, 5(1):2.
- Doctor, N. E., Ahmad, N. S. B., Pek, P. P., Yap, S., and Ong, M. E. H. (2017). The pan-asian resuscitation outcomes study (paros) clinical research network: what, where, why and how. *Singapore medical journal*, 58(7):456.
- Duchi, J. C. and Namkoong, H. (2021). Learning models with uniform performance via distributionally robust optimization. *The Annals of Statistics*, 49(3):1378–1406.
- Esfahani, P. M. and Kuhn, D. (2017). Data-driven distributionally robust optimization using the wasserstein metric: Performance guarantees and tractable reformulations.
- Farrell, M. H., Liang, T., and Misra, S. (2021). Deep neural networks for estimation and inference. *Econometrica*, 89(1):181–213.
- Ganin, Y., Ustinova, E., Ajakan, H., Germain, P., Larochelle, H., Laviolette, F., March, M., and Lempitsky, V. (2016). Domain-adversarial training of neural networks. *Journal of machine learning research*, 17(59):1–35.
- Guideline, I. et al. (2003). Stability testing of new drug substances and products. *Q1A (R2), current step*, 4(1-24).
- Hashimoto, T. B., Srivastava, M., Namkoong, H., and Liang, P. (2018). Fairness without demographics in repeated loss minimization.

- Hoffman, J., Tzeng, E., Park, T., Zhu, J.-Y., Isola, P., Saenko, K., Efros, A., and Darrell, T. (2018). Cycada: Cycle-consistent adversarial domain adaptation. In *International conference on machine learning*, pages 1989–1998. Pmlr.
- Hornik, K., Stinchcombe, M., and White, H. (1989). Multilayer feedforward networks are universal approximators. *Neural networks*, 2(5):359–366.
- Hu, Z. and Hong, L. J. (2013). Kullback-leibler divergence constrained distributionally robust optimization. *Available at Optimization Online*, 1(2):9.
- Huang, J., Gretton, A., Borgwardt, K., Schölkopf, B., and Smola, A. (2006). Correcting sample selection bias by unlabeled data. *Advances in neural information processing systems*, 19.
- Jang, E., Gu, S., and Poole, B. (2017). Categorical reparametrization with gumble-softmax. In *International Conference on Learning Representations (ICLR 2017)*. OpenReview. net.
- Jin, Y. and Rothenhäusler, D. (2023). Modular regression: improving linear models by incorporating auxiliary data. *Journal of Machine Learning Research*, 24(351):1–52.
- Kennedy, E. H. (2023). Towards optimal doubly robust estimation of heterogeneous causal effects. *Electronic Journal of Statistics*, 17(2):3008–3049.
- Li, S., Li, X., Yu, K., Wu, Q., Miao, D., Zhu, M., Yan, M., Ke, Y., D’Agostino, D., Ning, Y., et al. (2025a). Bridging data gaps in healthcare: a scoping review of transfer learning in structured data analysis. *Health Data Science*, 5:0321.
- Li, S., Liu, M., Tian, Z., Hong, C., and Liu, N. (2025b). Robust mixture models for algorithmic fairness under latent heterogeneity. *arXiv preprint arXiv:2509.17411*.
- Li, S., Miao, D., Wu, Q., Hong, C., D’Agostino, D., Li, X., Ning, Y., Shang, Y., Wang, Z., Liu, M., et al. (2024). Federated learning in healthcare: A benchmark comparison of engineering and statistical approaches for structured data analysis. *Health Data Science*, 4:0196.
- Li, S., Okada, Y., Gu, W., Chen, M. H., Do, S. N., Pham, Q. D., Hoang, Q. T., Ong, M. E. H., and Liu, N. (2025c). Leveraging ai and transfer learning to enhance out-of-hospital cardiac arrest outcome prediction in diverse setting. *npj Digital Medicine*, 8(1):716.
- Li, S., Wu, Q., Zhou, D., Li, X., Miao, D., Hong, C., Gu, W., Shang, Y., Okada, Y., Chen, M. H., et al. (2025d). Fairfml: Fair federated machine learning with a case study on reducing gender disparities in cardiac arrest outcome prediction. *npj Health Systems*, 2(1):29.
- Li, Y., Wei, Y., and Liu, M. (2025e). Adaptive learning with blockwise missing and semi-supervised data.
- Little, R. J. and Rubin, D. B. (2019). *Statistical analysis with missing data*. John Wiley & Sons.

- Long, M., Cao, Y., Wang, J., and Jordan, M. (2015). Learning transferable features with deep adaptation networks. In *International conference on machine learning*, pages 97–105. PMLR.
- National Heart, Lung, and Blood Institute (2024). Resuscitation Outcomes Consortium (ROC) Cardiac Epidemiologic Registry (Cardiac Epistry) Version 3. BioLINCC (Biologic Specimen and Data Repository Information Coordinating Center). Accession Number: HLB01801818a. Study period: April 2011 – June 2015.
- Nolan, J. P., Berg, R. A., Andersen, L. W., Bhanji, F., Chan, P. S., Donnino, M. W., Lim, S. H., Ma, M. H.-M., Nadkarni, V. M., Starks, M. A., et al. (2019). Cardiac arrest and cardiopulmonary resuscitation outcome reports: update of the utstein resuscitation registry template for in-hospital cardiac arrest: a consensus report from a task force of the international liaison committee on resuscitation (american heart association, european resuscitation council, australian and new zealand council on resuscitation, heart and stroke foundation of canada, interamerican heart foundation, resuscitation council of southern africa, resuscitation council of asia). *Circulation*, 140(18):e746–e757.
- Ong, M. E. H., Shin, S. D., Tanaka, H., Ma, M. H.-M., Khruerkarnchana, P., Hisamuddin, N., Atilla, R., Middleton, P., Kajino, K., Leong, B. S.-H., et al. (2011). Pan-asian resuscitation outcomes study (paros): rationale, methodology, and implementation. *Academic Emergency Medicine*, 18(8):890–897.
- Ribeiro, M. T., Singh, S., and Guestrin, C. (2016). ” why should i trust you?” explaining the predictions of any classifier. In *Proceedings of the 22nd ACM SIGKDD international conference on knowledge discovery and data mining*, pages 1135–1144.
- Rotnitzky, A., Smucler, E., and Robins, J. M. (2021). Characterization of parameters with a mixed bias property. *Biometrika*, 108(1):231–238.
- Sagawa, S., Koh, P. W., Hashimoto, T. B., and Liang, P. (2020). Distributionally robust neural networks for group shifts: On the importance of regularization for worst-case generalization.
- Shen, X. and Meinshausen, N. (2024). Engression: extrapolation through the lens of distributional regression. *Journal of the Royal Statistical Society Series B: Statistical Methodology*, page qkae108.
- Shimodaira, H. (2000). Improving predictive inference under covariate shift by weighting the log-likelihood function. *Journal of statistical planning and inference*, 90(2):227–244.
- Sion, M. (1958). On general minimax theorems. *Pacific Journal of Mathematics*, 8:171–176.
- Steinwart, I., Hush, D. R., Scovel, C., et al. (2009). Optimal rates for regularized least squares regression. In *COLT*, pages 79–93.
- Sugiyama, M., Krauledat, M., and Müller, K.-R. (2007). Covariate shift adaptation by importance weighted cross validation. *Journal of Machine Learning Research*, 8(5).

- Székely, G. J. and Rizzo, M. L. (2013). Energy statistics: A class of statistics based on distances. *Journal of statistical planning and inference*, 143(8):1249–1272.
- Van der Vaart, A. W. (2000). *Asymptotic statistics*, volume 3. Cambridge university press.
- Van Zyl, C., Badenhorst, M., Hanekom, S., and Heine, M. (2021). Unravelling ‘low-resource settings’: a systematic scoping review with qualitative content analysis. *BMJ global health*, 6(6).
- Wager, S. and Athey, S. (2018). Estimation and inference of heterogeneous treatment effects using random forests. *Journal of the American Statistical Association*, 113(523):1228–1242.
- Wahl, B., Cossy-Gantner, A., Germann, S., and Schwalbe, N. R. (2018). Artificial intelligence (ai) and global health: how can ai contribute to health in resource-poor settings? *BMJ global health*, 3(4):e000798.
- Wainwright, M. J. (2019). *High-dimensional statistics: A non-asymptotic viewpoint*, volume 48. Cambridge university press.
- Wang, Z., Li, S., Ong, M. E. H., and Liu, N. (2026). Communication-efficient federated risk difference estimation for time-to-event clinical outcomes. *arXiv preprint arXiv:2601.14609*.
- Weiss, K., Khoshgoftaar, T. M., and Wang, D. (2016). A survey of transfer learning. *Journal of Big data*, 3(1):9.
- Xiang, S., Yuan, L., Fan, W., Wang, Y., Thompson, P. M., Ye, J., Initiative, A. D. N., et al. (2014). Bi-level multi-source learning for heterogeneous block-wise missing data. *NeuroImage*, 102:192–206.
- Xue, F. and Qu, A. (2021). Integrating multisource block-wise missing data in model selection. *Journal of the American Statistical Association*, 116(536):1914–1927.
- Yang, C., Kors, J. A., Ioannou, S., John, L. H., Markus, A. F., Rekkas, A., de Ridder, M. A., Seinen, T. M., Williams, R. D., and Rijnbeek, P. R. (2022). Trends in the conduct and reporting of clinical prediction model development and validation: a systematic review. *Journal of the American Medical Informatics Association*, 29(5):983–989.
- Yang, J., Dung, N. T., Thach, P. N., Phong, N. T., Phu, V. D., Phu, K. D., Yen, L. M., Thy, D. B. X., Soltan, A. A., Thwaites, L., et al. (2024). Generalizability assessment of ai models across hospitals in a low-middle and high income country. *Nature Communications*, 15(1):8270.
- Yu, G., Li, Q., Shen, D., and Liu, Y. (2020). Optimal sparse linear prediction for block-missing multi-modality data without imputation. *Journal of the American Statistical Association*, 115(531):1406–1419.
- Yuan, L., Wang, Y., Thompson, P. M., Narayan, V. A., Ye, J., Initiative, A. D. N., et al. (2012). Multi-source feature learning for joint analysis of incomplete multiple heterogeneous neuroimaging data. *NeuroImage*, 61(3):622–632.

A Theoretical Justification and Proofs

A.1 Derivation of the Bias-Corrected Estimator

The bias reduction can be seen from the following expansion. Writing $\hat{f} = \bar{f} + (\hat{f} - \bar{f})$, the plug-in prediction decomposes as $\hat{m}(x) = m(x) + \Delta(x)$, where

$$m(x) = \mathbb{E}_{A \sim \mathbb{P}_{A|X}}[\bar{f}(x, A)], \quad \Delta(x) = \mathbb{E}_{A \sim \mathbb{P}_{A|X}}[(\hat{f} - \bar{f})(x, A)].$$

Since the generator is trained to minimize $\mathbb{E}_X[\hat{m}(X)^2]$ as in (8), expanding $(m(x) + \Delta(x))^2$ yields:

$$\mathbb{E}_X[\hat{m}(X)^2] = \underbrace{\mathbb{E}_X[m(X)^2]}_{\text{true objective}} + \underbrace{2\mathbb{E}_X[m(X) \cdot \Delta(X)]}_{\text{first-order in } (\hat{f} - \bar{f})} + \underbrace{\mathbb{E}_X[\Delta(X)^2]}_{\text{second-order}}. \quad (18)$$

The first-order bias is the middle term $2\mathbb{E}_X[m(X) \cdot \Delta(X)]$, which is $O(\|\hat{f} - \bar{f}\|)$.

To cancel this term, we introduce the density ratio $\omega(x, a) = \mathbb{Q}_{X,A}^{\bar{g}}(x, a) / \mathbb{P}_{X,A}^S(x, a)$, where \bar{g} is a fixed preliminary generator from uncorrected DRUM (denoted \hat{g} in Section 4.4). At the population level, the debiased loss takes the oracle form:

$$\mathcal{L}^{\text{deb}} = \mathbb{E}_{X \sim \mathbb{Q}_X}[\hat{m}(X)^2] + 2\mathbb{E}_{(X,A) \sim \mathbb{P}^S}[\omega(X, A) m(X) (Y - \hat{f}(X, A))]. \quad (19)$$

Since $m(X)$ is unknown, the implementable cross-fitted version replaces $m(X)$ with the plug-in estimate $\hat{\mu}_{\hat{\theta}}^{(-k)}(X)$ from the preliminary generator (Eq. (27)).

At the population level where $\hat{f} = \bar{f}$, the correction term vanishes by the tower property: since $\mathbb{E}[Y - \bar{f}(X, A) | X, A] = 0$, we have

$$\mathbb{E}_{\mathbb{P}^S}[\omega(X, A) m(X) (Y - \bar{f}(X, A))] = 0,$$

so the correction does not change the population minimizer. However, at the empirical level where \bar{f} is replaced by \hat{f} , the residual $\mathbb{E}[Y - \hat{f}(X, A) | X, A] = \bar{f}(X, A) - \hat{f}(X, A) \neq 0$, and the correction term becomes nonzero in a way that exactly cancels the first-order bias $2\mathbb{E}_X[m(X) \cdot \Delta(X)]$ from the plug-in expansion. The detailed cancellation argument, which uses the importance weighting identity $\mathbb{E}_{\mathbb{P}^S}[\omega \cdot h] = \mathbb{E}_{\mathbb{Q}^g}[h]$ to relate the correction term back to the first-order bias, is given in the proof of Theorem 3.

We note that our debiased estimator requires both \hat{f} and $\hat{\omega}$ to be consistent, unlike classical doubly robust estimators for average treatment effects. However, neither needs to converge at the parametric \sqrt{n} rate individually: by Corollary 1, the parametric rate is achieved whenever $\phi_f + \phi_\omega > 1/2$ (Rotnitzky et al., 2021).

The density ratio ω is estimated via probabilistic classification: pool source data $(X_i, A_i, S_i = 1)$ with synthetic target data $(X_j, \hat{g}(\cdot, \epsilon_j), S_j = 0)$ and train a classifier $\hat{p}(S = 1 | X, A)$; the density ratio is $\hat{\omega} = (1 - \hat{p})/\hat{p}$.

A.2 Theoretical Results

We first introduce additional assumptions and conditions.

Assumption 1 (Domain and Generator Regularity). We impose the following conditions:

- (i) $\mathcal{A} \subset \mathbb{R}^{d_A}$ is compact and convex;
- (ii) The generator parameter spaces $\Theta, \Phi \subset \mathbb{R}^p$ are compact;
- (iii) The generators g_θ, g_ϕ are measurable, and continuous in their parameters for almost every input.

Assumption 2 (Regularity of Conditional Mean and Generator). We impose the following regularity conditions on \bar{f} and g_θ :

- (i) The conditional mean function $\bar{f} : \mathbb{R}^{d_X} \times \mathbb{R}^{d_A} \rightarrow \mathbb{R}$ is bounded ($\sup_{x,a} |\bar{f}(x,a)| \leq M < \infty$) and Lipschitz continuous in a : there exists $L_f > 0$ such that

$$|\bar{f}(x, a_1) - \bar{f}(x, a_2)| \leq L_f \|a_1 - a_2\| \quad \text{for all } x, a_1, a_2.$$

- (ii) The generator g_θ is Lipschitz continuous in θ : there exists a measurable function $\ell(\epsilon)$ with $\mathbb{E}[\ell(\epsilon)^2] < \infty$ such that

$$\|g_{\theta_1}(\epsilon) - g_{\theta_2}(\epsilon)\| \leq \ell(\epsilon) \|\theta_1 - \theta_2\| \quad \text{for all } \theta_1, \theta_2 \in \Theta \text{ and a.e. } \epsilon.$$

Assumption 3 (Nuisance Estimator Quality). The nuisance estimators \hat{f} and $\hat{\omega}$ satisfy, as $n, N \rightarrow \infty$:

- (i) $\|\hat{\omega} - \omega\|_{L^2(P)} = O_P(n^{-\phi_\omega})$ for some $\phi_\omega > 0$ (convergence rate of classification model)
- (ii) $\|\hat{f} - \bar{f}\|_\infty = O_P(n^{-\phi_f})$ for some $\phi_f > 0$ (convergence rate of outcome model)
- (iii) $\sqrt{N} \cdot \|\hat{f} - \bar{f}\|_\infty \cdot \|\hat{\omega} - \omega\|_{L^2(P)} \xrightarrow{P} 0$ (rate condition)

Remark 1. Conditions (i)–(ii) are standard consistency requirements in the semiparametric inference literature (Chernozhukov et al., 2018; Kennedy, 2023). Condition (iii) requires the product of the two nuisance estimation errors to be $o(N^{-1/2})$, which is satisfied whenever $\phi_f + \phi_\omega > 1/2$. Under appropriate smoothness and dimensionality conditions, individual rates of $n^{-1/4}$ or faster are achieved by deep neural networks (Farrell et al., 2021), random forests (Wager and Athey, 2018), and kernel methods (Steinwart et al., 2009). For example, if $\|\hat{f} - \bar{f}\| = O_P(n^{-1/4})$ and $\|\hat{\omega} - \omega\| = O_P(n^{-1/4} + N^{-1/4})$, then

$$\sqrt{N} \cdot n^{-1/4} \cdot (n^{-1/4} + N^{-1/4}) = N^{1/2} n^{-1/2} + N^{1/4} n^{-1/4} \rightarrow 0$$

whenever $N = o(n)$. When $N > n$ as in the Japan external validation cohort in our study, the convergence rate is dominated by the source nuisance estimation terms $n^{-\phi_f}$ and $n^{-\phi_\omega}$ and the $N^{-1/2}$ sampling term becomes negligible.

Both conditions in Assumption 2 are standard and mild in practice. Condition (i) strengthens the continuity requirement of the earlier version of this assumption (Lipschitz implies continuous). Condition (ii) holds for neural networks with bounded weights, since the Lipschitz constant of a composition of Lipschitz functions is bounded by the product of the individual Lipschitz constants (Bartlett et al., 2017); weight decay regularization, used in our training procedures, ensures the weights remain bounded. Note that Condition (ii) strengthens the continuity requirement in Assumption 1 (iii), replacing continuity of $g_\theta(\epsilon)$ in θ with Lipschitz continuity.

When multiple minimizers exist, the robust predictor $m^*(x)$ may depend on the choice of g^* . In practice, gradient-based optimization selects one such minimizer. Our consistency results (Theorem 1) hold for any sequence of estimators converging to any minimizer.

Having established existence (Theorem 3.2), we now show that the empirical minimizer converges to a population minimizer, and characterize its rate. In Theorems 1–3, θ denotes generator parameters generically; the results apply to both the unconstrained ($g_\theta(\epsilon)$) and conditional ($g_\phi(x, \epsilon)$) parameterizations, with Θ representing the relevant compact parameter space in each case.

Theorem 1 (Convergence of Optimal Loss Value). Define the population and empirical objectives:

$$\mathcal{L}(\theta) = \mathbb{E}_{X \sim \mathbb{Q}_X} [\mathbb{E}_\epsilon [\bar{f}(X, g_\theta(\epsilon))]]^2 \quad (20)$$

$$\hat{\mathcal{L}}(\theta) = \frac{1}{N} \sum_{j=1}^N \left[\frac{1}{L} \sum_{l=1}^L \hat{f}(X_j, g_\theta(\epsilon_{jl})) \right]^2 \quad (21)$$

Let $\theta^* \in \arg \min_{\theta \in \Theta} \mathcal{L}(\theta)$ and $\hat{\theta} \in \arg \min_{\theta \in \Theta} \hat{\mathcal{L}}(\theta)$. Under Assumptions 1 and 2, as $n, N, L \rightarrow \infty$:

$$\mathcal{L}(\hat{\theta}) \xrightarrow{P} \mathcal{L}(\theta^*) \quad (22)$$

The following result refines the consistency guarantee by providing explicit convergence rates.

Theorem 2 (Convergence Rate of Optimal Loss Value). Under the conditions of Theorem 1 and Assumption 3, as $n, N \rightarrow \infty$, with L sufficiently large:

$$|\mathcal{L}(\hat{\theta}) - \mathcal{L}(\theta^*)| = O_P(n^{-\phi_f} + N^{-1/2}). \quad (23)$$

The rate consists of two terms: $n^{-\phi_f}$ from estimating \bar{f} using source data, and $N^{-1/2}$ from the finite target sample. The Monte Carlo approximation of $\mathbb{E}_\epsilon [\bar{f}(X, g_\theta(\epsilon))]$ using L draws introduces an additional $O(L^{-1})$ bias. While increasing L reduces this approximation error, it also increases the computational cost of evaluating $\hat{\mathcal{L}}(\theta)$ and its gradients, since each evaluation requires $N \times L$ forward passes through \hat{f} . Empirically, L could be fine-tuned as a hyperparameter; our experiments show that $L \leq 50$ provides a good balance between approximation accuracy and computational efficiency.

We introduce additional conditions first.

Assumption 4 (Overlap and Bounded Density Ratio). There exists a constant $M_\omega < \infty$ such that:

(i) $\|\omega\|_\infty \leq M_\omega$ (population overlap)

(ii) $\|\hat{\omega}\|_\infty \leq M_\omega$ (a.s.) (bounded estimator)

(ii) is satisfied when the density ratio estimator is clipped, i.e., $\hat{\omega}(x, a) \leftarrow \min(\hat{\omega}(x, a), M_\omega)$. In Algorithm 4, weights are clipped and then normalized to unit mean within each fold. The condition holds for each cross-fitting fold, i.e., for all $\hat{\omega}^{(-k)}$, $k = 1, \dots, K$.

Theorem 3 (Bias Reduction of the Debiased Objective). Under Assumptions 3 and 4, for any fixed generator $g \in \mathcal{G}$, the cross-fitted debiased loss (19) satisfies:

$$|\mathcal{L}^{\text{deb}}(\hat{\theta}) - \mathcal{L}(\theta^*)| = O_P\left(n^{-2\phi_f} + n^{-\phi_f} \cdot N^{-\phi_\omega} + N^{-1/2}\right) \quad (24)$$

The bound consists of three terms: $n^{-2\phi_f}$ from the squared estimation error of \bar{f} , $n^{-\phi_f} \cdot N^{-\phi_\omega}$ from the product of the two nuisance estimation errors, and $N^{-1/2}$ from the finite target sample. When $N \asymp n$, the bound simplifies to $O_P(n^{-(\phi_f + \phi_\omega)} + n^{-1/2})$, since $n^{-2\phi_f} \leq n^{-(\phi_f + \phi_\omega)}$ when $\phi_f \geq \phi_\omega$.

Corollary 1 (Parametric rate under product-of-rates condition). If $\phi_f + \phi_\omega > \frac{1}{2}$ and $n^{-2\phi_f} = O(N^{-1/2})$ (satisfied, e.g., when $N \asymp n$), then

$$\mathcal{L}(\hat{\theta}^{\text{deb}}) - \mathcal{L}(\theta^*) = O_P(N^{-1/2}). \quad (25)$$

Remark 2. Table 4 compares the plug-in (Theorem 2) and debiased (Theorem 3) rates under representative nuisance estimation scenarios, assuming $N \asymp n$. Regardless of the values of ϕ_f and

ϕ_f	ϕ_ω	Plug-in (Thm 2)	Debiased (Thm 3)
1/4	1/4	$O_P(N^{-1/4})$	$O_P(N^{-1/2})$
1/3	1/4	$O_P(N^{-1/3})$	$O_P(N^{-1/2})$
1/3	1/6	$O_P(N^{-1/3})$	$O_P(N^{-1/2})$
1/5	1/5	$O_P(N^{-1/5})$	$O_P(N^{-2/5})$
1/4	1/8	$O_P(N^{-1/4})$	$O_P(N^{-3/8})$

Table 4: Rate comparison under different nuisance estimation scenarios, assuming $N \asymp n$.

ϕ_ω , the debiased rate is never worse than the plug-in rate, since $N^{-(\phi_f + \phi_\omega)} \leq N^{-\phi_f}$ for any $\phi_\omega > 0$.

Proposition 1 (Existence — general setting). Suppose the uncertainty set $\mathcal{C}(\delta)$ is nonempty and weakly compact for each $\delta \geq 0$. Then under the Conditional Stability Assumption (3.1) and Assumption 2, the minimization problem (5) admits a solution $\mathbb{P}_{A|X}^* \in \mathcal{C}(\delta)$, and the robust prediction function is

$$m_\delta^*(x) = \mathbb{E}_{A \sim \mathbb{P}_{A|X=x}^*}[\bar{f}(x, A)].$$

When $\delta = 0$, this recovers the source-conditional prediction $m_0^*(x) = \mathbb{E}_{A \sim \mathbb{P}_{A|X=x}^S}[\bar{f}(x, A)]$. For increasing δ , the uncertainty set expands monotonically, yielding progressively more conservative robust predictors.

Remark 3 (Compactness of the energy-based uncertainty set). For the generator class used in our implementation—neural networks with bounded weights enforced via weight decay regularization—all induced distributions are supported on the compact set \mathcal{A} (Assumption 1), ensuring tightness by Prokhorov’s theorem. The sublevel set $\mathcal{C}_g(\delta) = \{g \in \mathcal{G} : \text{En}(g) - \text{En}(g^{\mathcal{S}}) \leq \delta\}$ is closed: the Lipschitz continuity of g_θ in θ (Assumption 2) ensures that $\text{En}(g_\theta)$ is continuous in θ by dominated convergence, so the sublevel set is a closed subset of the compact parameter space Θ , hence compact.

At the distribution level, substituting the closed-form optimizer $m^*(x)$ reduces the minimax problem to a direct minimization of $\mathbb{E}_X[m^*(X)^2]$ over $\mathcal{C}(\delta)$; existence of a minimizer follows from weak compactness (Prokhorov’s theorem). In our implementation, the adversary is restricted to distributions induced by neural generators with compact parameter space Θ , which ensures existence within the parameterized class though the induced set of distributions may not be convex. The energy-constrained primal-dual optimization (Algorithm 3) converges reliably across all settings examined.

A.3 Proofs

Revisit the definitions of the population, oracle empirical, and empirical objectives:

$$\begin{aligned}\mathcal{L}(\theta) &= \mathbb{E}_{X \sim \mathbb{Q}_X} \left[\mathbb{E}_{\epsilon \sim \mathcal{N}(0, I_q)} [\bar{f}(X, g_\theta(\epsilon))] \right]^2 \\ \tilde{\mathcal{L}}(\theta) &= \frac{1}{N} \sum_{j=1}^N \left[\frac{1}{L} \sum_{l=1}^L \bar{f}(X_j, g_\theta(\epsilon_{jl})) \right]^2 \\ \hat{\mathcal{L}}(\theta) &= \frac{1}{N} \sum_{j=1}^N \left[\frac{1}{L} \sum_{l=1}^L \hat{f}(X_j, g_\theta(\epsilon_{jl})) \right]^2\end{aligned}$$

where $X_j \sim \mathbb{Q}_X$ are target covariates, $\epsilon_{jl} \sim \mathcal{N}(0, I_q)$ are Monte Carlo draws, and \hat{f} is estimated from source data.

Proof of Theorem 3.2 (distributional formulation). Since \mathcal{A} is compact (Assumption 1 (i)), the set \mathcal{P}_A of Borel probability measures on \mathcal{A} is compact in the weak topology by Prokhorov’s theorem. Define the objective $\Psi(\rho) = \mathbb{E}_{X \sim \mathbb{Q}_X} [\mathbb{E}_{A \sim \rho} [\bar{f}(X, A)]]^2$. It suffices to show Ψ is continuous in the weak topology. For any weakly convergent sequence $\rho_n \xrightarrow{w} \rho_0$, the map $a \mapsto \bar{f}(x, a)$ is bounded and continuous in a for each fixed x (Assumption 2 (i)), so the definition of weak convergence gives $\mathbb{E}_{A \sim \rho_n} [\bar{f}(x, A)] \rightarrow \mathbb{E}_{A \sim \rho_0} [\bar{f}(x, A)]$ for each x .

Since $|\mathbb{E}_{A \sim \rho} [\bar{f}(x, A)]| \leq M$ uniformly over ρ and x , the dominated convergence theorem yields $\Psi(\rho_n) \rightarrow \Psi(\rho_0)$. By the Weierstrass extreme value theorem, Ψ attains its minimum on the compact set \mathcal{P}_A . The identification follows from the derivation of (4) with $\mathbb{P}_{A|X}$ replaced by the marginal ρ^* .

□

Proof of Theorem 3.2 (parameterized formulation). We verify the conditions of the Weierstrass extreme value theorem.

First, the parameter space Θ is compact by Assumption 1 (ii).

Next, we show $\mathcal{L}(\theta)$ is continuous. Let $\theta_n \rightarrow \theta_0$ be any convergent sequence in Θ . Define

$$\mu_\theta(x) = \mathbb{E}_\epsilon[\bar{f}(x, g_\theta(\epsilon))].$$

For the inner expectation: By Assumption 1 (iii), $g_{\theta_n}(\epsilon) \rightarrow g_{\theta_0}(\epsilon)$ for almost every ϵ . By Assumption 2, \bar{f} is continuous, so $\bar{f}(x, g_{\theta_n}(\epsilon)) \rightarrow \bar{f}(x, g_{\theta_0}(\epsilon))$. Since $|\bar{f}| \leq M$, the dominated convergence theorem allows us to interchange the limit and expectation:

$$\lim_{n \rightarrow \infty} \mu_{\theta_n}(x) = \lim_{n \rightarrow \infty} \mathbb{E}_\epsilon[\bar{f}(x, g_{\theta_n}(\epsilon))] = \mathbb{E}_\epsilon \left[\lim_{n \rightarrow \infty} \bar{f}(x, g_{\theta_n}(\epsilon)) \right] = \mathbb{E}_\epsilon[\bar{f}(x, g_{\theta_0}(\epsilon))] = \mu_{\theta_0}(x).$$

For the outer expectation: Since $|\mu_\theta(x)| \leq M$ for all θ and x , and $\mu_{\theta_n}(x) \rightarrow \mu_{\theta_0}(x)$ pointwise, the dominated convergence theorem allows us again to interchange the limit and expectation:

$$\lim_{n \rightarrow \infty} \mathbb{E}_X[\mu_{\theta_n}(X)] = \mathbb{E}_X \left[\lim_{n \rightarrow \infty} \mu_{\theta_n}(X) \right] = \mathbb{E}_X[\mu_{\theta_0}(X)].$$

Then, by the Weierstrass extreme value theorem, a continuous function on a compact set attains its minimum. Hence there exists $\theta^* \in \Theta$ such that $\mathcal{L}(\theta^*) = \min_{\theta \in \Theta} \mathcal{L}(\theta)$.

From the derivation in Section 3, for any fixed generator g_θ , the inner maximization over $m(\cdot)$ in (3) yields $m_\theta(x) = \mathbb{E}_\epsilon[\bar{f}(x, g_\theta(\epsilon))]$. At the optimal θ^* , this gives

$$m^*(x) = \mathbb{E}_{\epsilon \sim \mathcal{N}(0, I_q)}[\bar{f}(x, g_{\theta^*}(\epsilon))].$$

□

Proof of Theorem 1. Decompose the difference:

$$\hat{\mathcal{L}}(\theta) - \mathcal{L}(\theta) = \underbrace{[\hat{\mathcal{L}}(\theta) - \tilde{\mathcal{L}}(\theta)]}_{(A)} + \underbrace{[\tilde{\mathcal{L}}(\theta) - \mathcal{L}(\theta)]}_{(B)}$$

For term (A), define $\hat{\mu}_\theta(X) = \frac{1}{L} \sum_l \hat{f}(X, g_\theta(\epsilon_l))$ and $\bar{\mu}_\theta(X) = \frac{1}{L} \sum_l \bar{f}(X, g_\theta(\epsilon_l))$. Using $|a^2 - b^2| \leq 2M|a - b|$ (since $|\bar{f}|, |\hat{f}| \leq M$):

$$\sup_{\theta \in \Theta} |\hat{\mathcal{L}}(\theta) - \tilde{\mathcal{L}}(\theta)| \leq \frac{2M}{N} \sum_{j=1}^N |\hat{\mu}_\theta(X_j) - \bar{\mu}_\theta(X_j)| \leq 2M \|\hat{f} - \bar{f}\|_\infty \xrightarrow{P} 0$$

by Assumption 3.

For term (B), define $h_\theta(x, \epsilon_{1:L}) = \left[\frac{1}{L} \sum_{l=1}^L \bar{f}(x, g_\theta(\epsilon_l)) \right]^2$ and let $\mathcal{L}_L(\theta) = \mathbb{E}_{X, \epsilon_{1:L}}[h_\theta(X, \epsilon_{1:L})]$.

We further decompose term (B):

$$|\tilde{\mathcal{L}}(\theta) - \mathcal{L}(\theta)| \leq \underbrace{|\tilde{\mathcal{L}}(\theta) - \mathcal{L}_L(\theta)|}_{(B_1)} + \underbrace{|\mathcal{L}_L(\theta) - \mathcal{L}(\theta)|}_{(B_2)}$$

For term (B_1) : Since $|h_\theta| \leq M^2$, the function class $\{h_\theta : \theta \in \Theta\}$ is uniformly bounded and continuous in θ on compact Θ . By the uniform law of large numbers (Wainwright, 2019), as $N \rightarrow \infty$:

$$\sup_{\theta \in \Theta} |\tilde{\mathcal{L}}(\theta) - \mathcal{L}_L(\theta)| \xrightarrow{P} 0$$

For term (B_2) : By expanding the square and using independence of $\epsilon_1, \dots, \epsilon_L$:

$$\mathcal{L}_L(\theta) = \mathcal{L}(\theta) + \frac{1}{L} \mathbb{E}_X [\text{Var}_\epsilon(\bar{f}(X, g_\theta(\epsilon)))]$$

Since $|\bar{f}| \leq M$, the variance term is bounded by M^2 , so:

$$\sup_{\theta \in \Theta} |\mathcal{L}_L(\theta) - \mathcal{L}(\theta)| \leq \frac{M^2}{L} \rightarrow 0 \quad \text{as } L \rightarrow \infty$$

Combining (B_1) and (B_2) :

$$\sup_{\theta \in \Theta} |\tilde{\mathcal{L}}(\theta) - \mathcal{L}(\theta)| \xrightarrow{P} 0 \quad \text{as } N, L \rightarrow \infty$$

Finally, since $\hat{\theta}$ minimizes $\hat{\mathcal{L}}$ and θ^* minimizes \mathcal{L} :

$$\hat{\mathcal{L}}(\hat{\theta}) \leq \hat{\mathcal{L}}(\theta^*) \quad \text{and} \quad \mathcal{L}(\theta^*) \leq \mathcal{L}(\hat{\theta})$$

Adding and subtracting, we obtain:

$$\begin{aligned} 0 \leq \mathcal{L}(\hat{\theta}) - \mathcal{L}(\theta^*) &= \mathcal{L}(\hat{\theta}) - \hat{\mathcal{L}}(\hat{\theta}) + \hat{\mathcal{L}}(\hat{\theta}) - \mathcal{L}(\theta^*) \\ &\leq \mathcal{L}(\hat{\theta}) - \hat{\mathcal{L}}(\hat{\theta}) + \hat{\mathcal{L}}(\theta^*) - \mathcal{L}(\theta^*) \\ &\leq |\mathcal{L}(\hat{\theta}) - \hat{\mathcal{L}}(\hat{\theta})| + |\hat{\mathcal{L}}(\theta^*) - \mathcal{L}(\theta^*)| \\ &\leq 2 \sup_{\theta \in \Theta} |\hat{\mathcal{L}}(\theta) - \mathcal{L}(\theta)| \end{aligned}$$

Therefore $\sup_{\theta \in \Theta} |\hat{\mathcal{L}}(\theta) - \mathcal{L}(\theta)| \xrightarrow{P} 0$ and thus $\mathcal{L}(\hat{\theta}) - \mathcal{L}(\theta^*) \xrightarrow{P} 0$, which gives $\mathcal{L}(\hat{\theta}) \xrightarrow{P} \mathcal{L}(\theta^*)$. \square

Proof of Theorem 2. From the proof of Theorem 1, we have

$$0 \leq \mathcal{L}(\hat{\theta}) - \mathcal{L}(\theta^*) \leq 2 \left[\underbrace{\sup_{\theta} |\hat{\mathcal{L}}(\theta) - \tilde{\mathcal{L}}(\theta)|}_{(A)} + \underbrace{\sup_{\theta} |\tilde{\mathcal{L}}(\theta) - \mathcal{L}(\theta)|}_{(B)} \right] \quad (26)$$

where $\tilde{\mathcal{L}}(\theta)$ is the oracle empirical objective. It remains to establish the rate for each term.

For rate for term (A) , using the same notation $\hat{\mu}_\theta$ and $\bar{\mu}_\theta$ as in the proof of Theorem 1, and the bound $|a^2 - b^2| \leq 2M|a - b|$ gives:

$$\sup_{\theta} |\hat{\mathcal{L}}(\theta) - \tilde{\mathcal{L}}(\theta)| \leq 2M \sup_{\theta} \frac{1}{N} \sum_{j=1}^N |\hat{\mu}_\theta(X_j) - \bar{\mu}_\theta(X_j)|$$

Since

$$|\hat{\mu}_\theta(X) - \bar{\mu}_\theta(X)| = \left| \frac{1}{L} \sum_{l=1}^L [\hat{f}(X, g_\theta(\epsilon_l)) - \bar{f}(X, g_\theta(\epsilon_l))] \right| \leq \frac{1}{L} \sum_{l=1}^L |\hat{f}(X, g_\theta(\epsilon_l)) - \bar{f}(X, g_\theta(\epsilon_l))| \leq \|\hat{f} - \bar{f}\|_\infty$$

we obtain

$$\sup_{\theta} |\hat{\mathcal{L}}(\theta) - \tilde{\mathcal{L}}(\theta)| \leq 2M \|\hat{f} - \bar{f}\|_\infty = O_P(n^{-\phi_f})$$

by Assumption 3. This bound is uniform over θ since the sup norm does not depend on θ .

For rate for term (B), using the same decomposition as in the proof of Theorem 1 gives:

$$\sup_{\theta} |\tilde{\mathcal{L}}(\theta) - \mathcal{L}(\theta)| \leq \sup_{\theta} \underbrace{|\tilde{\mathcal{L}}(\theta) - \mathcal{L}_L(\theta)|}_{(B_1)} + \sup_{\theta} \underbrace{|\mathcal{L}_L(\theta) - \mathcal{L}(\theta)|}_{(B_2)}$$

For term (B₂), we have showed $\sup_{\theta} |\mathcal{L}_L(\theta) - \mathcal{L}(\theta)| \leq M^2/L$, which is negligible for L sufficiently large.

For term (B₁), recall that

$$\tilde{\mathcal{L}}(\theta) - \mathcal{L}_L(\theta) = \frac{1}{N} \sum_{j=1}^N [h_\theta(X_j, \epsilon_{j\cdot}) - \mathbb{E}[h_\theta]],$$

where $h_\theta(x, \epsilon_{1:L}) = \left[\frac{1}{L} \sum_{l=1}^L \bar{f}(x, g_\theta(\epsilon_l)) \right]^2$ as defined in the proof of Theorem 1, and X_1, \dots, X_N are i.i.d. draws from \mathbb{Q}_X .

We consider Example 19.7 of Van der Vaart (2000): the function class $\mathcal{H} = \{h_\theta : \theta \in \Theta\}$, where $\Theta \subset \mathbb{R}^p$ is compact (Assumption 1 (ii)).

This requires verifying a Lipschitz condition: there exists a measurable function $m(x, \epsilon_{1:L})$ with $\mathbb{E}[m^2] < \infty$ such that

$$|h_{\theta_1}(x, \epsilon_{1:L}) - h_{\theta_2}(x, \epsilon_{1:L})| \leq m(x, \epsilon_{1:L}) \|\theta_1 - \theta_2\| \quad \text{for all } \theta_1, \theta_2 \in \Theta.$$

Define $\mu_\theta(x, \epsilon_{1:L}) = \frac{1}{L} \sum_{l=1}^L \bar{f}(x, g_\theta(\epsilon_l))$, so that $h_\theta = \mu_\theta^2$. Then

$$\begin{aligned} |h_{\theta_1} - h_{\theta_2}| &= |\mu_{\theta_1} + \mu_{\theta_2}| \cdot |\mu_{\theta_1} - \mu_{\theta_2}| \\ &\leq 2M \cdot \frac{1}{L} \sum_{l=1}^L |\bar{f}(x, g_{\theta_1}(\epsilon_l)) - \bar{f}(x, g_{\theta_2}(\epsilon_l))| \\ &\leq 2ML_f \cdot \frac{1}{L} \sum_{l=1}^L \|g_{\theta_1}(\epsilon_l) - g_{\theta_2}(\epsilon_l)\| \\ &\leq \frac{2ML_f}{L} \sum_{l=1}^L \ell(\epsilon_l) \cdot \|\theta_1 - \theta_2\|, \end{aligned}$$

where the second inequality uses the Lipschitz continuity of \bar{f} in a (Assumption 2 (i)) and the third uses the Lipschitz continuity of g_θ in θ (Assumption 2 (ii)).

Setting $m(x, \epsilon_{1:L}) = \frac{2ML_f}{L} \sum_{l=1}^L \ell(\epsilon_l)$, we have $\mathbb{E}[m^2] \leq (2ML_f)^2 \mathbb{E}[\ell(\epsilon)^2] < \infty$ by Assumption 2 (ii).

Since $\Theta \subset \mathbb{R}^p$ is compact and $\mathbb{E}[m^2] < \infty$, the conditions of Example 19.7 in Van der Vaart (2000) are satisfied, and \mathcal{H} is a Donsker class which implies that $\sup_{\theta \in \Theta} \sqrt{N} |\tilde{\mathcal{L}}(\theta) - \mathcal{L}_L(\theta)|$ is $O_P(1)$, yielding the $O_P(N^{-1/2})$ rate (Donsker theorem (Van der Vaart, 2000, Theorem 19.3)):

$$\sup_{\theta \in \Theta} |\tilde{\mathcal{L}}(\theta) - \mathcal{L}_L(\theta)| = O_P(N^{-1/2}).$$

Finally, collecting the results for terms (A), (B₁), and (B₂):

$$\begin{aligned} \sup_{\theta \in \Theta} |\hat{\mathcal{L}}(\theta) - \mathcal{L}(\theta)| &\leq \sup_{\theta} |\hat{\mathcal{L}}(\theta) - \tilde{\mathcal{L}}(\theta)| + \sup_{\theta} |\tilde{\mathcal{L}}(\theta) - \mathcal{L}_L(\theta)| + \sup_{\theta} |\mathcal{L}_L(\theta) - \mathcal{L}(\theta)| \\ &= O_P(n^{-\phi_f}) + O_P(N^{-1/2}) + \frac{M^2}{L}. \end{aligned}$$

For L sufficiently large that M^2/L is dominated by the other terms, we obtain

$$\sup_{\theta \in \Theta} |\hat{\mathcal{L}}(\theta) - \mathcal{L}(\theta)| = O_P(n^{-\phi_f} + N^{-1/2}).$$

Since $\hat{\theta}$ minimizes $\hat{\mathcal{L}}$ and θ^* minimizes \mathcal{L} , the same sandwich argument as in the proof of Theorem 1 gives:

$$0 \leq \mathcal{L}(\hat{\theta}) - \mathcal{L}(\theta^*) \leq 2 \sup_{\theta \in \Theta} |\hat{\mathcal{L}}(\theta) - \mathcal{L}(\theta)| = O_P(n^{-\phi_f} + N^{-1/2}),$$

which completes the proof. □

Proof of Theorem 3. We use the generator notation $\mu_{\bar{\theta}}(x) = \mathbb{E}_{\epsilon}[\bar{f}(x, g_{\bar{\theta}}(\epsilon))]$ and $\Delta_{\bar{\theta}}(x) = \mathbb{E}_{\epsilon}[(\hat{f} - \bar{f})(x, g_{\bar{\theta}}(\epsilon))]$, corresponding to $m(x)$ and $\Delta(x)$ in the main text evaluated at the preliminary generator $\bar{\theta}$.

We first take a detailed look at the cross-fitting used in Algorithm 4. Following its construction, with K -fold cross-fitting, we partition the source indices into folds $\mathcal{I}_1, \dots, \mathcal{I}_K$ and target indices into $\mathcal{J}_1, \dots, \mathcal{J}_K$. For fold k , let $\hat{f}^{(-k)}$ and $\hat{\omega}^{(-k)}$ denote nuisance estimates trained on all folds except k .

Then the cross-fitted debiased objective is:

$$\hat{\mathcal{L}}^{\text{deb}}(\theta) = \frac{1}{K} \sum_{k=1}^K \left[\underbrace{\frac{1}{|\mathcal{J}_k|} \sum_{j \in \mathcal{J}_k} \left[\frac{1}{L} \sum_{l=1}^L \hat{f}^{(-k)}(X_j, g_{\theta}(\epsilon_{jl})) \right]^2}_{\hat{\mathcal{L}}_k(\theta)} + \underbrace{\frac{2}{|\mathcal{I}_k|} \sum_{i \in \mathcal{I}_k} \hat{\omega}_i^{(-k)} \cdot \hat{\mu}_{\bar{\theta}}^{(-k)}(X_i) \cdot (Y_i - \hat{f}_i^{(-k)})}_{\hat{C}_k} \right] \quad (27)$$

where $\bar{\theta}$ denotes the preliminary generator parameters from uncorrected DRUM, $\hat{f}_i^{(-k)} = \hat{f}^{(-k)}(X_i, A_i)$, $\hat{\omega}_i^{(-k)} = \hat{\omega}^{(-k)}(X_i, A_i)$, and

$$\hat{\mu}_{\bar{\theta}}^{(-k)}(x) = \frac{1}{L} \sum_{l=1}^L \hat{f}^{(-k)}(x, g_{\bar{\theta}}(\epsilon_l)).$$

The formal proof follows the same structure as Theorems 1 and 2, with additional analysis of the correction term. By the same sandwich argument as in Theorem 2:

$$0 \leq \mathcal{L}(\hat{\theta}^{\text{deb}}) - \mathcal{L}(\theta^*) \leq 2 \sup_{\theta \in \Theta} |\hat{\mathcal{L}}^{\text{deb}}(\theta) - \mathcal{L}(\theta)|,$$

it suffices to bound the right-hand side.

As mentioned above, by cross-fitting, it suffices to analyze a single fold k . Conditional on the training folds, the nuisance estimates $\hat{f}^{(-k)}$ and $\hat{\omega}^{(-k)}$ are deterministic functions. We suppress the superscript $(-k)$ for readability.

Decompose:

$$\hat{\mathcal{L}}^{\text{deb}}(\theta) - \mathcal{L}(\theta) = \underbrace{[\hat{\mathcal{L}}(\theta) - \tilde{\mathcal{L}}(\theta)]}_{(A)} + \underbrace{[\tilde{\mathcal{L}}(\theta) - \mathcal{L}(\theta)]}_{(B)} + \underbrace{\hat{C}}_{(C)}, \quad (28)$$

where $\hat{\mathcal{L}}(\theta)$ is the plug-in empirical objective, $\tilde{\mathcal{L}}(\theta)$ is the oracle empirical objective, and \hat{C} is the correction term.

For term (B), using the same decomposition $B = B_1 + B_2$ in Theorem 2 gives:

$$\sup_{\theta \in \Theta} |\tilde{\mathcal{L}}(\theta) - \mathcal{L}(\theta)| = O_P(N^{-1/2}) + O(L^{-1}). \quad (29)$$

For the correction term $\hat{C} = \frac{2}{|\mathcal{I}_k|} \sum_{i \in \mathcal{I}_k} \hat{\omega}(X_i, A_i) \cdot \hat{\mu}_{\bar{\theta}}(X_i) \cdot (Y_i - \hat{f}(X_i, A_i))$, we first obtain the conditional expectation:

$$\mathbb{E}[\hat{C} \mid \hat{f}, \hat{\omega}] = 2 \mathbb{E}_{(X,A) \sim \mathbb{P}^S} \left[\hat{\omega}(X, A) \cdot \hat{\mu}_{\bar{\theta}}(X) \cdot (\bar{f}(X, A) - \hat{f}(X, A)) \right] \quad (30)$$

given that \hat{f} and $\hat{\omega}$ are fixed (by cross-fitting) and $\mathbb{E}[Y_i \mid X_i, A_i] = \bar{f}(X_i, A_i)$.

For further decomposition, we first write $\hat{\omega} = \omega + (\hat{\omega} - \omega)$ and $\hat{\mu}_{\bar{\theta}} = \mu_{\bar{\theta}} + \Delta_{\bar{\theta}}$, where $\Delta_{\bar{\theta}}(x) = \hat{\mu}_{\bar{\theta}}(x) - \mu_{\bar{\theta}}(x) = \frac{1}{L} \sum_{l=1}^L (\hat{f} - \bar{f})(x, g_{\bar{\theta}}(\epsilon_l))$.

Substituting both into (30) and expanding the product $\hat{\omega} \cdot \hat{\mu}_{\bar{\theta}} = [\omega + (\hat{\omega} - \omega)][\mu_{\bar{\theta}} + \Delta_{\bar{\theta}}]$:

$$\begin{aligned} \mathbb{E}[\hat{C} \mid \hat{f}, \hat{\omega}] &= 2 \mathbb{E}_{\mathbb{P}^S} \left[\hat{\omega} \cdot \hat{\mu}_{\bar{\theta}} \cdot (\bar{f} - \hat{f}) \right] \\ &= 2 \mathbb{E}_{\mathbb{P}^S} \left[\omega \cdot \mu_{\bar{\theta}} \cdot (\bar{f} - \hat{f}) \right] + 2 \mathbb{E}_{\mathbb{P}^S} \left[\omega \cdot \Delta_{\bar{\theta}} \cdot (\bar{f} - \hat{f}) \right] \\ &\quad + 2 \mathbb{E}_{\mathbb{P}^S} \left[(\hat{\omega} - \omega) \cdot \mu_{\bar{\theta}} \cdot (\bar{f} - \hat{f}) \right] + 2 \mathbb{E}_{\mathbb{P}^S} \left[(\hat{\omega} - \omega) \cdot \Delta_{\bar{\theta}} \cdot (\bar{f} - \hat{f}) \right] \end{aligned} \quad (31)$$

Combining the last two terms:

$$\mathbb{E}[\hat{C} \mid \hat{f}, \hat{\omega}] = \underbrace{2 \mathbb{E}_{\mathbb{P}^S} \left[\omega \cdot \mu_{\bar{\theta}} \cdot (\bar{f} - \hat{f}) \right]}_{T_1} + \underbrace{2 \mathbb{E}_{\mathbb{P}^S} \left[\omega \cdot \Delta_{\bar{\theta}} \cdot (\bar{f} - \hat{f}) \right]}_{T_2} + \underbrace{2 \mathbb{E}_{\mathbb{P}^S} \left[(\hat{\omega} - \omega) \cdot \hat{\mu}_{\bar{\theta}} \cdot (\bar{f} - \hat{f}) \right]}_{T_3}. \quad (32)$$

Note that the above three terms have distinct orders in estimation error: T_1 is first-order in $(\hat{f} - \bar{f})$; T_2 is second-order since both $\Delta_{\bar{\theta}}$ and $(\bar{f} - \hat{f})$ are $O(\|\hat{f} - \bar{f}\|_\infty)$; T_3 is a mixed product of two independent estimation errors.

For term T_1 , recall the density ratio in Section 4, by the change-of-measure (importance weighting) identity, for any measurable h , we have:

$$\mathbb{E}_{(X,A) \sim \mathbb{P}^S}[\omega(X, A) \cdot h(X, A)] = \mathbb{E}_{(X,A) \sim \mathbb{Q}^{g_{\bar{\theta}}}}[h(X, A)].$$

Note that this holds for both DRUM (unconstrained) and DRUM because ω is defined as the density ratio between the target-generator joint and the source joint in both cases.

Therefore for T_1 , with $h(x, a) = \mu_{\bar{\theta}}(x) \cdot (\bar{f}(x, a) - \hat{f}(x, a))$, we have:

$$\begin{aligned} T_1 &= 2 \mathbb{E}_{(X,A) \sim \mathbb{P}^S} \left[\omega(X, A) \cdot \mu_{\bar{\theta}}(X) \cdot (\bar{f}(X, A) - \hat{f}(X, A)) \right] \\ &= 2 \mathbb{E}_{(X,A) \sim \mathbb{Q}^{g_{\bar{\theta}}}} \left[\mu_{\bar{\theta}}(X) \cdot (\bar{f}(X, A) - \hat{f}(X, A)) \right] \\ &= 2 \mathbb{E}_{X \sim \mathbb{Q}_X} \left[\mu_{\bar{\theta}}(X) \cdot \mathbb{E}_{A \sim \rho_{\bar{\theta}}(\cdot|X)} \left[(\bar{f} - \hat{f})(X, A) \right] \right] \\ &= 2 \mathbb{E}_{X \sim \mathbb{Q}_X} \left[\mu_{\bar{\theta}}(X) \cdot \left(\underbrace{\mathbb{E}_{\epsilon}[\bar{f}(X, g_{\bar{\theta}}(\cdot))]}_{=\mu_{\bar{\theta}}(X)} - \underbrace{\mathbb{E}_{\epsilon}[\hat{f}(X, g_{\bar{\theta}}(\cdot))]}_{=\mu_{\bar{\theta}}(X) + \Delta_{\bar{\theta}}(X)} \right) \right] \\ &= 2 \mathbb{E}_{X \sim \mathbb{Q}_X} \left[\mu_{\bar{\theta}}(X) \cdot (-\Delta_{\bar{\theta}}(X)) \right] \\ &= -2 \mathbb{E}_{X \sim \mathbb{Q}_X} [\mu_{\bar{\theta}}(X) \cdot \Delta_{\bar{\theta}}(X)] \end{aligned}$$

which we show next that actually cancels with the first order term of (A).

Write term (A) at the population level. Expanding $\hat{\mu}_{\bar{\theta}} = \mu_{\bar{\theta}} + \Delta_{\bar{\theta}}$:

$$\begin{aligned} \mathbb{E}_X [\hat{\mu}_{\bar{\theta}}(X)^2 - \mu_{\bar{\theta}}(X)^2] &= \mathbb{E}_X [(\mu_{\bar{\theta}} + \Delta_{\bar{\theta}})^2 - \mu_{\bar{\theta}}^2] \\ &= \underbrace{2 \mathbb{E}_X [\mu_{\bar{\theta}} \cdot \Delta_{\bar{\theta}}]}_{\text{first-order: } O(\|\hat{f} - \bar{f}\|_{\infty})} + \underbrace{\mathbb{E}_X [\Delta_{\bar{\theta}}^2]}_{\text{second-order: } O(\|\hat{f} - \bar{f}\|_{\infty}^2)}. \end{aligned} \quad (33)$$

Adding (33) to $T_1 = -2 \mathbb{E}_X [\mu_{\bar{\theta}} \cdot \Delta_{\bar{\theta}}]$:

$$\underbrace{2 \mathbb{E}_X [\mu_{\bar{\theta}} \cdot \Delta_{\bar{\theta}}]}_{\text{first-order part of (A)}} + \underbrace{(-2 \mathbb{E}_X [\mu_{\bar{\theta}} \cdot \Delta_{\bar{\theta}}])}_{T_1} = 0. \quad (34)$$

Therefore the first-order terms cancel exactly. The surviving contribution from (A) is only the second-order remainder:

$$\mathbb{E}_X [\Delta_{\bar{\theta}}(X)^2] \leq \|\hat{f} - \bar{f}\|_{\infty}^2 = O_P(n^{-2\phi_f}). \quad (35)$$

For T_2 , taking absolute values inside the expectation:

$$|T_2| \leq 2 \mathbb{E}_{\mathbb{P}^S} \left[|\omega(X, A)| \cdot |\Delta_{\bar{\theta}}(X)| \cdot |(\bar{f} - \hat{f})(X, A)| \right]. \quad (36)$$

We bound each factor:

- $|\omega(X, A)| \leq M_{\omega}$ (bounded density ratio);
- $|\Delta_{\bar{\theta}}(X)| = |\mathbb{E}_{\epsilon}[(\hat{f} - \bar{f})(X, g_{\bar{\theta}}(\epsilon))]| \leq \|\hat{f} - \bar{f}\|_{\infty}$ (triangle inequality);

- $|(\bar{f} - \hat{f})(X, A)| \leq \|\hat{f} - \bar{f}\|_\infty$.

Therefore:

$$|T_2| \leq 2M_\omega \cdot \|\hat{f} - \bar{f}\|_\infty \cdot \|\hat{f} - \bar{f}\|_\infty = 2M_\omega \|\hat{f} - \bar{f}\|_\infty^2 = O_P(n^{-2\phi_f}). \quad (37)$$

For T_3 , taking absolute values and factoring out $|\hat{\mu}_{\bar{\theta}}(X)| \leq M$:

$$\begin{aligned} |T_3| &\leq 2 \mathbb{E}_{\mathbb{P}^S} \left[|(\hat{\omega} - \omega)(X, A)| \cdot |\hat{\mu}_{\bar{\theta}}(X)| \cdot |(\bar{f} - \hat{f})(X, A)| \right] \\ &\leq 2M \mathbb{E}_{\mathbb{P}^S} \left[|(\hat{\omega} - \omega)(X, A)| \cdot |(\bar{f} - \hat{f})(X, A)| \right]. \end{aligned} \quad (38)$$

Since $|(\bar{f} - \hat{f})(X, A)| \leq \|\hat{f} - \bar{f}\|_\infty$ is a constant (conditional on \hat{f}), it can be pulled out of the expectation:

$$\begin{aligned} |T_3| &\leq 2M \|\hat{f} - \bar{f}\|_\infty \cdot \mathbb{E}_{\mathbb{P}^S} [|(\hat{\omega} - \omega)(X, A)|] \\ &\leq 2M \|\hat{f} - \bar{f}\|_\infty \cdot \|\hat{\omega} - \omega\|_{L^2(\mathbb{P}^S)}, \end{aligned} \quad (39)$$

where the last step uses Jensen's inequality: $\mathbb{E}[|Z|] \leq (\mathbb{E}[Z^2])^{1/2} = \|Z\|_{L^2}$.

Finally, the debiased error at $\theta = \bar{\theta}$ consists of:

- Second-order remainder from (A): $\mathbb{E}_X[\Delta_{\bar{\theta}}^2] \leq \|\hat{f} - \bar{f}\|_\infty^2$ (Eq. 35)

- $|T_2| \leq 2M_\omega \|\hat{f} - \bar{f}\|_\infty^2$ (Eq. 37)

- $|T_3| \leq 2M \|\hat{f} - \bar{f}\|_\infty \cdot \|\hat{\omega} - \omega\|_{L^2}$ (Eq. 39)

- Term (B): $O_P(N^{-1/2}) + O(L^{-1})$ (from Theorem 2)

- Stochastic fluctuation of \hat{C} : $O_P(n^{-1/2})$

First, stochastic fluctuation of \hat{C} around its conditional expectation is $O_P(|\mathcal{I}_k|^{-1/2})$ by the central limit theorem, since each summand is bounded (Assumptions 2 and 4).

Then, combining:

$$\begin{aligned} |\hat{\mathcal{L}}^{\text{deb}}(\bar{\theta}) - \mathcal{L}(\bar{\theta})| &\leq \underbrace{(1 + 2M_\omega) \|\hat{f} - \bar{f}\|_\infty^2}_{\text{from (A) remainder} + T_2} + \underbrace{2M \|\hat{f} - \bar{f}\|_\infty \cdot \|\hat{\omega} - \omega\|_{L^2}}_{T_3} \\ &\quad + \underbrace{O_P(N^{-1/2})}_{\text{term (B}_1)} + \underbrace{O(L^{-1})}_{\text{term (B}_2)} + \underbrace{O_P(n^{-1/2})}_{\hat{C} \text{ fluctuation}}. \end{aligned} \quad (40)$$

For L sufficiently large that $O(L^{-1})$ is negligible, and using $n^{-1/2} = O(N^{-1/2})$ when $N \leq n$:

$$|\hat{\mathcal{L}}^{\text{deb}}(\bar{\theta}) - \mathcal{L}(\bar{\theta})| = O_P\left(\|\hat{f} - \bar{f}\|_\infty^2 + \|\hat{f} - \bar{f}\|_\infty \cdot \|\hat{\omega} - \omega\|_{L^2} + N^{-1/2}\right). \quad (41)$$

By Assumption 3, this becomes

$$|\hat{\mathcal{L}}^{\text{deb}}(\bar{\theta}) - \mathcal{L}(\bar{\theta})| = O_P\left(n^{-2\phi_f} + n^{-\phi_f} \cdot N^{-\phi_\omega} + N^{-1/2}\right). \quad (42)$$

Note that this bound holds uniformly over Θ : term (A) is bounded by $\|\hat{f} - \bar{f}\|_\infty^2$ which does not depend on θ ; term (B) has a uniform bound by the same argument as in Theorem 2; and the correction term \hat{C} depends only on the fixed preliminary generator $\bar{\theta}$, not on the variable θ .

Finally, since $\hat{\theta}^{\text{deb}}$ minimizes $\hat{\mathcal{L}}^{\text{deb}}$ and θ^* minimizes \mathcal{L} , the same sandwich argument as in Theorem 2 gives:

$$0 \leq \mathcal{L}(\hat{\theta}^{\text{deb}}) - \mathcal{L}(\theta^*) \leq 2 \sup_{\theta \in \Theta} |\hat{\mathcal{L}}^{\text{deb}}(\theta) - \mathcal{L}(\theta)| = O_P\left(n^{-2\phi_f} + n^{-\phi_f} \cdot N^{-\phi_\omega} + N^{-1/2}\right). \quad (43)$$

□

B Detailed Algorithmic Procedures

This section provides pseudocode for the algorithms described in Section 3.

Algorithm 1: DRUM (unconstrained)

Input : Source data $\mathcal{D}_S = \{X_i, A_i, Y_i\}_{i=1}^n$; target data $\mathcal{D}_T = \{X_j\}_{j=1}^N$; learning rates η_f, η_g , epochs E_f, E_g , batch sizes B_S, B_T , Monte Carlo samples L .

Output: Robust predictor $\hat{m}(\cdot)$.

// Stage 1: Estimate conditional mean \bar{f}

- 1 Initialize neural network parameters ψ
- 2 **for** $epoch=1$ to E_f **do**
- 3 **for** $mini\text{-}batch \{X_i, A_i, Y_i\}_{i=1}^{B_S}$ from \mathcal{D}_S **do**
- 4 $\mathcal{L}_f(\psi) = \frac{1}{B_S} \sum_{i=1}^{B_S} (Y_i - \hat{f}_\psi(X_i, A_i))^2$
- 5 $\psi \leftarrow \psi - \eta_f \nabla_\psi \mathcal{L}_f(\psi)$
- 6 **end**
- 7 **end**
- 8 Freeze ψ

// Stage 2: Train worst-case generator g_θ .

- 9 Initialize neural network parameters θ
- 10 **for** $epoch = 1$ to E_g **do**
- 11 **for** $mini\text{-}batch \{X_j\}_{j=1}^{B_T}$ from \mathcal{D}_T **do**
- 12 Sample $\{\epsilon_{jl}\}_{l=1}^L \stackrel{\text{iid}}{\sim} \mathcal{N}(0, I_q)$
- 13 **for** $j = 1$ to B_T **do**
- 14 $\bar{m}_j \leftarrow \frac{1}{L} \sum_{l=1}^L \hat{f}_\psi(X_j, g_\theta(\epsilon_{jl}))$
- 15 **end**
- 16 $\mathcal{L}_g(\theta) \leftarrow \frac{1}{B_T} \sum_{j=1}^{B_T} (\bar{m}_j)^2$
- 17 $\theta \leftarrow \theta - \eta_g \nabla_\theta \mathcal{L}_g(\theta)$
- 18 **end**
- 19 **end**

// Stage 3: Prediction function $m^*(x)$

- 20 **Function** $\text{Predict}(x)$:
- 21 Sample $\{\epsilon_l\}_{l=1}^L \stackrel{\text{iid}}{\sim} \mathcal{N}(0, I_q)$
- 22 **return** $\hat{m}(x) = \frac{1}{L} \sum_{l=1}^L \hat{f}_\psi(x, g_\theta(\epsilon_l))$

Algorithm 2: DRUM

Input : Source data $\mathcal{D}_S = \{(X_i, A_i, Y_i)\}_{i=1}^n$; target covariates $\mathcal{D}_T = \{X_j\}_{j=1}^N$; learning rates $\eta_f, \eta_{g^S}, \eta_g$; epochs E_f, E_{g^S}, E_g ; batch sizes B_S, B_T ; Monte Carlo samples L ; uncertainty radius δ .

Output: Robust predictor $\hat{m}_{\text{local}}(\cdot)$.

// Stage 1: Estimate conditional mean \bar{f}

1 Initialize neural network parameters ψ

2 **for** $epoch = 1$ to E_f **do**

3 **for** mini-batch $\{(X_i, A_i, Y_i)\}_{i=1}^{B_S}$ from \mathcal{D}_S **do**

4 $\mathcal{L}_f(\psi) \leftarrow \frac{1}{B_S} \sum_{i=1}^{B_S} (Y_i - \hat{f}_\psi(X_i, A_i))^2$

5 $\psi \leftarrow \psi - \eta_f \nabla_\psi \mathcal{L}_f(\psi)$

6 **end**

7 **end**

8 Freeze ψ

// Stage 2a: Learn source conditional generator g^S

9 Initialize neural network parameters ϕ

10 **for** $epoch = 1$ to E_{g^S} **do**

11 **for** mini-batch $\{(X_i, A_i)\}_{i=1}^{B_S}$ from \mathcal{D}_S **do**

12 Sample $\{\epsilon_i\}_{i=1}^{B_S}, \{\epsilon'_i\}_{i=1}^{B_S} \stackrel{\text{iid}}{\sim} \mathcal{N}(0, I_q)$

13 $\hat{A}_i \leftarrow g_\phi^S(X_i, \epsilon_i), \quad \hat{A}'_i \leftarrow g_\phi^S(X_i, \epsilon'_i)$

14 $En(\phi) \leftarrow \frac{1}{B_S} \sum_{i=1}^{B_S} \|A_i - \hat{A}_i\|_2 - \frac{1}{2B_S} \sum_{i=1}^{B_S} \|\hat{A}_i - \hat{A}'_i\|_2$

15 $\phi \leftarrow \phi - \eta_{g^S} \nabla_\phi En(\phi)$

16 **end**

17 **end**

18 Store $\phi^S \leftarrow \phi$ and baseline energy $En(g_{\phi^S}^S)$

// Stage 2b: Solve energy-constrained optimization

19 $\phi^* \leftarrow$ **Algorithm 3**($\hat{f}_\psi, g_{\phi^S}^S, En(g_{\phi^S}^S), \mathcal{D}_S, \mathcal{D}_T, \delta$)

// Stage 3: Prediction function

20 **Function** Predict(x):

21 Sample $\{\epsilon_l\}_{l=1}^L \stackrel{\text{iid}}{\sim} \mathcal{N}(0, I_q)$

22 **return** $\hat{m}_{\text{local}}(x) = \frac{1}{L} \sum_{l=1}^L \hat{f}_\psi(x, g_{\phi^*}(x, \epsilon_l))$

Algorithm 3: Energy-Constrained Optimization (Primal-Dual)

Input : Predictor \hat{f}_ψ ; source generator $g_{\phi_S}^S$; baseline energy $En(g^S)$; source data \mathcal{D}_S ; target covariates \mathcal{D}_T ; uncertainty radius δ ; learning rates η_ϕ, η_λ ; epochs E ; batch sizes B_S, B_T ; Monte Carlo samples L .

Output: Optimal generator parameters ϕ^* .

```
1 Initialize  $\phi \leftarrow \phi^S$  // Initialize from source generator
2 Initialize dual variable  $\lambda \leftarrow 0$ 
3 for epoch = 1 to  $E$  do
4   for mini-batches  $\{(X_i, A_i)\}_{i=1}^{B_S}$  from  $\mathcal{D}_S$ ,  $\{X_j\}_{j=1}^{B_T}$  from  $\mathcal{D}_T$  do
5     // Compute primal objective on target data
6     Sample  $\{\epsilon_{jl}\}_{l=1}^L \stackrel{\text{iid}}{\sim} \mathcal{N}(0, I_q)$  for each  $j$ 
7     for  $j = 1$  to  $B_T$  do
8       |  $\bar{m}_j \leftarrow \frac{1}{L} \sum_{l=1}^L \hat{f}_\psi(X_j, g_\phi(X_j, \epsilon_{jl}))$ 
9     end
10     $\mathcal{L}_{\text{obj}} \leftarrow \frac{1}{B_T} \sum_{j=1}^{B_T} (\bar{m}_j)^2$ 
11    // Compute energy gap on source data
12    Sample  $\{\epsilon_i\}_{i=1}^{B_S}, \{\epsilon'_i\}_{i=1}^{B_S} \stackrel{\text{iid}}{\sim} \mathcal{N}(0, I_q)$ 
13     $En(g_\phi) \leftarrow \frac{1}{B_S} \sum_{i=1}^{B_S} \|A_i - g_\phi(X_i, \epsilon_i)\|_2 - \frac{1}{2B_S} \sum_{i=1}^{B_S} \|g_\phi(X_i, \epsilon_i) - g_\phi(X_i, \epsilon'_i)\|_2$ 
14     $\Delta En \leftarrow En(g_\phi) - En(g^S)$ 
15    // Primal-dual updates
16     $\mathcal{L}(\phi, \lambda) \leftarrow \mathcal{L}_{\text{obj}} + \lambda \cdot (\Delta En - \delta)$ 
17     $\phi \leftarrow \phi - \eta_\phi \nabla_\phi \mathcal{L}(\phi, \lambda)$ 
18     $\lambda \leftarrow \max(0, \lambda + \eta_\lambda \cdot (\Delta En - \delta))$ 
19  end
20 end
21 return  $\phi$ 
```

Algorithm 4: DRUM-Debiased

Input : Source data $\mathcal{D}_S = \{X_i, A_i, Y_i\}_{i=1}^n$; Target data $\mathcal{D}_T = \{X_j\}_{j=1}^N$; Preliminary generator $g^{(0)}$ from Algorithm 1; learning rates $\eta_f, \eta_\omega, \eta_g, \eta_F$; epochs E_f, E_ω, E_g, E_F ; Monte Carlo samples L .

Output: $m_{deb}^*(x)$.

// Stage 1: Partition data

- 1 Partition \mathcal{D}_S into 3 folds: $\mathcal{I}_1, \mathcal{I}_2, \mathcal{I}_3$
- 2 Partition \mathcal{D}_T into 3 folds: $\mathcal{J}_1, \mathcal{J}_2, \mathcal{J}_3$

// Stage 2: Cross-fitted nuisance estimation

- 3 **for** $k = 1, 2, 3$ (indices mod 3) **do**

// Estimate \hat{f} and residuals

- 4 Train $\hat{f}^{(k)}$ on \mathcal{I}_k using MSE loss
- 5 Compute $\hat{R}_i \leftarrow Y_i - \hat{f}^{(k)}(X_i, A_i)$ for $i \in \mathcal{I}_{k+1}$

// Estimate density ratio $\hat{\omega}$

- 6 Generate $\tilde{A}_j = g^{(0)}(\epsilon_j)$, $\epsilon_j \sim \mathcal{N}(0, I_q)$ for $j \in \mathcal{J}_k$
- 7 Train $\hat{p}^{(k)}(X, A) \approx P(S = 1 | X, A)$ on $\{(X_i, A_i, 1)\}_{i \in \mathcal{I}_k} \cup \{(X_j, \tilde{A}_j, 0)\}_{j \in \mathcal{J}_k}$
- 8 Compute $\hat{\Omega}_i \leftarrow (1 - \hat{p}^{(k)}(X_i, A_i)) / \hat{p}^{(k)}(X_i, A_i)$ for $i \in \mathcal{I}_{k+1}$
- 9 Normalize: $\hat{\Omega}_{\mathcal{I}_{k+1}} \leftarrow \hat{\Omega}_{\mathcal{I}_{k+1}} / \text{mean}(\hat{\Omega}_{\mathcal{I}_{k+1}})$

10 **end**

// Stage 3: Cross-fitted debiased generator

- 11 **for** $k = 1, 2, 3$ **do**

- 12 Train $\hat{g}^{(k)}$ on $(\mathcal{I}_k, \mathcal{J}_k)$ using $(\hat{R}_{\mathcal{I}_k}, \hat{\Omega}_{\mathcal{I}_k}, \hat{f}^{(k-1)})$ with loss (19)
- 13 Compute $\hat{F}_j \leftarrow \frac{1}{L} \sum_{l=1}^L \hat{f}^{(k-1)}(X_j, \hat{g}^{(k)}(\epsilon_{jl}))$ for $j \in \mathcal{J}_{k+1}$

14 **end**

// Stage 4: Influence function and final estimator

- 15 Let $r = n/N$

- 16 Compute $F_i \leftarrow \hat{\Omega}_i \cdot \hat{R}_i$ for $i = 1, \dots, n$ (source)
 - 17 Compute $F_{n+j} \leftarrow r \cdot \hat{F}_j$ for $j = 1, \dots, N$ (target)
 - 18 Pool data: $X_{pool} \leftarrow [X_S; X_T]$, $F_{pool} \leftarrow [F_1, \dots, F_{n+N}]^\top$
 - 19 Train final estimator $m_{deb}^*(x)$ by regressing F_{pool} on X_{pool} for E_F epochs
-

C Experiment Details

C.1 Simulation Details

C.2 Setting I.

Parameter Details The coefficient matrix $B \in \mathbb{R}^{d_X \times d_A}$ in the conditional model (15) is defined as follows. The first 10 rows (corresponding to X_0, \dots, X_9) are:

$$B_I = \begin{pmatrix} 1.0 & 0.5 & 0.3 & 0.2 & 0.1 \\ 0.8 & 1.0 & 0.4 & 0.1 & 0.2 \\ 0.5 & 0.3 & 1.0 & 0.5 & 0.3 \\ 0.3 & 0.2 & 0.6 & 1.0 & 0.4 \\ 0.2 & 0.4 & 0.2 & 0.3 & 1.0 \\ 0.1 & 0.1 & 0.3 & 0.2 & 0.5 \\ 0.0 & 0.2 & 0.1 & 0.4 & 0.3 \\ 0.1 & 0.0 & 0.2 & 0.1 & 0.2 \\ 0.0 & 0.2 & 0.0 & 0.2 & 0.1 \\ 0.0 & 0.3 & 0.0 & 0.0 & 0.1 \end{pmatrix},$$

and the remaining rows $B_{11:15} = \mathbf{0} \in \mathbb{R}^{5 \times 5}$.

Implementation Details All hyperparameters were selected via grid search using a held-out validation set comprising 20% of the source data (because only source data are labeled). For each method and each hyperparameter configuration, models were trained on the remaining 80% of source data, and the configuration minimizing validation mean squared error was selected. The tuning was performed once on the source data and the selected hyperparameters were held fixed across all perturbation scales and Monte Carlo test datasets.

DRUM methods. For the conditional mean estimator \hat{f}_ψ (shared across DRUM variants): learning rate $\eta_f = 10^{-5}$, $E_f = 100$ epochs, two hidden layers of width 128 with ReLU activations. For DRUM (unconstrained): generator learning rate $\eta_g = 10^{-5}$, $E_g = 300$ epochs, latent dimension $q = 4$, Monte Carlo samples $L = 256$, two hidden layers of width 128. For DRUM: source Engresion trained with learning rate $\eta_{gS} = 5 \times 10^{-4}$, hidden dimension 16, noise dimension 32, $E_{gS} = 500$ epochs; energy-constrained optimization with primal learning rate $\eta_\phi = 2 \times 10^{-4}$, dual learning rate $\eta_\lambda = 10^{-4}$, gradient clipping at 2.0, $\delta = 0.3$, 80 fine-tuning steps. For DRUM-Debiased: density ratio classifier learning rate $\eta_\omega = 10^{-5}$, $E_\omega = 200$ epochs; final estimator learning rate $\eta_F = 10^{-5}$, $E_F = 300$ epochs; three-fold cross-fitting for all nuisance estimates.

Standard baselines. For Baseline-ERM: selected learning rate 10^{-3} , 20 epochs. For Baseline-DRO (Duchi and Namkoong, 2021): selected learning rate 5×10^{-4} , 50 epochs, $\rho = 0.25$. Both use the same architecture as \hat{f}_ψ but take only X as input.

Importance weighting baselines. For IW-KMM, density ratio weights were estimated via kernel

Method	Parameter	Search range
DRUM (unconstrained)	η_f	$\{10^{-6}, 5 \times 10^{-6}, 10^{-5}\}$
	E_f	$\{100, 150, 200\}$
	η_g	$\{5 \times 10^{-5}, 10^{-4}, 5 \times 10^{-4}\}$
	E_g	$\{150, 200, 300\}$
DRUM	δ	$\{0.15, 0.2, 0.3\}$
	η_ϕ	$\{10^{-5}, 10^{-4}, 10^{-3}\}$
	η_λ	$\{10^{-5}, 10^{-4}, 10^{-3}\}$
	hidden dim	$\{4, 8\}$
DRUM-Debiased	η_ω	$\{10^{-5}, 10^{-4}, 10^{-3}\}$
	η_F	$\{10^{-5}, 10^{-4}, 10^{-3}\}$
	E_ω	$\{200, 300\}$
	E_F	$\{200, 300\}$
Baseline-ERM, Baseline-IW-KMM, Baseline-IW-Classify, Baseline-PL+ERM	learning rate	$\{5 \times 10^{-5}, 10^{-4}, 5 \times 10^{-4}, 10^{-3}\}$
	epochs	$\{20, 30, 50\}$
Baseline-DRO, Baseline-PL+DRO	learning rate	$\{5 \times 10^{-5}, 10^{-4}, 5 \times 10^{-4}, 10^{-3}\}$
	epochs	$\{20, 30, 50\}$
	ρ	$\{0.25, 0.5, 0.75, 1.0, 1.25, 1.5\}$

Table 5: Hyperparameter search grids for all methods in Setting I. ERM-based methods search over 12 configurations; DRO-based methods search over 72 configurations.

mean matching (Huang et al., 2006) using a Gaussian kernel with bandwidth selected by the median heuristic, upper bound $B = 1,000$, and constraint tolerance $\epsilon = (\sqrt{m} - 1)/\sqrt{m}$. For IW-Classify, density ratio weights were estimated via a logistic regression classifier trained to distinguish source from target observations using X only. Both methods produce per-observation weights $\hat{w}(x_i)$ that are used to train a weighted MSE regression on source data. The effective sample size ($\text{ESS} = (\sum_i w_i)^2 / \sum_i w_i^2$, measuring the effective number of independent observations after reweighting) was 1,576/4,000 for KMM and 3,539/4,000 for the classifier, indicating moderate weight concentration. Selected hyperparameters: IW-KMM (lr = 10^{-3} , 30 epochs), IW-Classify (lr = 5×10^{-4} , 50 epochs).

Pseudo-label baselines. Target outcomes Y were treated as missing and imputed using source $Y | X$ relationships via three methods: mean imputation, MICE (iterative imputation with Bayesian ridge regression, 20 iterations), and MissForest (iterative imputation with random forests, 100 trees, max depth 10, 25 iterations). The imputed target observations were pooled with source data and used to train $Y \sim X$ models via ERM or DRO, yielding six variants. The imputation hyperparameters were set to standard defaults; tuning these would further favor the pseudo-label baselines.

All models were trained with the Adam optimizer and batch size 128. Prediction samples at test time: $L = 256$ for DRUM (unconstrained), $L = 256$ for DRUM. Table 5 summarizes the hyperparameter search ranges for each method.

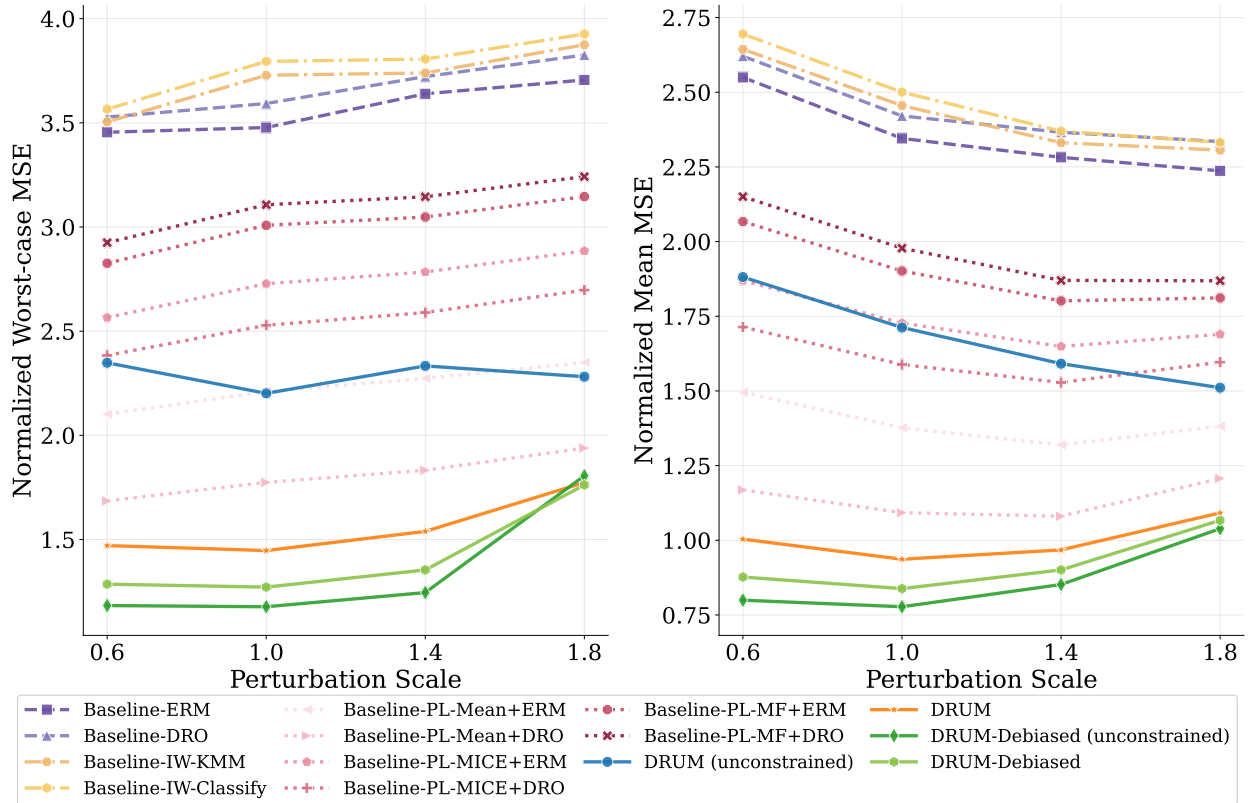


Figure 8: Ablation comparison of all four DRUM variants alongside the standard baselines for Setting I. Results are computed over 100 Monte Carlo test datasets at each scale. MSE is normalized by the source outcome variance $\widehat{\text{Var}}(Y^S)$.

Full Results Figure 8 and Table 6 present the full comparison among all four DRUM variants alongside the standard baselines for Setting I. Among the plug-in estimators, DRUM consistently outperforms DRUM (unconstrained) across all scales, suggesting that preserving the conditional structure $A | X$ during generator training yields a more robust predictor. Both debiased variants outperform their plug-in counterparts at $s \leq 1.4$, with DRUM-Debiased (unconstrained) achieving the best worst-case MSE. At $s = 1.8$, the plug-in DRUM remains competitive while the debiased variants show some degradation.

Table 6: Full numerical results for Setting I: Normalized worst-case and mean MSE across perturbation scales s , for all methods. Results are computed over 100 Monte Carlo test datasets at each scale. MSE is normalized by the source outcome variance $\widehat{\text{Var}}(Y^S)$. Best performance in each column is in bold.

Method	Normalized Worst-case MSE			
	$s=0.6$	$s=1.0$	$s=1.4$	$s=1.8$
Baseline-ERM	3.455	3.478	3.639	3.706
Baseline-DRO	3.527	3.593	3.722	3.826
Baseline-IW-KMM	3.505	3.728	3.740	3.875
Baseline-IW-Classify	3.566	3.795	3.806	3.926
Baseline-PL-Mean+ERM	2.102	2.210	2.274	2.349
Baseline-PL-Mean+DRO	1.685	1.774	1.832	1.939
Baseline-PL-MICE+ERM	2.565	2.728	2.784	2.885
Baseline-PL-MICE+DRO	2.384	2.528	2.589	2.697
Baseline-PL-MF+ERM	2.826	3.008	3.048	3.146
Baseline-PL-MF+DRO	2.925	3.107	3.145	3.242
DRUM (unconstrained)	2.348	2.201	2.333	2.281
DRUM	1.471	1.447	1.539	1.774
DRUM-Debiased (unconstrained)	1.183	1.177	1.245	1.806
DRUM-Debiased	1.286	1.271	1.354	1.762

Method	Normalized Mean MSE			
	$s=0.6$	$s=1.0$	$s=1.4$	$s=1.8$
Baseline-ERM	2.550	2.345	2.282	2.237
Baseline-DRO	2.621	2.421	2.366	2.335
Baseline-IW-KMM	2.644	2.455	2.331	2.306
Baseline-IW-Classify	2.695	2.500	2.370	2.332
Baseline-PL-Mean+ERM	1.495	1.377	1.319	1.382
Baseline-PL-Mean+DRO	1.169	1.092	1.081	1.207
Baseline-PL-MICE+ERM	1.870	1.727	1.649	1.690
Baseline-PL-MICE+DRO	1.714	1.589	1.528	1.596
Baseline-PL-MF+ERM	2.067	1.902	1.802	1.811
Baseline-PL-MF+DRO	2.150	1.978	1.870	1.869
DRUM (unconstrained)	1.881	1.712	1.591	1.511
DRUM	1.004	0.937	0.968	1.092
DRUM-Debiased (unconstrained)	0.800	0.777	0.852	1.039
DRUM-Debiased	0.877	0.838	0.901	1.067

C.3 Setting II

Parameter Details The coefficient matrix $B \in \mathbb{R}^{d_X \times d_A}$ in the conditional model (17) is defined as follows. The first 10 rows (corresponding to X_0, \dots, X_9) are:

$$B_{II} = \begin{pmatrix} 1.0 & 0.5 & 0.3 & 0.2 & 0.1 \\ 0.8 & 1.0 & 0.4 & 0.1 & 0.2 \\ 0.5 & 0.3 & 1.0 & 0.5 & 0.3 \\ 0.3 & 0.2 & 0.6 & 1.0 & 0.4 \\ 0.2 & 0.4 & 0.2 & 0.3 & 1.0 \\ 0.1 & 0.1 & 0.3 & 0.2 & 0.5 \\ 0.0 & 0.2 & 0.1 & 0.4 & 0.3 \\ 0.1 & 0.0 & 0.2 & 0.1 & 0.2 \\ 0.0 & 0.2 & 0.0 & 0.2 & 0.1 \\ 0.0 & 0.3 & 0.0 & 0.0 & 0.1 \\ 0.3 & 0.2 & 0.2 & 0.0 & 0.4 \\ 0.1 & 0.4 & 0.0 & 0.3 & 0.1 \\ 0.0 & 0.2 & 0.3 & 0.1 & 0.2 \\ 0.2 & 0.0 & 0.1 & 0.4 & 0.0 \\ 0.1 & 0.3 & 0.2 & 0.0 & 0.3 \\ 0.0 & 0.0 & 0.0 & 0.0 & 0.0 \end{pmatrix}$$

Implementation Details All DRUM methods use the same hyperparameter search procedure as Setting I. For a simplified fair comparison, the two original baselines use fixed hyperparameters: Baseline-ERM with learning rate 10^{-3} , 50 epochs; Baseline-DRO with learning rate 10^{-3} , 50 epochs, $\rho = 0.5$. Both use the same architecture as \hat{f}_ψ but take only X as input.

For the additional baselines, the same tuning grids as Setting I (Table 5) were used, with hyperparameters selected by validation MSE on held-out source data. Selected hyperparameters: IW-KMM (lr = 10^{-3} , 50 epochs), IW-Classify (lr = 10^{-3} , 50 epochs), PL-Mean+ERM (lr = 10^{-3} , 20 epochs), PL-Mean+DRO (lr = 10^{-3} , 20 epochs, $\rho = 0.25$), PL-MICE+ERM (lr = 10^{-3} , 30 epochs), PL-MICE+DRO (lr = 10^{-3} , 30 epochs, $\rho = 0.25$), PL-MF+ERM (lr = 10^{-3} , 50 epochs), PL-MF+DRO (lr = 10^{-3} , 50 epochs, $\rho = 0.25$). All DRO pseudo-label variants selected the minimum $\rho = 0.25$, indicating negligible benefit from the DRO penalty on pooled imputed data.

Full Results Figure 9 and Table 7 present the full comparison among all four DRUM variants alongside the standard baselines for Setting II.

Table 7: Full numerical results for Setting II: Normalized worst-case and mean MSE across perturbation scales s , for all methods. Results are computed over 100 Monte Carlo test datasets at each scale. MSE is normalized by the source outcome variance $\widehat{\text{Var}}(Y^S)$. Best performance in each column is in bold.

Method	Normalized Worst-case MSE			
	$s=0.6$	$s=1.0$	$s=1.4$	$s=1.8$
Baseline-ERM	4.292	4.982	4.700	4.881
Baseline-DRO	4.339	5.026	4.736	4.918
Baseline-IW-KMM	3.845	4.439	4.998	5.200
Baseline-IW-Classify	3.862	4.458	5.015	5.213
Baseline-PL-Mean+ERM	2.179	2.642	3.069	3.244
Baseline-PL-Mean+DRO	2.159	2.621	3.045	3.219
Baseline-PL-MICE+ERM	2.349	2.817	3.248	3.421
Baseline-PL-MICE+DRO	2.337	2.803	3.229	3.400
Baseline-PL-MF+ERM	3.429	4.039	4.573	4.746
Baseline-PL-MF+DRO	3.410	4.017	4.549	4.721
DRUM (unconstrained)	1.632	2.020	2.784	2.590
DRUM	1.580	2.010	2.276	2.424
DRUM-Debiased (unconstrained)	1.407	1.822	2.381	2.584
DRUM-Debiased	1.921	2.396	2.173	2.407

Method	Normalized Mean MSE			
	$s=0.6$	$s=1.0$	$s=1.4$	$s=1.8$
Baseline-ERM	2.724	2.580	2.544	2.633
Baseline-DRO	2.766	2.613	2.570	2.639
Baseline-IW-KMM	2.623	2.588	2.521	2.544
Baseline-IW-Classify	2.638	2.605	2.538	2.559
Baseline-PL-Mean+ERM	1.362	1.382	1.401	1.529
Baseline-PL-Mean+DRO	1.347	1.368	1.389	1.518
Baseline-PL-MICE+ERM	1.481	1.488	1.491	1.608
Baseline-PL-MICE+DRO	1.473	1.480	1.484	1.601
Baseline-PL-MF+ERM	2.269	2.234	2.171	2.215
Baseline-PL-MF+DRO	2.253	2.219	2.158	2.203
DRUM (unconstrained)	1.058	1.069	1.159	1.321
DRUM	0.879	0.891	0.999	1.188
DRUM-Debiased (unconstrained)	0.780	0.807	0.931	1.143
DRUM-Debiased	1.095	1.082	1.171	1.347

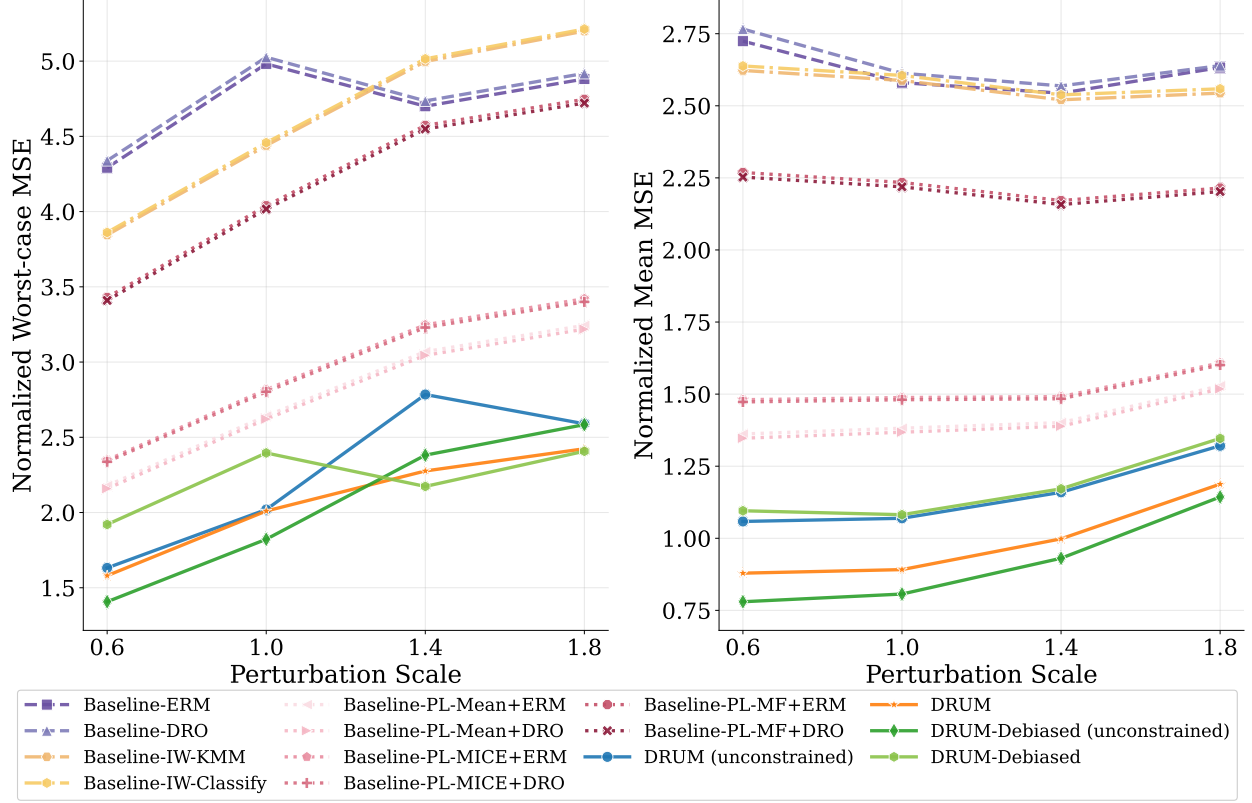


Figure 9: Ablation comparison of all four DRUM variants alongside the standard baselines for Setting II. Results are computed over 100 Monte Carlo test datasets at each scale. MSE is normalized by the source outcome variance $\widehat{\text{Var}}(Y^S)$.

C.4 Setting III

Parameter Details The coefficient matrix $B \in \mathbb{R}^{d_X \times d_A}$ in the conditional model (17) for setting III is defined as follows:

$$B_{III} = \begin{pmatrix} 1.0 & 0.5 & 0.3 & 0.2 & 0.1 & 0.4 & 0.2 & 0.1 & 0.3 & 0.2 \\ 0.4 & 1.0 & 0.4 & 0.1 & 0.2 & 0.3 & 0.5 & 0.2 & 0.1 & 0.1 \\ 0.5 & 0.3 & 1.0 & 0.5 & 0.3 & 0.2 & 0.1 & 0.4 & 0.2 & 0.3 \\ 0.3 & 0.2 & 0.6 & 1.0 & 0.4 & 0.1 & 0.3 & 0.5 & 0.1 & 0.2 \\ 0.2 & 0.4 & 0.2 & 0.3 & 1.0 & 0.3 & 0.2 & 0.1 & 0.5 & 0.4 \\ 0.1 & 0.1 & 0.3 & 0.2 & 0.5 & 1.0 & 0.4 & 0.3 & 0.2 & 0.1 \\ 0.0 & 0.2 & 0.1 & 0.4 & 0.3 & 0.3 & 1.0 & 0.2 & 0.4 & 0.2 \\ 0.1 & 0.0 & 0.2 & 0.1 & 0.2 & 0.2 & 0.3 & 1.0 & 0.1 & 0.3 \\ 0.0 & 0.2 & 0.0 & 0.2 & 0.1 & 0.1 & 0.2 & 0.3 & 1.0 & 0.2 \\ 0.0 & 0.3 & 0.0 & 0.0 & 0.1 & 0.2 & 0.1 & 0.2 & 0.3 & 1.0 \\ 0.3 & 0.2 & 0.2 & 0.0 & 0.4 & 0.1 & 0.0 & 0.1 & 0.2 & 0.3 \\ 0.1 & 0.4 & 0.0 & 0.3 & 0.1 & 0.2 & 0.1 & 0.0 & 0.1 & 0.2 \\ 0.0 & 0.2 & 0.3 & 0.1 & 0.2 & 0.0 & 0.2 & 0.1 & 0.0 & 0.1 \\ 0.2 & 0.0 & 0.1 & 0.4 & 0.0 & 0.1 & 0.0 & 0.2 & 0.1 & 0.0 \\ 0.1 & 0.3 & 0.2 & 0.0 & 0.3 & 0.0 & 0.1 & 0.0 & 0.2 & 0.1 \\ 0.0 & 0.0 & 0.0 & 0.0 & 0.0 & 0.0 & 0.0 & 0.0 & 0.0 & 0.0 \end{pmatrix}$$

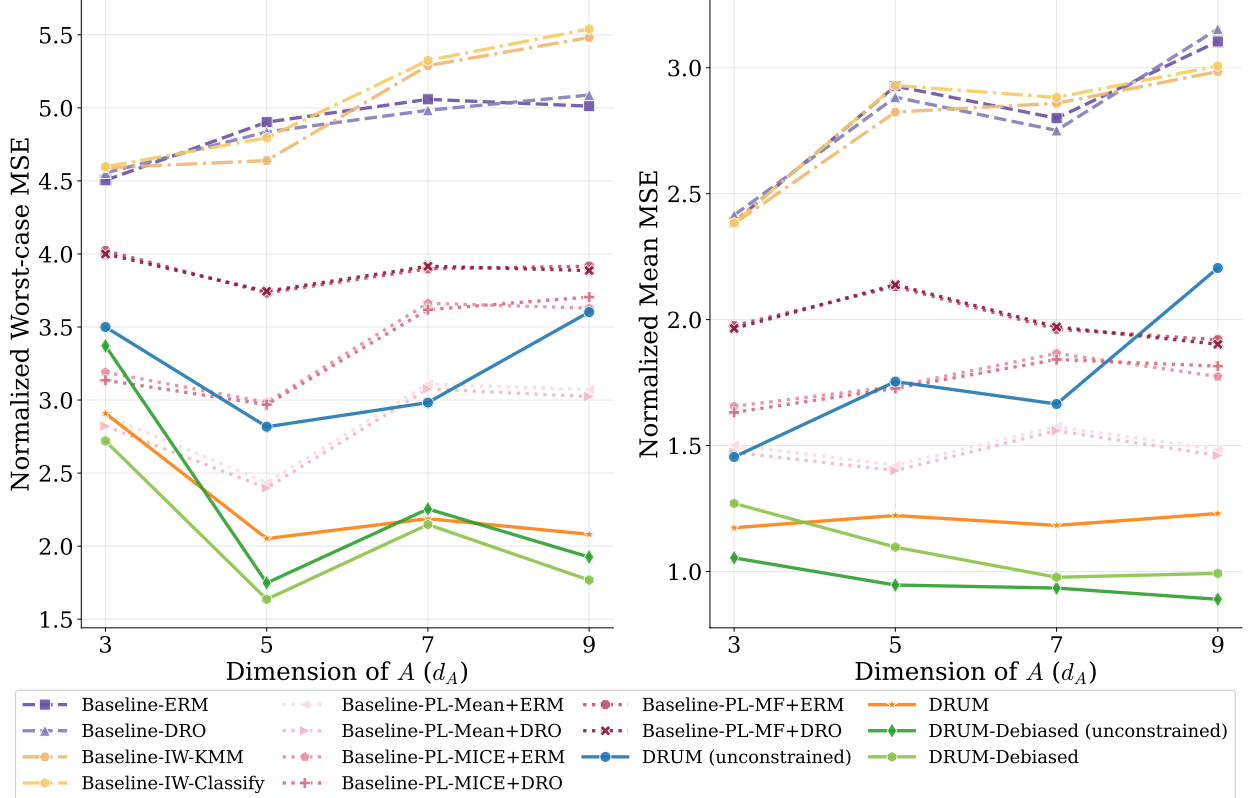


Figure 10: Ablation comparison of all four DRUM variants alongside the standard baselines for Setting III. Results are computed over 100 Monte Carlo test datasets at each scale. MSE is normalized by the source outcome variance $\widehat{\text{Var}}(Y^S)$.

Implementation Details For the DRUM variants, all hyperparameters are kept fixed (identical to Setting II) across d_A , adjusting only the generator latent dimension as $q = \max(4, d_A)$. For the original baselines (ERM and DRO), a grid search over network architecture, learning rate, and regularization parameters is performed at each d_A to ensure a fair comparison as problem complexity increases (Table 9). For the additional baselines (IW-KMM, IW-Classify, and all pseudo-label variants), the same tuning grids as Settings I and II (Table 5) were used with a fixed [128, 128] architecture, and hyperparameters were re-tuned at each d_A . Across all d_A values, the IW and pseudo-label baselines consistently selected $\text{lr} = 10^{-3}$ with epochs between 20 and 50; all DRO pseudo-label variants selected $\rho = 0.25$ (with a single exception of $\rho = 0.5$ for PL-MICE+DRO at $d_A = 9$), suggesting the negligible benefit of the DRO penalty observed in Settings I and II.

Full Results Figure 10 and Table 8 present the full comparison among all four DRUM variants alongside the standard baselines for Setting III.

Table 8: Full numerical results for Setting III: Normalized worst-case and mean MSE across dimensions d_A with fixed perturbation scale $s = 1.8$. Results are computed over 100 Monte Carlo test datasets at each dimension. MSE is normalized by the source outcome variance $\widehat{\text{Var}}(Y^{\mathcal{S}})$. Best performance in each column is in bold.

Method	Normalized Worst-case MSE			
	$d_A=3$	$d_A=5$	$d_A=7$	$d_A=9$
Baseline-ERM	4.504	4.902	5.058	5.012
Baseline-DRO	4.555	4.835	4.984	5.088
Baseline-IW-KMM	4.590	4.639	5.290	5.481
Baseline-IW-Classify	4.597	4.795	5.325	5.540
Baseline-PL-Mean+ERM	2.895	2.434	3.109	3.072
Baseline-PL-Mean+DRO	2.822	2.398	3.076	3.023
Baseline-PL-MICE+ERM	3.191	2.984	3.662	3.629
Baseline-PL-MICE+DRO	3.135	2.969	3.619	3.705
Baseline-PL-MF+ERM	4.023	3.734	3.898	3.916
Baseline-PL-MF+DRO	4.000	3.745	3.916	3.886
DRUM (unconstrained)	3.500	2.817	2.983	3.602
DRUM	2.909	2.052	2.188	2.081
DRUM-Debiased (unconstrained)	3.371	1.748	2.255	1.925
DRUM-Debiased	2.720	1.636	2.148	1.768

Method	Normalized Mean MSE			
	$d_A=3$	$d_A=5$	$d_A=7$	$d_A=9$
Baseline-ERM	2.387	2.927	2.799	3.104
Baseline-DRO	2.415	2.883	2.751	3.154
Baseline-IW-KMM	2.381	2.824	2.859	2.985
Baseline-IW-Classify	2.384	2.929	2.882	3.007
Baseline-PL-Mean+ERM	1.502	1.422	1.575	1.485
Baseline-PL-Mean+DRO	1.473	1.401	1.559	1.461
Baseline-PL-MICE+ERM	1.655	1.735	1.866	1.774
Baseline-PL-MICE+DRO	1.632	1.727	1.842	1.815
Baseline-PL-MF+ERM	1.976	2.131	1.962	1.920
Baseline-PL-MF+DRO	1.965	2.138	1.971	1.902
DRUM (unconstrained)	1.455	1.754	1.665	2.205
DRUM	1.174	1.222	1.183	1.230
DRUM-Debiased (unconstrained)	1.054	0.946	0.934	0.889
DRUM-Debiased	1.270	1.097	0.977	0.992

Method	Parameter	Search range
Baseline-ERM	architecture	[128, 128], [256, 128], [128, 128, 64], [256, 256, 128]*
	learning rate	$\{5 \times 10^{-5}, 10^{-4}, 5 \times 10^{-4}, 10^{-3}\}$
	epochs	{20, 30, 50}
Baseline-DRO	architecture	[128, 128], [256, 128], [128, 128, 64], [256, 256, 128]*
	learning rate	$\{5 \times 10^{-5}, 10^{-4}, 5 \times 10^{-4}, 10^{-3}\}$
	epochs	{20, 30, 50}
	ρ	{0.25, 0.5, 0.75, 1.0, 1.25, 1.5}
All ERM baselines [†]	learning rate	$\{5 \times 10^{-5}, 10^{-4}, 5 \times 10^{-4}, 10^{-3}\}$
	epochs	{20, 30, 50}
All DRO baselines [†]	learning rate	$\{5 \times 10^{-5}, 10^{-4}, 5 \times 10^{-4}, 10^{-3}\}$
	epochs	{20, 30, 50}
	ρ	{0.25, 0.5, 0.75, 1.0, 1.25, 1.5}

Table 9: Hyperparameter search grids for Setting III. Baseline-ERM and Baseline-DRO include architecture search; all other baselines use a fixed [128, 128] architecture. *[256, 256, 128] included only for $d_A \geq 8$. [†]IW-KMM, IW-Classify, and all PL variants.

C.5 Real-world Data Experiment details

Data Details The source population comprised out-of-hospital cardiac arrest (OHCA) patients treated by emergency medical services (EMS) providers, as recorded in the Resuscitation Outcomes Consortium (ROC) Cardiac Epidemiologic Registry (Epistry) (Version 3, covering the period from April 1, 2011, to June 30, 2015). The ROC, a North American database established in 2004, aims to advance clinical research on cardiopulmonary arrest. Ethical approval was obtained from the National University of Singapore Institutional Review Board (IRB), which granted an exemption for this study (IRB Reference Number: NUS-IRB-2023-451).

The Pan-Asian Resuscitation Outcomes Study (PAROS) data were approved by the relevant ethics committees at each participating site and by the Centralized Institutional Review Board and Domain Specific Review Board for Singapore (reference numbers: 2010-270-C, C-10-545, 2013/604/C, and 2013/00929). Informed consent was waived for both datasets due to the retrospective, observational nature of the study, and all data were de-identified prior to analysis.

The target population comprised adult OHCA patients recorded in the PAROS database from April 2010 to December 2016 in Singapore, January 2011 to December 2014 in South Korea, January 2009 to December 2014 in Japan and August 2014 to March 2018 in Vietnam. The Vietnamese cohort ($n = 235$, 5 favorable outcomes) is included as supplementary validation in this appendix but excluded from the main analysis due to insufficient positive events for reliable metric estimation. With only 5 outcomes, calibration estimates and classification comparisons lack statistical power, and performance differences between methods cannot be meaningfully assessed. Nonetheless, the DRUM pipeline (generator training, bias correction, and prediction) runs without modification on this cohort, confirming that the framework remains operationally stable for deployment at sites

with very small sample sizes.

For cohort formation, we retained adult patients (aged 18 and older) with known sex, determinable initial cardiac rhythm, and non-missing values for all shared covariates. Continuous variables were standardized using source population statistics. We note that EMS response time is recorded at some PAROS sites, though not uniformly across all deployment populations. Because epinephrine dose and blood pH are consistently absent across all PAROS sites, and our framework requires a common set of structurally missing covariates across deployment populations, we treat all three prehospital variables as structurally missing for consistency.

Table 10 presents baseline characteristics across all study populations. Several notable differences are apparent. The source population (US-ROC) was younger on average (mean age 63.8 years) compared to the Asian populations, with Japan having the oldest patients (mean age 72.4 years). The rate of shockable initial rhythm was highest in the US (43.4%) and lowest in Vietnam (5.1%). Favorable neurological outcome rates varied substantially, from 2.1% in Vietnam to 19.3% in the source US population and 3.1% in the target Singapore population. These differences in outcome rates and covariate distributions across populations illustrate the challenge of cross-regional clinical prediction and the need for robust ML methods.

Hyperparameter Fine-tuning For the DRUM variants, we use the same three-stage estimation procedure described in Section 4. The primary hyperparameter ranges were taken from the simulation experiments. In the retrospective OHCA benchmark, a held-out 20% Singapore subset was used only to confirm the final choice within this narrow prespecified grid, using Brier score as the criterion. The selected values were identical or close to the simulation-default values.

In Stage 1, we fix the outcome model \hat{f} (trained on source data) and tune the unconstrained generator, general generator (Engression), and baseline parameters independently. In Stage 2, we fix the best Engression configuration from Stage 1 and tune only the debiasing parameters (density ratio and final estimator). The density ratio $\hat{\omega}$ was estimated via probabilistic classification within each cross-fitting fold (Algorithm 4). Weights were clipped to satisfy Assumption 4 and then normalized to unit mean within each fold, mitigating instability from regions of poor overlap between the source and generator-induced distributions. External sites (Japan, Korea, Vietnam) were never used during hyperparameter selection.

Table 11 summarizes the search grids for all methods. Pseudo-label baselines (PL-Mean, PL-MICE, PL-MissForest, each with ERM and DRO) use the same architecture and tuning grids as Baseline-ERM and Baseline-DRO respectively, trained on the pooled source and imputed target data. IW-KMM uses Gaussian kernel with bandwidth $\sigma = 1.277$ (median heuristic), $B = 1,000$, $ESS = 4,355/7,793$. IW-Classify uses logistic regression with domain classification $AUC = 0.649$, $ESS = 6,049/7,793$.

Full Results The full Brier score and calibration plots with all 14 methods, for all four sites (Singapore, Korea, Japan and Vietnam) are shown in Figures 11 and 12.

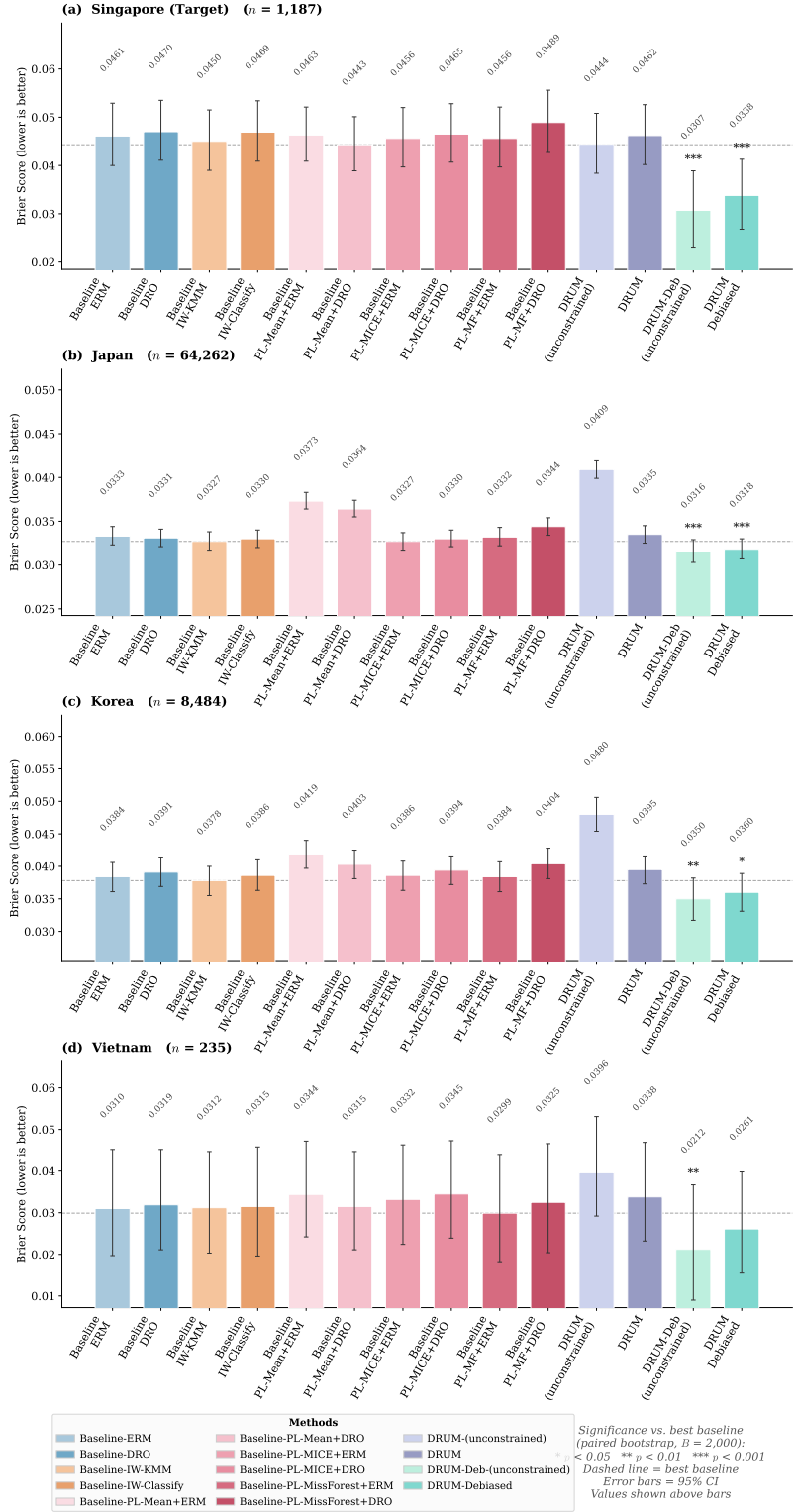


Figure 11: Brier score of all methods across four OHCA populations. Bars show Brier scores (lower is better) with 95% bootstrap CIs for all baselines and four DRUM variants.

Table 10: Baseline characteristics of the OHCA study populations. Continuous variables are presented as mean (SD) or median [IQR]; categorical variables as n (%). The prehospital care variables (A) were available only in the US-ROC source data.

		Source	Target	External		
		US-ROC $n = 9,755$	Singapore $n = 5,933$	Japan $n = 64,262$	Korea $n = 8,484$	Vietnam $n = 235$
<i>Stable covariates (X)</i>						
Age, mean (SD)		63.8 (16.0)	65.2 (18.4)	72.4 (18.3)	64.6 (19.1)	54.6 (17.9)
Sex, n (%)	Female	3,427 (35.1)	2,072 (34.9)	27,460 (42.7)	3,079 (36.3)	60 (25.5)
	Male	6,328 (64.9)	3,861 (65.1)	36,802 (57.3)	5,405 (63.7)	175 (74.5)
Rhythm, n (%)	Non-shock.	5,519 (56.6)	4,901 (82.6)	59,795 (93.0)	7,284 (85.9)	223 (94.9)
	Shockable	4,236 (43.4)	1,032 (17.4)	4,467 (7.0)	1,200 (14.1)	12 (5.1)
Witness/CPR, n (%)	No/No	1,869 (19.2)	1,354 (22.8)	21,706 (33.8)	2,498 (29.4)	59 (25.1)
	No/Yes	1,503 (15.4)	1,057 (17.8)	15,829 (24.6)	1,535 (18.1)	2 (0.9)
	Yes/No	2,351 (24.1)	1,475 (24.9)	11,530 (17.9)	1,862 (21.9)	103 (43.8)
	Yes/Yes	4,032 (41.3)	2,047 (34.5)	15,197 (23.6)	2,589 (30.5)	71 (30.2)
<i>Missing covariates (A, source only)</i>						
Response time (min)		5.40 [4.15, 6.90]	—	—	—	—
Epinephrine dose (mg)		2.00 [1.00, 3.00]	—	—	—	—
Blood pH		7.18 [7.02, 7.29]	—	—	—	—
<i>Outcome (Y)</i>						
Neuro outcome, n (%)	Good	1,885 (19.3)	183 (3.1)	2,217 (3.4)	354 (4.2)	5 (2.1)
	Poor	7,870 (80.7)	5,750 (96.9)	62,045 (96.6)	8,130 (95.8)	230 (97.9)

Discrimination Analysis Figure 13 and 14 present the overall AUROC and AUPRC values. For both metrics, DRUM variants achieve comparable performance on smaller samples (Singapore, Vietnam), with modest reductions on large-sample sites where statistical power detects small absolute differences, consistent with DRUM targeting calibration rather than discrimination.

Table 12 evaluates classification performance at fixed probability cutoffs $t \in \{0.03, 0.05, 0.10, 0.15\}$, which correspond to clinically meaningful decision thresholds near the observed outcome prevalence in the four Asian OHCA populations (2–4%). In practice, a clinician or risk stratification system may flag patients with predicted probability exceeding a threshold t for prioritized intervention; the choice of t reflects the desired trade-off between identifying high-risk patients and limiting false alarms.

DRUM-Debiased (unconstrained) achieves the highest precision and specificity at every cutoff and site examined, and the highest F1 at all sites for $t \leq 0.10$. Baselines achieve higher recall at all cutoffs, which is a direct consequence of miscalibration: because baseline methods systematically over-predict outcome probabilities in these low-prevalence populations, a larger proportion of patients, including most true positives, receive predicted probabilities exceeding any fixed thresh-

Table 11: Hyperparameter search grids for the OHCA application. DRUM hyperparameters were initially guided by simulation settings and adjusted based on preliminary source validation; final values were confirmed on a held-out Singapore subset. Baseline hyperparameters were selected via source validation. External sites (Japan, Korea, Vietnam) were never used during any training or selection step.

Method	Parameter	Search range	Selected
Outcome model \hat{f}	learning rate	$\{10^{-5}, 10^{-4}\}$	10^{-5}
	epochs	$\{50, 100, 200\}$	50
Unconstrained generator	learning rate	$\{5 \times 10^{-5}, 10^{-4}, 5 \times 10^{-4}\}$	5×10^{-5}
	epochs	$\{100, 150, 200\}$	150
General generator	δ	$\{0.05, 0.1, 0.15, 0.2, 0.3, 0.5\}$	0.3
	hidden dim	$\{4, 8, 16\}$	4
	noise dim	$\{4, 8, 16\}$	8
	$\text{lr}_{\text{primal}}$	$\{10^{-5}, 10^{-4}, 10^{-3}\}$	10^{-5}
	lr_{dual}	$\{10^{-5}, 10^{-4}, 10^{-3}\}$	10^{-4}
	Engression epochs	$\{200, 300\}$	200
Debiased (unconstrained & general)	finetune steps	$\{80, 150, 250\}$	150
	lr_{ω}	$\{10^{-5}, 10^{-4}, 5 \times 10^{-4}, 10^{-3}\}$	10^{-4}
	lr_{F_x}	$\{10^{-5}, 10^{-4}, 5 \times 10^{-4}, 10^{-3}\}$	10^{-4}
	ω epochs	$\{100, 200, 300\}$	300
	F_x epochs	$\{100, 200, 300\}$	300
Baseline-ERM	architecture	$[64, 64], [128, 128], [128, 64]$	$[64, 64]$
	learning rate	$\{10^{-4}, 5 \times 10^{-4}, 10^{-3}\}$	10^{-4}
	epochs	$\{30, 50, 100\}$	30
Baseline-DRO	architecture	$[64, 64], [128, 128], [128, 64]$	$[64, 64]$
	learning rate	$\{10^{-4}, 5 \times 10^{-4}, 10^{-3}\}$	10^{-3}
	epochs	$\{30, 50, 100\}$	100
	ρ	$\{0.25, 0.5, 1.0\}$	0.5
IW-KMM	architecture	$[64, 64], [128, 128], [128, 64]$	$[128, 64]$
	learning rate	$\{10^{-4}, 5 \times 10^{-4}, 10^{-3}\}$	5×10^{-4}
	epochs	$\{30, 50, 100\}$	30
IW-Classify	architecture	$[64, 64], [128, 128], [128, 64]$	$[128, 128]$
	learning rate	$\{10^{-4}, 5 \times 10^{-4}, 10^{-3}\}$	5×10^{-4}
	epochs	$\{30, 50, 100\}$	100

old. This inflates sensitivity but at the cost of many false positives, resulting in lower precision and specificity. DRUM-Debiased produces well-calibrated probabilities concentrated near the true prevalence, so fewer patients exceed a given threshold, but those who do are substantially more likely to be true positives.

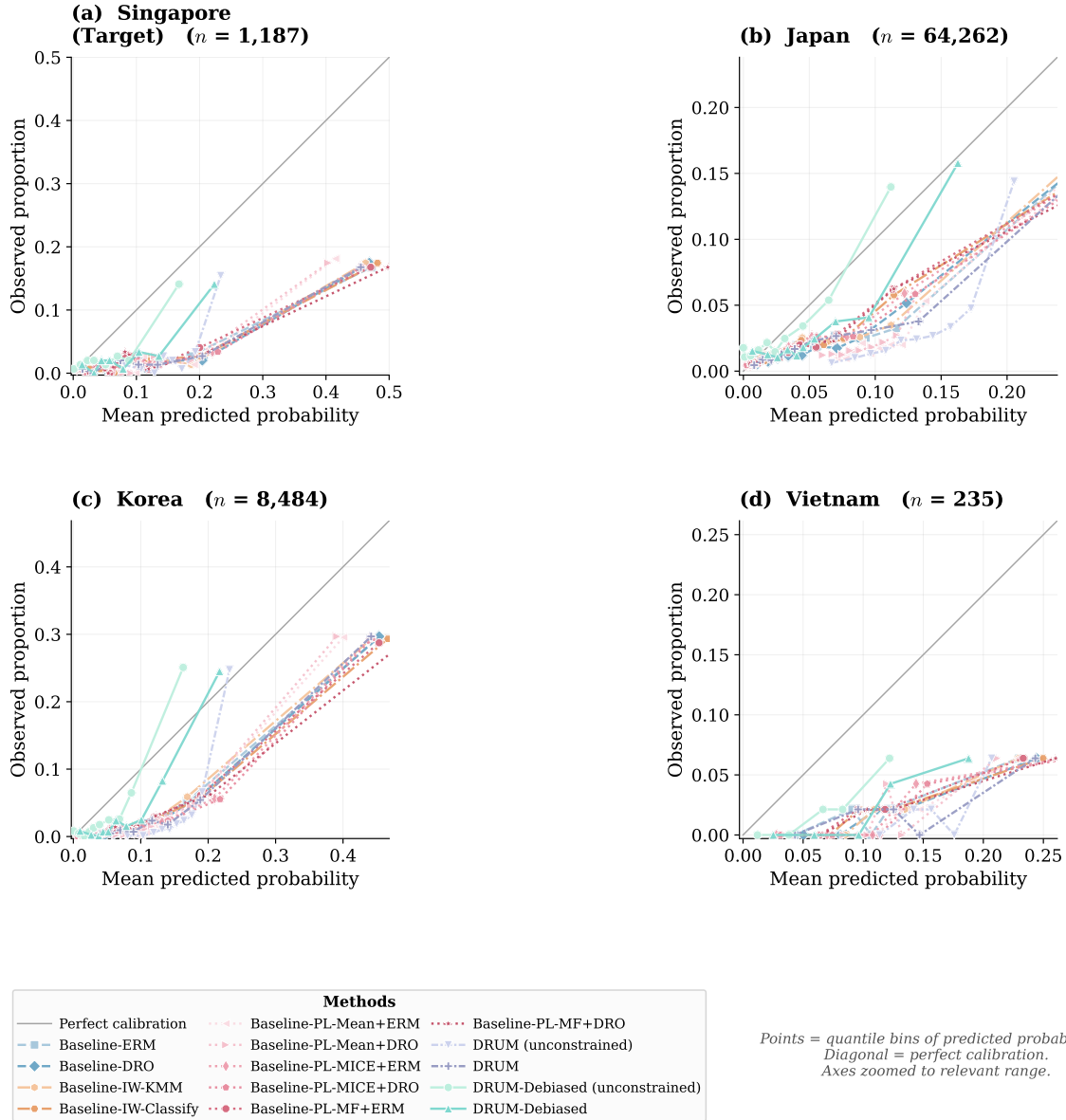
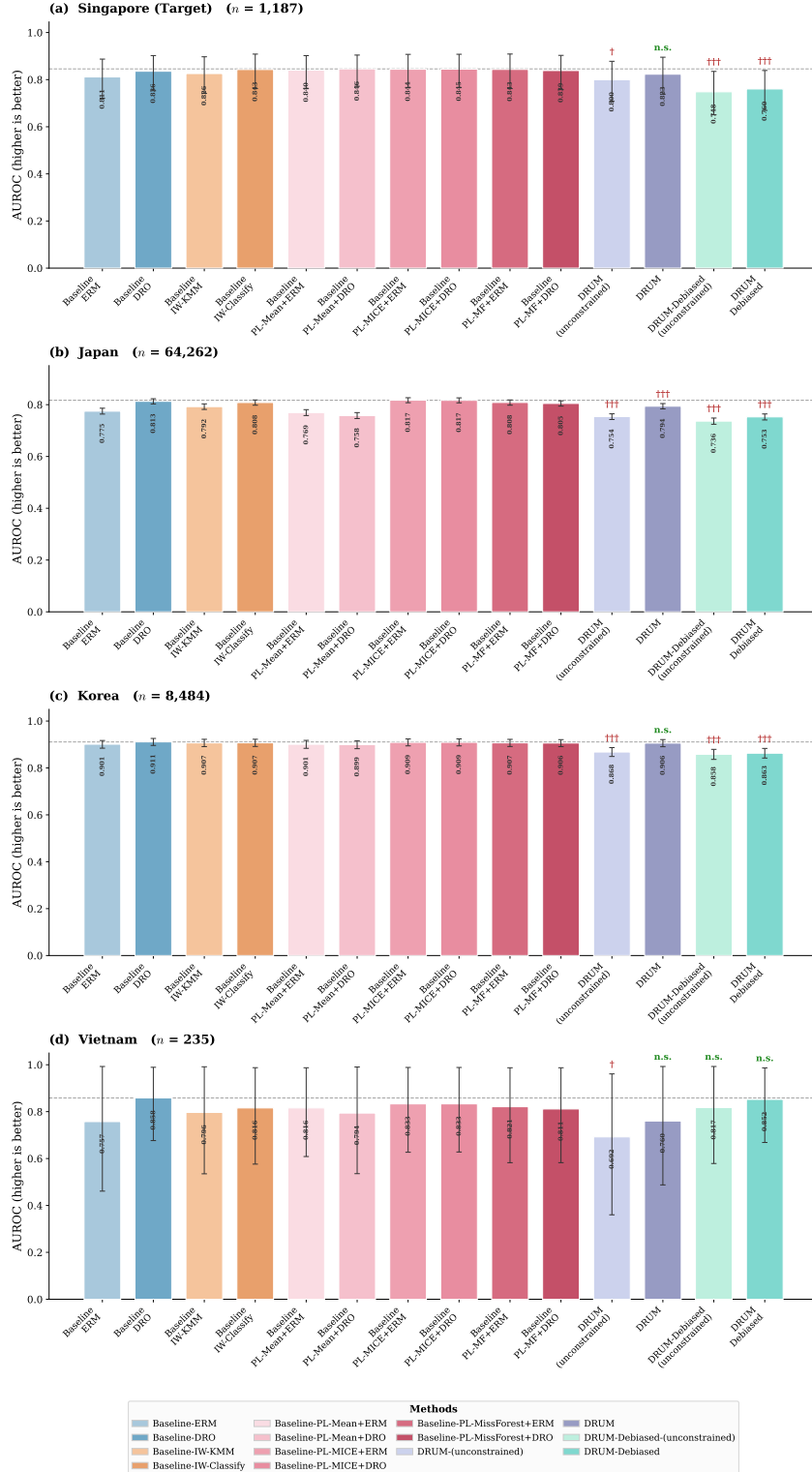


Figure 12: Calibration plots of all methods across four OHCA populations. Points show mean predicted probability vs observed proportion in quantile bins (axes truncated for visibility). Diagonal = perfect calibration.



vs. best baseline (paired bootstrap, B=2,000): * ($p < 0.05$) ** ($p < 0.01$) *** ($p < 0.001$) | † worse ($p < 0.05$) †† ($p < 0.01$) ††† ($p < 0.001$) | n.s. = not significant | Dashed line = best baseline | Error bars = 95% CI

Figure 13: AUROC across all four Asian OHCA populations. Bars show AUROC (higher is better) with 95% bootstrap CIs. Dashed line = best baseline. Annotations: n.s. = not significantly different from the best baseline ($p \geq 0.05$); † = significantly worse (paired bootstrap, B = 2,000).

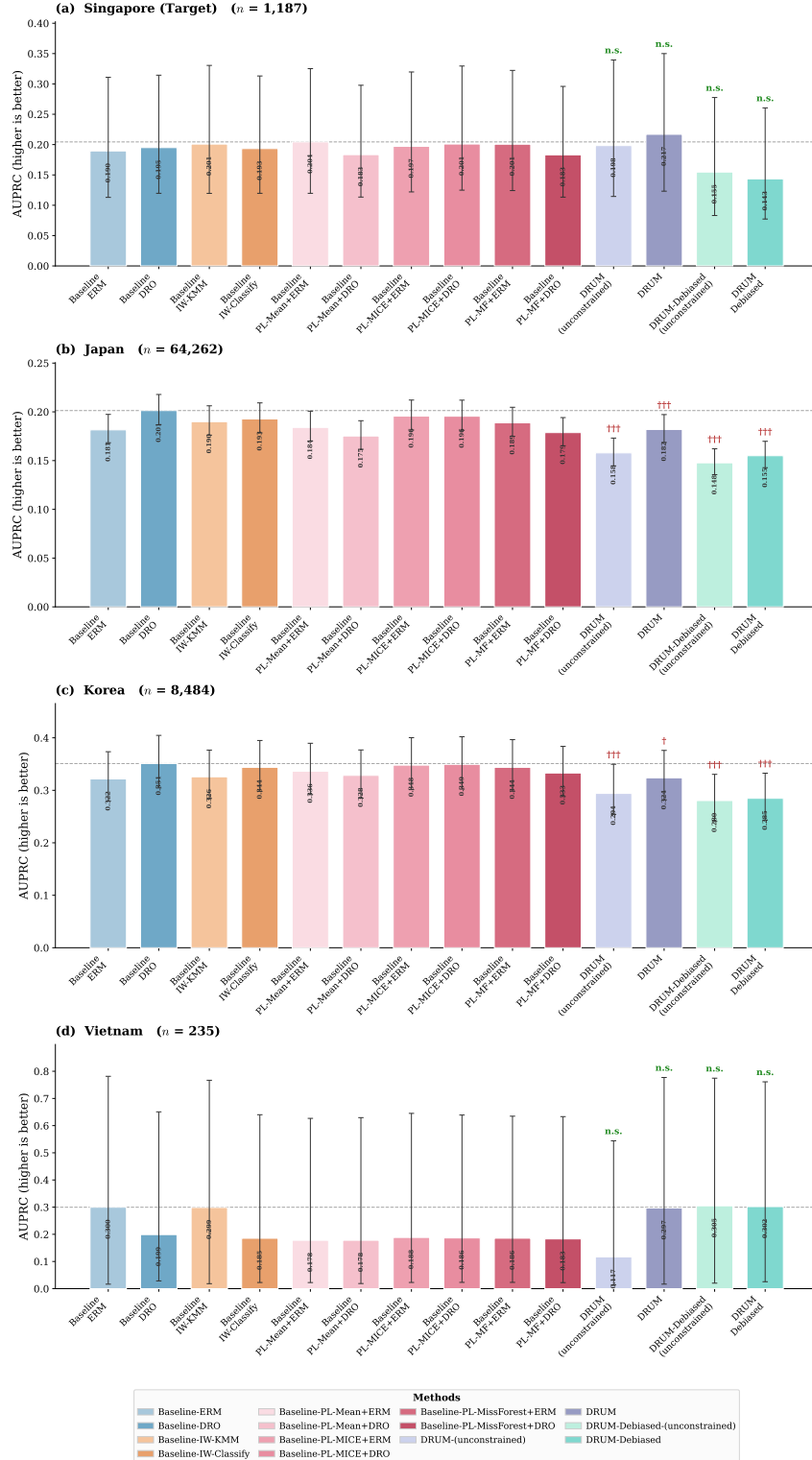


Figure 14: AUPRC across four Asian OHCA populations. Bars show AUPRC (higher is better) with 95% bootstrap CIs. Dashed line = best baseline. Annotations: n.s. = not significantly different from the best baseline ($p \geq 0.05$); † = significantly worse (paired bootstrap, $B = 2,000$).

Table 12: Classification performance at fixed probability cutoffs across four OHCA populations. Best baseline is selected per site from all 10 baselines (oracle selection). Bold indicates the best value across all methods at each site.

t	Method	F1 Score				Precision				Recall				Specificity			
		<i>Singapore</i>	<i>Japan</i>	<i>Korea</i>	<i>Vietnam</i>	<i>Singapore</i>	<i>Japan</i>	<i>Korea</i>	<i>Vietnam</i>	<i>Singapore</i>	<i>Japan</i>	<i>Korea</i>	<i>Vietnam</i>	<i>Singapore</i>	<i>Japan</i>	<i>Korea</i>	<i>Vietnam</i>
0.03	Best BL*	0.084	0.115	0.110	0.046	0.044	0.062	0.058	0.024	1.000	1.000	1.000	1.000	0.279	0.528	0.305	0.100
	DRUM-U	0.064	0.067	0.080	0.042	0.033	0.034	0.042	0.021	1.000	1.000	1.000	1.000	0.000	0.000	0.000	0.000
	DRUM	0.075	0.094	0.095	0.044	0.039	0.050	0.050	0.022	0.974	0.913	0.997	1.000	0.182	0.373	0.176	0.048
	DRUM-Deb-U	0.084	0.123	0.133	0.055	0.045	0.068	0.071	0.028	0.795	0.701	0.932	1.000	0.422	0.655	0.472	0.257
	DRUM-Deb	0.071	0.084	0.095	0.046	0.037	0.044	0.050	0.023	0.949	0.886	0.977	1.000	0.164	0.315	0.186	0.096
0.05	Best BL*	0.096	0.140	0.135	0.052	0.051	0.074	0.073	0.027	1.000	0.999	1.000	1.000	0.413	0.658	0.455	0.209
	DRUM-U	0.064	0.067	0.080	0.042	0.033	0.034	0.042	0.021	1.000	0.999	1.000	1.000	0.003	0.004	0.001	0.000
	DRUM	0.088	0.115	0.114	0.048	0.046	0.062	0.060	0.024	0.974	0.827	0.989	1.000	0.316	0.550	0.331	0.130
	DRUM-Deb-U	0.105	0.156	0.180	0.067	0.056	0.090	0.100	0.034	0.769	0.576	0.870	1.000	0.564	0.792	0.660	0.391
	DRUM-Deb	0.089	0.122	0.129	0.054	0.047	0.067	0.069	0.028	0.897	0.747	0.952	1.000	0.380	0.626	0.445	0.243
0.10	Best BL*	0.134	0.213	0.214	0.074	0.073	0.128	0.121	0.038	0.974	0.760	0.980	1.000	0.633	0.841	0.711	0.557
	DRUM-U	0.070	0.084	0.091	0.043	0.036	0.044	0.048	0.022	0.949	0.920	0.997	1.000	0.149	0.288	0.135	0.043
	DRUM	0.112	0.165	0.173	0.059	0.060	0.095	0.096	0.030	0.821	0.658	0.941	1.000	0.564	0.775	0.612	0.309
	DRUM-Deb-U	0.207	0.221	0.354	0.121	0.128	0.208	0.253	0.071	0.538	0.235	0.590	0.400	0.875	0.968	0.924	0.887
	DRUM-Deb	0.127	0.200	0.229	0.085	0.070	0.126	0.134	0.044	0.692	0.488	0.805	1.000	0.687	0.878	0.773	0.530
0.15	Best BL*	0.204	0.285	0.333	0.171	0.118	0.208	0.210	0.100	0.769	0.567	0.862	0.800	0.814	0.939	0.868	0.883
	DRUM-U	0.103	0.134	0.147	0.056	0.055	0.075	0.080	0.029	0.821	0.654	0.918	0.800	0.518	0.711	0.540	0.413
	DRUM	0.171	0.261	0.285	0.088	0.097	0.175	0.171	0.048	0.744	0.512	0.845	0.600	0.764	0.914	0.822	0.739
	DRUM-Deb-U	0.216	0.165	0.379	0.333	0.167	0.279	0.352	0.286	0.308	0.117	0.410	0.400	0.948	0.989	0.967	0.978
	DRUM-Deb	0.222	0.249	0.356	0.162	0.140	0.233	0.257	0.094	0.538	0.267	0.579	0.600	0.888	0.969	0.927	0.874

*Best baseline selected per site from: ERM, DRO, IW-KMM, IW-Classify, and six PL variants (oracle selection favoring baselines).

Cutoff t : classify $\hat{Y} = 1$ if predicted probability $\geq t$.

DRUM-U/DRUM/DRUM-Deb-U/DRUM-Deb = DRUM (unconstrained)/DRUM/DRUM-Debiased (unconstrained)/DRUM-Debiased.

Diagnostic: worst-case $A \mid X$ recovered by DRUM generators. Since A is structurally absent in the target, direct validation against the target $A \mid X$ distribution is impossible. We instead examine the behavior of the DRUM generators relative to the source $A \mid X$ distribution.

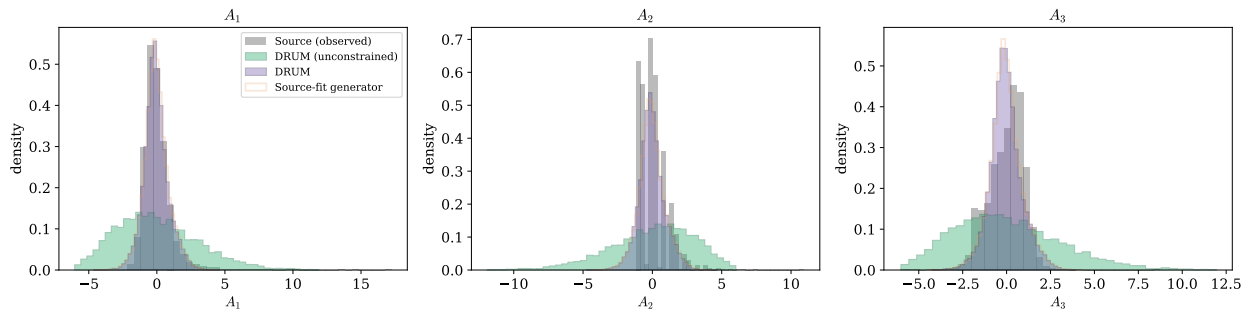


Figure 15: Marginal distributions of each structurally missing covariate A in the source (observed) compared with samples from the DRUM (unconstrained) and DRUM. Source A has approximately zero mean and unit standard deviation due to standardization.

Figure 15 compares marginal distributions of each A variable under three scenarios: the source-observed distribution, samples from the DRUM (unconstrained) worst-case generator, and samples from the DRUM worst-case generator (pooled over X). The unconstrained generator produces a substantially wider marginal distribution, reflecting its protection against arbitrary marginal shifts, while the general generator remains close to the source marginal, consistent with its bounded-perturbation design.

Model Interpretability Analysis To assess whether DRUM-Debiased variants rely on different features than baseline methods, we applied LIME (Ribeiro et al., 2016) to all methods on each evaluation site. For each method, 200 randomly sampled test instances were explained using 5,000 perturbation samples, with source training data providing feature statistics for the LIME explainer. Table 13 and Table 14 present the results across all four sites.

The feature importance patterns are remarkably consistent across populations. All baseline methods and non-debiased DRUM variants rank initial cardiac rhythm (shockable vs. non-shockable) as the dominant predictor. The DRUM-Debiased variants exhibit a qualitatively different pattern. Both DRUM-Debiased (unconstrained) and DRUM-Debiased rank sex as the top feature (coefficient ≈ 0.055), with rhythm, age, and witness/bystander CPR status contributing more evenly. The redistribution of feature importance away from a single dominant predictor suggests that the debiasing procedure encourages more balanced use of available covariates, rather than relying heavily on the feature most predictive in the US source population.

Local Supervised Baselines (Oracle Reference) As an additional reference, we trained local ERM models using data from sites (Vietnam is excluded) with sufficient sample size. For each site (Singapore, Japan, and Korea), we performed a stratified 80/20 train-test split and trained three

Table 13: Local feature importance (LIME) on Singapore (Target) and Japan. Values are mean absolute LIME coefficients averaged over 200 explained instances per site. Underline = top-ranked feature for that method.

Method	Rhythm	Age	Sex	Wit+BCPR	Wit+noBCPR	noWit+BCPR
<i>(a) Singapore (Target)</i>						
Baseline-ERM	<u>0.232</u>	0.086	0.025	0.048	0.004	0.063
Baseline-DRO	<u>0.226</u>	0.087	0.043	0.096	0.038	0.021
Baseline-IW-KMM	<u>0.221</u>	0.085	0.046	0.079	0.020	0.022
Baseline-IW-Classify	<u>0.235</u>	0.087	0.049	0.099	0.038	0.009
Baseline-PL-Mean+ERM	<u>0.154</u>	0.056	0.029	0.061	0.024	0.014
Baseline-PL-Mean+DRO	<u>0.157</u>	0.065	0.026	0.065	0.016	0.012
Baseline-PL-MICE+ERM	<u>0.230</u>	0.085	0.043	0.106	0.044	0.017
Baseline-PL-MICE+DRO	<u>0.230</u>	0.083	0.037	0.101	0.038	0.023
Baseline-PL-MF+ERM	<u>0.236</u>	0.082	0.045	0.100	0.041	0.018
Baseline-PL-MF+DRO	<u>0.231</u>	0.085	0.042	0.102	0.044	0.019
DRUM (unconstrained)	<u>0.068</u>	0.056	0.001	0.013	0.001	0.020
DRUM	<u>0.208</u>	0.082	0.035	0.059	0.018	0.053
DRUM-Debiased (unconstrained)	0.033	0.047	<u>0.056</u>	0.034	0.002	0.003
DRUM-Debiased	0.029	0.040	<u>0.057</u>	0.044	0.004	0.015
<i>(b) Japan</i>						
Baseline-ERM	<u>0.229</u>	0.097	0.025	0.047	0.004	0.062
Baseline-DRO	<u>0.223</u>	0.098	0.042	0.094	0.038	0.021
Baseline-IW-KMM	<u>0.218</u>	0.096	0.045	0.078	0.020	0.022
Baseline-IW-Classify	<u>0.232</u>	0.097	0.048	0.098	0.038	0.009
Baseline-PL-Mean+ERM	<u>0.151</u>	0.062	0.029	0.060	0.023	0.014
Baseline-PL-Mean+DRO	<u>0.154</u>	0.074	0.026	0.064	0.016	0.012
Baseline-PL-MICE+ERM	<u>0.227</u>	0.095	0.043	0.105	0.044	0.017
Baseline-PL-MICE+DRO	<u>0.227</u>	0.093	0.036	0.100	0.037	0.023
Baseline-PL-MF+ERM	<u>0.233</u>	0.093	0.044	0.098	0.040	0.018
Baseline-PL-MF+DRO	<u>0.227</u>	0.097	0.041	0.101	0.043	0.019
DRUM (unconstrained)	<u>0.068</u>	0.063	0.001	0.013	0.001	0.021
DRUM	<u>0.206</u>	0.093	0.035	0.058	0.018	0.053
DRUM-Debiased (unconstrained)	0.032	0.051	<u>0.054</u>	0.033	0.001	0.003
DRUM-Debiased	0.028	0.045	<u>0.055</u>	0.043	0.004	0.015

Rhythm = initial cardiac rhythm (shockable); Wit+BCPR = witnessed with bystander CPR; Wit+noBCPR = witnessed without bystander CPR; noWit+BCPR = unwitnessed with bystander CPR. LIME: 200 instances \times 5,000 perturbation samples.

Table 14: Local feature importance (LIME) on Korea and Vietnam (continued from Table 13). Same format and settings.

Method	Rhythm	Age	Sex	Wit+BCPR	Wit+noBCPR	noWit+BCPR
<i>(c) Korea</i>						
Baseline-ERM	<u>0.232</u>	0.091	0.025	0.048	0.004	0.063
Baseline-DRO	<u>0.225</u>	0.093	0.043	0.095	0.039	0.021
Baseline-IW-KMM	<u>0.220</u>	0.090	0.046	0.079	0.020	0.022
Baseline-IW-Classify	<u>0.234</u>	0.093	0.049	0.099	0.038	0.009
Baseline-PL-Mean+ERM	<u>0.153</u>	0.059	0.029	0.061	0.024	0.014
Baseline-PL-Mean+DRO	<u>0.156</u>	0.069	0.026	0.065	0.016	0.012
Baseline-PL-MICE+ERM	<u>0.229</u>	0.091	0.043	0.106	0.044	0.017
Baseline-PL-MICE+DRO	<u>0.229</u>	0.088	0.037	0.101	0.038	0.023
Baseline-PL-MF+ERM	<u>0.236</u>	0.087	0.045	0.100	0.041	0.018
Baseline-PL-MF+DRO	<u>0.230</u>	0.091	0.042	0.102	0.044	0.019
DRUM (unconstrained)	<u>0.068</u>	0.059	0.001	0.013	0.001	0.021
DRUM	<u>0.208</u>	0.086	0.035	0.059	0.018	0.053
DRUM-Debiased (unconstrained)	0.032	0.049	<u>0.056</u>	0.034	0.002	0.003
DRUM-Debiased	0.028	0.042	<u>0.057</u>	0.043	0.004	0.015
<i>(d) Vietnam</i>						
Baseline-ERM	<u>0.234</u>	0.086	0.025	0.048	0.004	0.062
Baseline-DRO	<u>0.228</u>	0.089	0.043	0.095	0.039	0.020
Baseline-IW-KMM	<u>0.223</u>	0.085	0.045	0.078	0.020	0.022
Baseline-IW-Classify	<u>0.237</u>	0.089	0.048	0.098	0.038	0.009
Baseline-PL-Mean+ERM	<u>0.155</u>	0.056	0.029	0.060	0.024	0.014
Baseline-PL-Mean+DRO	<u>0.159</u>	0.065	0.026	0.064	0.016	0.011
Baseline-PL-MICE+ERM	<u>0.231</u>	0.089	0.043	0.106	0.045	0.017
Baseline-PL-MICE+DRO	<u>0.231</u>	0.085	0.036	0.101	0.038	0.023
Baseline-PL-MF+ERM	<u>0.239</u>	0.082	0.044	0.099	0.041	0.018
Baseline-PL-MF+DRO	<u>0.233</u>	0.085	0.042	0.102	0.044	0.019
DRUM (unconstrained)	<u>0.068</u>	0.057	0.001	0.013	0.001	0.020
DRUM	<u>0.210</u>	0.081	0.035	0.058	0.018	0.053
DRUM-Debiased (unconstrained)	0.033	0.049	<u>0.056</u>	0.034	0.002	0.004
DRUM-Debiased	0.029	0.039	<u>0.057</u>	0.044	0.005	0.016

Rhythm = initial cardiac rhythm (shockable); Wit+BCPR = witnessed with bystander CPR; Wit+noBCPR = witnessed without bystander CPR; noWit+BCPR = unwitnessed with bystander CPR. LIME: 200 instances \times 5,000 perturbation samples.

standard models on the local training set: logistic regression (with 5-fold cross-validation over the regularization parameter $C \in \{0.01, 0.1, 1, 10\}$), random forest (with 5-fold cross-validation over tree depth, number of estimators, and minimum leaf size), and a two-layer neural network (with grid search over 50 architecture-learning rate-epoch combinations, selected by validation loss). All models were evaluated on the held-out 20% local test set with 2,000 bootstrap resamples for confidence intervals. Table 15 reports the results: the local models achieved similar performance to each other, with neural networks and random forests performing comparably to logistic regression. Note that this comparison is asymmetric: DRUM is designed for unsupervised transfer learning setting and therefore the training uses no local labeled data, while the local models are trained on 80% of local labeled data and evaluated on the remaining 20%. The comparison is intended to contextualize DRUM’s transfer performance relative to models with direct access to local labels.

Table 15: Performance of local baseline models trained and evaluated on site-specific data (80/20 stratified split). Metrics are reported as point estimate (95% bootstrap CI). These models use local labeled data, unlike DRUM which uses no local labels.

Site	Method	Brier Score	AUROC	AUPRC
Singapore	Logistic Regression	0.0287 (0.0213, 0.0371)	0.8264 (0.7563, 0.8882)	0.1628 (0.0941, 0.2846)
	Random Forest	0.0283 (0.0210, 0.0370)	0.8183 (0.7407, 0.8836)	0.1852 (0.1021, 0.3213)
	Neural Network	0.0284 (0.0211, 0.0369)	0.8299 (0.7602, 0.8906)	0.1741 (0.1016, 0.2985)
Japan	Logistic Regression	0.0298 (0.0273, 0.0323)	0.8607 (0.8443, 0.8772)	0.2080 (0.1779, 0.2482)
	Random Forest	0.0296 (0.0271, 0.0322)	0.8597 (0.8424, 0.8763)	0.2158 (0.1832, 0.2548)
	Neural Network	0.0295 (0.0270, 0.0320)	0.8639 (0.8477, 0.8800)	0.2151 (0.1841, 0.2558)
Korea	Logistic Regression	0.0338 (0.0273, 0.0410)	0.8798 (0.8397, 0.9167)	0.3076 (0.2188, 0.4176)
	Random Forest	0.0335 (0.0269, 0.0407)	0.8712 (0.8243, 0.9142)	0.3079 (0.2188, 0.4169)
	Neural Network	0.0338 (0.0271, 0.0408)	0.8788 (0.8333, 0.9191)	0.3147 (0.2235, 0.4236)